Comprehensive Evaluation of Multistrand Post-Tensioning Anchorage Systems for Seismic Resilient Rocking Wall Structures

A THESIS
SUBMITTED TO THE FACULTY OF THE GRADUATE SCHOOL
OF THE UNIVERSITY OF MINNESOTA
BY

Daniel A. Abramson

IN PARTIAL FULFILLMENT OF THE REQUIREMENTS
FOR THE DEGREE OF
MASTER OF SCIENCE

Eshan V. Dave

May 2013

ACKNOWLEDGEMENTS

This research was funded by the National Science Foundation (NSF) and the George E. Brown, Jr. Network for Earthquake Engineering Simulation (NEES) Research (NEESR) as a part of the *Unbonded Post-Tensioned Rocking Walls for Seismic Resilient Structures* project.

Grateful acknowledgement is given to each of the professors who served as advisors during my time of research and study at the University of Minnesota Duluth (UMD) including Dr. Andrea Schokker (Co-PI), Dr. Eric Musselman (Co-PI), and Dr. Eshan Dave. A special thank you to Dr. Schokker for providing me with the research opportunity, Dr. Musselman for taking me on as an advisee following Dr. Schokker's promotion, and Dr. Dave for his willingness to serve as an advisor in an unfamiliar field of research. Each of you have been invaluable mentors and resources. Thank you also to Dr. Emmanuel Enemuoh for serving as a member of my committee.

Acknowledgement is also given to each of the project participants: Dr. Sri Sritharan (PI) and Dr. Sriram Aaleti of Iowa State University (ISU), Dr. Catherine French (Co-PI) and Andy Liu of the University of Minnesota (UMN), and Susie Nakaki, PE, of the Nakaki Bashaw Group, Inc. Thank you also to Paul Bergson, PE, operations manager of the UMN civil engineering lab, for his assistance in equipment setup and training.

In addition, acknowledgement is given to the following post-tensioning materials manufacturers for their willingness to donate materials and participate in the project: DYWIDAG Systems International, Hayes Specialty Machining, Ltd., Sumiden Wire Products Corporation, and VSL of Structural Group. Special thanks is given to Randy Draginis of Hayes Specialty Machining, Ltd. for sharing his valuable knowledge of post-tensioning wedges.

Last, but in no way least, acknowledgement is given to the students and professionals who provided their time and expertise to ensure a successful testing program: Andrew Morgan and Melynda Jensen (UMN), Matt Fournier (UMD), Owen Steffans (ISU), and Darrell Anderson (UMD).

DEDICATION

To my family, who has provided unconditional love and support in all that I have attempted. I owe each of my accomplishments to you.

ABSTRACT

The motivation to develop seismic resilient structures stems from the substantial economic losses that can be caused by earthquake damage. One method of achieving seismic resiliency is to design buildings with self-centering structural systems capable of resisting lateral earthquake loads, dissipating energy, and minimizing significant structural damage. The growing popularity of unbonded post-tensioned (PT) precast concrete rocking walls designed for seismic resiliency in conjunction with recent research indicating the inability of PT anchorage systems to meet current industry certification standards has prompted the need to further test and better understand PT anchorage systems. Recent research has focused on single strand PT anchorages in an attempt to better understand the failure mechanisms and ultimate stress and strain capacities of these systems. However, virtually no published literature is available regarding the certification of multistrand anchorages due to the Post-Tensioning Institute's recommendation to test only one strand at a time in multistrand anchorages. Furthermore, results from the anchorage validation tests, conducted by anchor manufacturers, are typically not available for public access. These uncertainties and the necessity to better understand the unique phenomena that exist in multistrand systems loaded with multiple strands at once, call for a comprehensive evaluation of multistrand post-tensioning anchorage systems.

This thesis presents results from a comprehensive laboratory evaluation of the fracture and ultimate strength and deformation capacities of multistrand PT anchorage systems for use in seismic resilient rocking wall structures. The testing program encompassed two anchorage manufacturers, two anchorage alignment configurations, and two wedge geometries under both monotonic and cyclic loading.

CONTENTS

LIST OF TABLES

LIST OF FIGURES

CHAPTER 1: INTRODUCTION AND BACKGROUND

1.1 Overview

The growing popularity of unbonded post-tensioned (PT) precast concrete rocking walls designed for seismic resiliency in conjunction with recent research indicating the inability of PT anchorage systems to meet current industry certification standards has prompted the need to further test and better understand PT anchorage systems. Recent research has focused on single strand PT anchorages in an attempt to better understand the failure mechanisms and ultimate stress and strain capacities of these systems. However, virtually no published literature is available regarding the certification of multistrand anchorages due to the Post-Tensioning Institute's recommendation to test only one strand at a time in multistrand anchorages (PTI 1998). Furthermore, results from the anchorage validation tests, conducted by anchor manufacturers, are typically not available for public access. These uncertainties and the necessity to better understand the unique phenomena that exist in multistrand systems loaded with multiple strands at once, call for a comprehensive evaluation of multistrand post-tensioning anchorage systems.

1.2 Objectives

In accordance with the research need in this area, the primary objectives of this report are:

(1) To review current design, testing, and usage guidelines for unbonded PT anchorage systems;

(2) To investigate the fracture and ultimate strength and strain capacities of representative multistrand PT anchorage configurations under monotonic and cyclic tensile loading;

(3) To make recommendations for the acceptance testing of unbonded multistrand PT anchorage systems; and

(4) To make recommendations for the design of unbonded multistrand PT for use in seismic resilient rocking wall structures.

1.3 Scope and Approach

This report presents fracture and ultimate strength and strain results from a comprehensive laboratory evaluation of multistrand PT anchorage systems under monotonic and cyclic loading parameters. The following multistrand anchorage configurations are included in the research: (1) anchorage manufacturer; (2) wedge geometry; and (3) anchorage alignment.

It should be noted that the results presented in this report are limited to the specimens tested. Many strand/anchorage/wedge configurations exist that were not considered in this research due to limited time and resources. Additionally, the test results are limited by the specimen sample pool size for each of the configurations considered.

1.4 Organization of Report

The remainder of this report begins with background information useful for understanding the origins of the overarching research project, followed by a review of the literature in the areas of prestressed concrete, post-tensioned rocking wall structures, and previous PT anchorage research conducted. The testing apparatus, methodology, instrumentation, configurations, and analysis are then discussed. A summary of the test results in terms of stress capacity, strain capacity, and modulus of elasticity of the PT strand are then presented. The report concludes with a summary, conclusions and recommendations for future testing of unbonded multistrand PT anchorage systems and the design and implementation of unbonded PT in seismic resilient rocking wall structures.

1.5 Unbonded Post-Tensioned Rocking Walls for Seismic Resilient Structures

The research presented in this report is a portion of a George E. Brown, Jr. Network for Earthquake Engineering Simulation (NEES) Research (NEESR) project titled *Unbonded Post-Tensioned Rocking Walls for Seismic Resilient Structures*. The research project included Iowa State University (ISU), the University of Minnesota Twin

Cities (UMN), and the University of Minnesota Duluth (UMD) and utilized NEES facilities located at UMN and the University of Nevada at Reno.

The motivation to develop seismic resilient structures stems from the substantial economic losses that can be caused by earthquake damage. One method of achieving seismic resiliency is to design buildings with self-centering structural systems capable of resisting lateral earthquake loads, dissipating energy, and minimizing significant structural damage. Using unbonded post-tensioning (PT) tendons and energy dissipating connectors, a cost-effective, self-centering wall system known as PreWEC (i.e., Precast Wall with two End Columns) was developed at ISU (Aaleti and Sritharan 2007). In this system (discussed further in Section 2.2.1), as well as in single rocking walls designed with unbonded PT, the response is dominated by a rocking mode.

While these systems have shown excellent seismic performance with minimal structural damage both analytically and experimentally, there are still several areas that require further investigation. One such area is the modes of energy dissipation. Significant effort will be placed on the identification of different energy dissipation sources of rocking walls such as impact (or radiation damping), viscous damping and hysteretic damping, and the influence of hysteretic damping on the impact energy loss (NEES@Nevada 2010). Contact damping, or the energy loss caused by the wall impacting the foundation during rocking, has not historically been given consideration in design due to lack of knowledge on this subject. However, significant evidence suggests that this mechanism alone may be sufficient to dissipate the seismic energy (NEES@Nevada 2010).

Another research area requiring further attention is the interaction of surrounding structural components, especially floors and gravity columns, with the seismic resistant systems. To ensure a fully resilient structure, these interactions must be addressed by understanding the wall-floor connection responses (Sritharan 2010).

Lastly, recent research has called into question the ability of PT anchoring devices to meet current industry standards and, therefore, the high strain demands of rocking wall structures. PT anchorage systems are a key component in a rocking wall's ability to self-

center following a seismic event. While a substantial amount of literature is available on monostrand PT anchorage evaluations, there is very little public data available on multistrand PT anchorage systems. The objective of this report is to meet the need for additional research in this area and, in turn, make design recommendations with regard to post-tensioning in rocking wall structures.

1.6 Motivation for Multistrand PT Anchorage Evaluations

Post-tensioning anchorages are required to provide a specified strand elongation and percentage of the strand's strength under tensile loads. Currently, there is considerable variation amongst governing institutions and code writing bodies in this area, which is due largely to recent changes in certification procedures promulgated by the Post-Tensioning Institute (PTI) and subsequently accepted by the American Association of State Highway and Transportation Officials (AASHTO) and many state Departments of Transportation (DOTs) (Hayes and Draginis 2010, b). In the mid-1990's, PTI replaced he term "GUTS" (guaranteed ultimate tensile strength) by two definitions: "MUTS" (minimum ultimate tensile strength) and "AUTS" (actual ultimate tensile strength) (FHWA 2013). In doing so, PTI made a fundamental shift in anchorage certification requirements from the strand's GUTS to AUTS. GUTS is the tensile strength of the strand that can be assured by the manufacturer and is expressed as a stress (i.e., force per area). AUTS is the actual breaking strength obtained in free-length fracture tests of a single representative strand and is expressed as a force. MUTS is the force equal to the nominal cross-sectional area of the strand times its nominal ultimate tensile stress.

Previously, PTI certification required anchorage systems to provide a minimum of 95 percent of GUTS. However, the new PTI certification requires the anchorages provide a minimum of 95 percent of AUTS, which can be significantly greater than GUTS. This change has made the certification requirement considerably more stringent by effectively increasing the required strength of the system. Subsequently, PT anchoring devices commonly used in practice now fail certification testing in a substantial number of cases (Hayes and Draginis 2010, b).

However, not all code writing bodies have accepted this new criterion, the most notable of which is the American Concrete Institute (ACI) in their Building Code Requirements for Structural Concrete (ACI 318-08). Section 18.21 of ACI 318-08 requires that PT anchorages develop at least 95 percent of the specified tensile strength of the prestressing steel (f_{pu}) and conform to the 2 percent elongation requirements in ACI 301 when tested in an unbonded condition, which is essentially the old PTI requirement.

The failure of the 7-wire strand in a PT system at values below the strand's ultimate capacity results from the interaction between the strand and the wedge system. Notching of the strand by the wedges and an unevenly distributed load over the length of the wedge at high stress levels causes a stress concentration at the nose of the wedge and a premature fracture of an individual wire. The importance of PT anchorage performance in the rocking wall structure being evaluated prompted the need to further investigate these failure mechanisms. Additionally, the vast majority of research in this area is conducted on monostrand anchorage systems whereas the experimental program described in this report will focus on the multistrand systems that will actually be implemented in the proposed rocking wall structures. Typically, when multistrand anchorages are tested, only one strand at a time is used, as specified by the Post-Tensioning Institute (PTI 1998) due to uncertainties associated with loading multiple strands simultaneously. However, there are several phenomena that are unique to the multistrand system and cannot effectively be evaluated using a single strand in a multistrand anchorage. Among these are disproportionate strand loading, strand eccentricity, twist, and fretting. By conducting tests on a multistrand system and applying virtually the same acceptance criteria as a monostrand system, the aforementioned phenomena can be better understood.

CHAPTER 2: LITERATURE REVIEW

2.1 Prestressed Concrete

Prestressed concrete is a method of placing a structural concrete member in compression prior to the application of service loads to overcome concrete's inherent weakness in tension. High strength steel strands located in regions where the concrete is prone to high tensile strains are tensioned and locked in place. This tensile force places the concrete member in compression, allowing for longer clear spans, thinner slabs, fewer beams, more slender elements and better crack control than conventionally reinforced concrete (PTI 2000). Schematic drawings in Figure 2.1 depict the concept of prestressed concrete in a beam application.

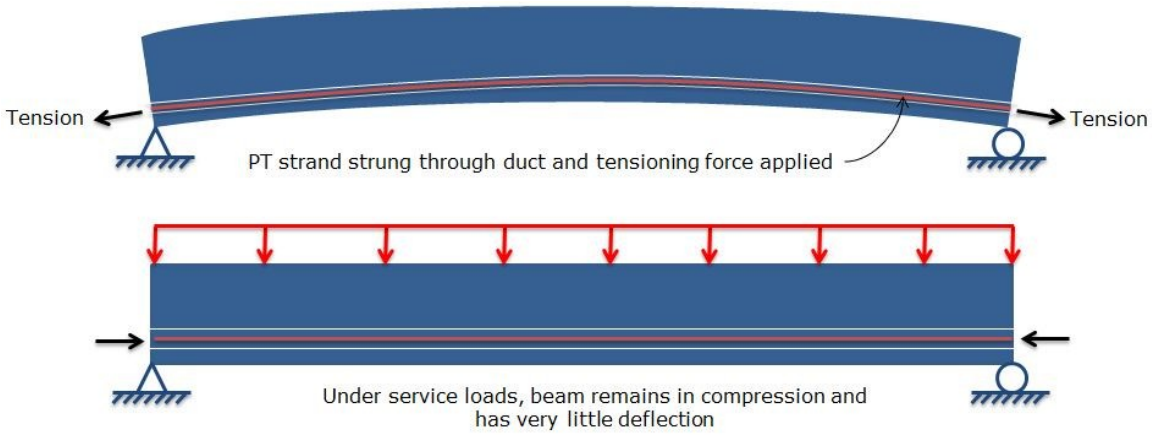

Figure 2.1: Prestressed concrete concept.

Introduced conceptually as early as the mid-to-late 1800's, prestressed concrete came to the United States following World War II (Aalami 2007). Its first use in the United States was in the 1951 construction of the Walnut Lane Bridge in Philadelphia, Pennsylvania (Dinges 2009). By 1957, prestressed concrete was brought into the mainstream of American construction practice (Billington 2004). Originally used exclusively for precast bridges, a wide variety of prestressed concrete applications quickly developed including building beams and slabs, parking structures, and slabs-on-ground (PTI 2000).

The three types of prestressed concrete are pre-tensioned, and bonded and unbonded post-tensioned. Pre-tensioned and post-tensioned concrete differ in the time at which the PT strands are stressed. In the case of pre-tensioned concrete, the strands are stressed in a casting bed and the concrete is placed around the strands. Once the concrete has adequately cured, the strands are cut, transferring the tensile force of the strands to the concrete. In the case of post-tensioned concrete, the concrete member is cast with either a hollow duct or a tendon coated in a sheathing that allows it to move along its length. Strands are run through the duct and stressed after the concrete has adequately cured.

Bonded and unbonded post-tensioning differ in the manner in which the strand's tensile stresses are transferred to the concrete member. In bonded applications, cementitious grout is pumped into the duct after the strands have been stressed. The grout provides corrosion protection to the strand and bonds the tendon to the surrounding concrete. The bond created by the grout offers a mechanism for load transfer of over the length of the tendon. In unbonded applications, the strands are coated with corrosion-inhibiting grease and encased in an extruded plastic protective sheathing to prevent them from bonding to the surrounding concrete. In this system, the strand's tensile force is transferred to the concrete only through embedded anchors located at each end of the tendon (PTI 2000). Unbonded strands are able to move freely relative to the surrounding concrete which results in a uniform distribution of strand strains and eliminates tensile stress transfer to the concrete as the strands elongate under lateral loading, reducing concrete cracking. These properties make unbonded post-tensioning ideal for use in rocking wall structures.

2.1.1 Post-Tensioning Anchorages

Post-tensioning anchorages are a critical element in PT systems, especially in unbonded applications since they are the exclusive source of load transfer. The anchorage system is made up of three primary components: (1) the anchor; (2) the wedge plate; and (3) the wedges. The anchor is embedded in the end of the concrete member and commonly consists of multiple bearing planes to ensure effective load transfer to the

concrete. The wedge plate is located outside of the concrete member and bears directly against the anchor. The wedge plate has tapered through holes in which conical wedges seat and grip the PT strand after stressing is complete. The wedges typically consist of two or three independent wedge pieces which have a smooth, cone-shaped exterior and threaded teeth for gripping the strand on their interior. Figure 2.2 shows a multistrand PT anchorage assembly with each of the components labeled.

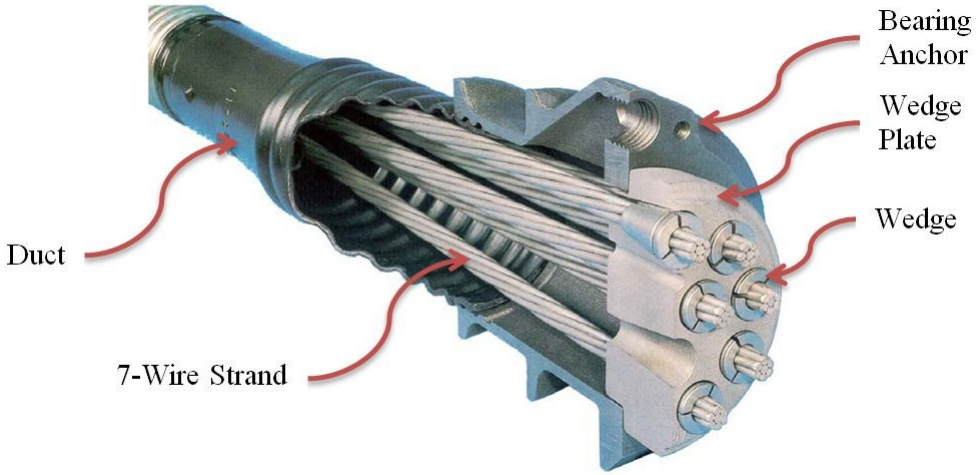

Figure 2.2: Tendons strung through an open duct and anchored in place using tapered wedges (DSI 2006).

2.1.2 Published Performance Requirements for Post-Tensioning Anchorages

Due to the gripping mechanism of the anchorage system in which the wedge teeth penetrate the exterior wires of the strand, the failure mechanism of anchored PT strand is brittle in nature and occurs within the anchor at the nose of the wedge (Walsh and Kurama 2009) (Figure 2.3). Several governing institutions and code writing bodies in the PT industry have published strength and deformation requirements that the anchoring system must allow the strand to achieve prior to failure. As discussed in Section 1.6, discrepancies exist amongst the published requirements because of a recent shift in certification requirements by PTI from GUTS to AUTS. Table 2.1 summarizes the published certification requirements for PT strand and strand/anchor systems.

Table 2.1: Published strength and deformation requirements.

Component	Publication	Required Strength (ksi)	Required Elongation at Ultimate Load	Required Gage Length (in.)
Strand	ASTM A416 Section 6	$1.00f_{pu}$, $f_{pm,free\text{-}length} > f_{pu}$	3.5%	24
Strand/Anchor System	ACI 318-08 Section 18.21.1	$0.95f_{pu}$	2.0%	N/A
Strand/Anchor System	ACI 423.7-07 Section 2.6	$0.95f_{pm,free\text{-}length}$	2.0%	36
Strand/Anchor System	ACI 423.3R-05 Section 4.1	$0.95f_{pm,free\text{-}length}$	2.0%	36
Strand/Anchor System	PTI-2000 Section 2.2.1	$0.95f_{pm,free\text{-}length}$	2.0%	36
Strand/Anchor System	ICC-ES AC303	$0.95f_{pm,free\text{-}length}$	2.0%	42

The subscript naming convention used in Table 2.1 is consistent with Walsh and Kurama 2009. For all intents and purposes of this research, f_{pu} can be taken as equivalent to GUTS and $f_{pm,free\text{-}length}$ can be taken as equivalent to AUTS divided by the nominal cross-sectional area of the seven-strand system (i.e., 0.217 in^2 * 7 = 1.519 in^2). All strand used in this research was grade 270 (i.e., f_{pu} = 270 ksi).

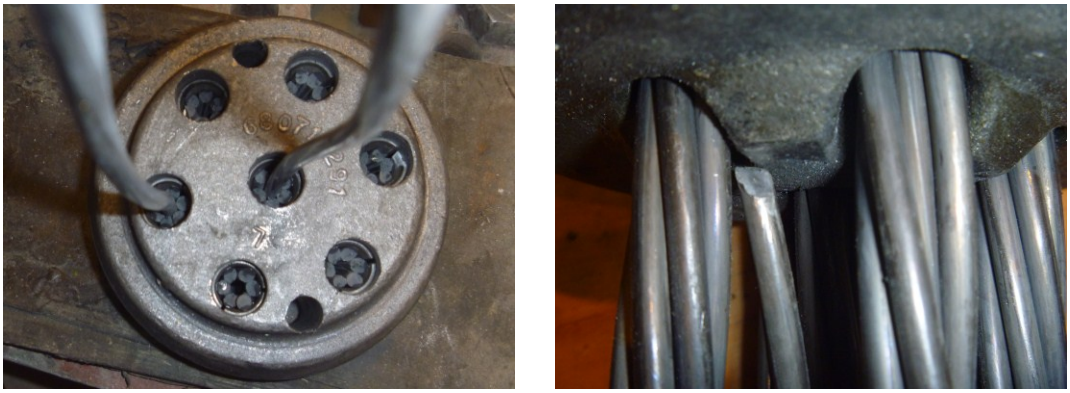

Figure 2.3: Wire fracture occurring within anchorage at the nose of the wedge.

2.2 Post-Tensioned Rocking Wall Systems

Prompted by the Chilean earthquakes of May, 1960, the study of structures being controlled by a rocking mode was first investigated through the free vibration of rigid

rocking blocks (Housner 1963). Based largely on the principles quantified by Housner, since the 1990s several structural rocking wall systems have been developed for the purpose of dissipating energy and minimizing damage during seismic events (e.g., Priestley and Tao 1993; El-Sheikh et al. 1999; Kurama el al. 1999; Priestley el al. 1999; Holden et al. 2003; Perez et al. 2004, 2007; Kurama 2005). In each of the structural rocking systems investigated, unbonded post-tensioning was used to join precast concrete members to achieve the lateral resistance required under seismic loads as well to provide self-centering capability. Additional benefits of unbonded PT over monolithic cast-in-place reinforced concrete in this application include better quality control, construction efficiency, and an ability to undergo large nonlinear lateral displacements without sustaining significant damage (Walsh and Kurama 2009).

From 1989 to 1999, researchers from the University of California at San Diego worked on the Precast Seismic Structural Systems (PRESSS) research program. The testing program culminated with a large-scale five-story precast concrete building constructed to 60 percent scale being tested under simulated seismic loading conditions. The building included several seismic resilient components, including an unbonded post-tensioned jointed rocking wall system. The primary objectives of this program were: (1) to develop comprehensive and rational design recommendations needed for a broader acceptance in seismic zones; and (2) to develop new materials, concepts, and technologies for precast concrete construction in different seismic zones (Priestley, et al. 1999).

While the PRESSS building's performance was touted as extremely satisfactory, several deficiencies of the jointed rocking wall system were identified through this testing program that limited its implementation in practice. Reduced moment capacity and expensive stainless steel energy dissipating shear connectors made the cost of the jointed wall system prohibitive in comparison to monolithic concrete wall construction (Sritharan, Aaleti, et al. 2008).

Another self-centering wall system concept is the hybrid wall (Kurama, Weldon and Shen 2006; Restrepo and Rahman 2007). This system combines a single post-

tensioned precast concrete wall with mild steel energy dissipating bars placed across the wall-foundation interface. The hybrid wall system addressed the reduced moment capacity deficiency while still providing sufficient energy dissipation. However, a new resiliency deficiency arose with the use of mild steel reinforcing bars as an energy dissipation element. The bars are likely to undergo low-cycle fatigue fracture during a large seismic event and cannot be cost-effectively replaced (Sritharan, Aaleti, et al. 2008).

2.2.1 Precast Wall with two End Columns (PreWEC)

To address the deficiencies identified above, a new structural wall system was developed (Aaleti and Sritharan 2007) at Iowa State University. The system consists of a Precast Wall with two End Columns (PreWEC). It utilizes inexpensive, easily replaceable mild steel oval-shaped flexural plate connectors (O-connectors) to dissipate energy (Henry, et al. 2010) and lightly prestressed unbonded post-tensioning to self-center after a seismic event.

As shown in Figure 2.4, the system consists of a single precast concrete wall with two end columns, all with unbonded post-tensioning. The end columns can be made up of steel columns, concrete filled steel tubes, or precast concrete columns. Walls and columns are anchored to the foundation via unbonded post-tensioning and joined together with energy dissipating O-connectors (Figure 2.5a). Unbonded post-tensioning strands or rods can be placed evenly along the wall or centered within the wall. Using unbonded PT ensures a constant strain distribution over the length of the strand and prevents localized strains at critical sections compared to bonded systems (Sritharan, Aaleti, et al. 2008). This allows the wall to withstand significant levels of drift without sustaining substantial structural damage.

Conceptually, the PreWEC system allows the wall and end columns to rock independently during a seismic event. Unlike most post-tensioning applications, the tendons will only be initially stressed to about fifty percent of ultimate design strength (f_{pu}) instead of the typical initial stress of about seventy percent of f_{pu}. This reduction in initial stressing is implemented so that the tendons will remain elastic for the duration of

the design seismic forces. The energy absorbed within the tendons is transferred back into the wall system and, ultimately, energy dissipating O-connectors.

Following a seismic event, the wall will re-center due to the restoring force of the elongated PT strands. The primary source of hysteretic damping in the system is forced to the mild steel O-connectors as they transfer energy laterally between precast segments and dissipate energy through inelastic flexural yielding (Figure 2.5b). After a significant seismic event, these connectors can be easily and economically replaced. Additionally, the PreWEC system can be designed to obtain a moment capacity comparable to that of a monolithic reinforced concrete wall (Aaleti and Sritharan 2007) ensuring a fully resilient system (Sritharan, Aaleti, et al. 2008).

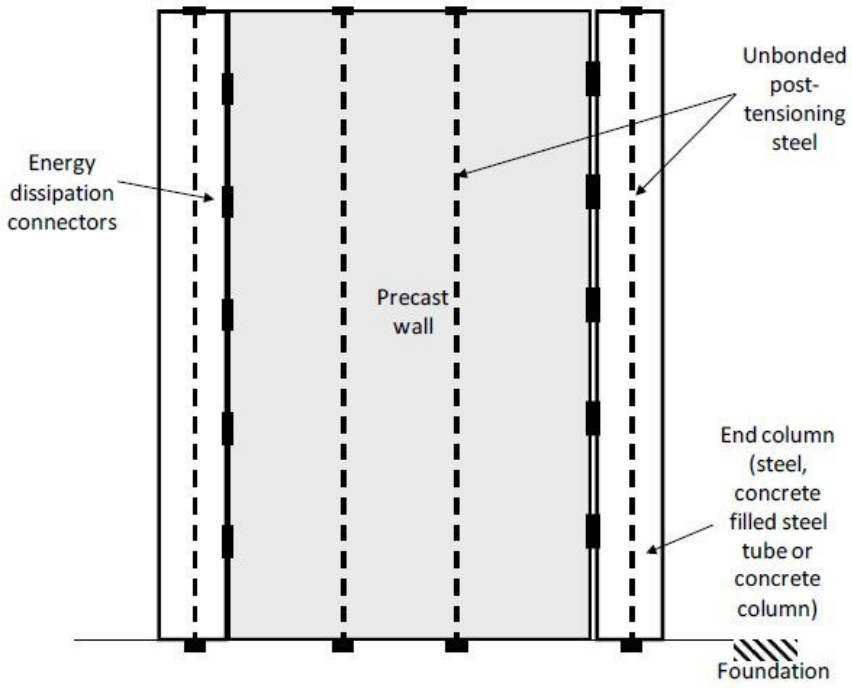

Figure 2.4: Schematic drawings of the PreWEC concept (Sritharan, Aaleti, et al. 2008).

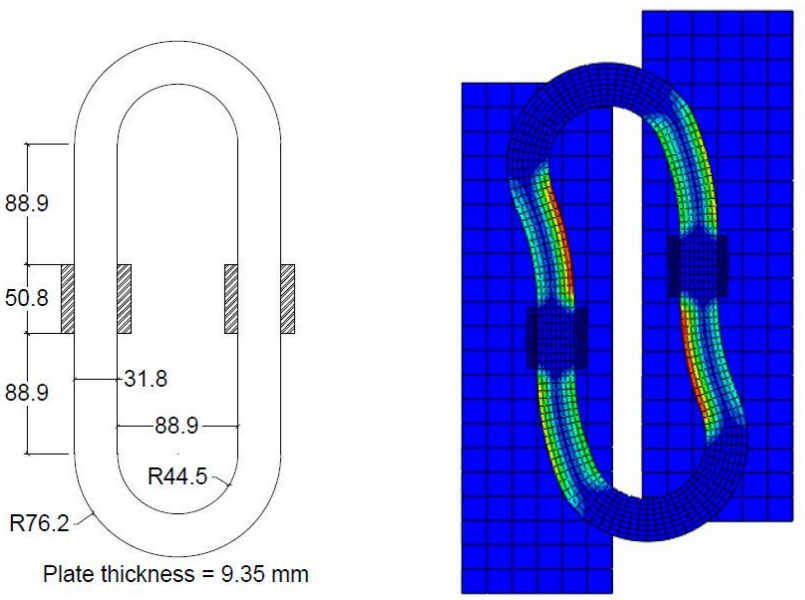

Figure 2.5: Energy dissipating O-connectors: (a) dimensions and (b) deformed shape from finite element modeling (Henry, et al. 2010).

2.3 Previous Research Conducted

Previous research in the area PT strand/anchorage performance evaluations is limited. However, a few key testing programs have recently produced conflicting results and raised questions about the performance of current systems and industry acceptance criteria. These studies will be discussed in detail as they played an important role in prompting the multistrand evaluations presented in this report. Additionally, a study of PT strand instrumentation will be reviewed as its methods and procedures were adopted in the tests presented in this report.

2.3.1 Monostrand Post-Tensioning Anchorage Evaluations

Published research in the area of post-tensioning anchorage evaluation tests in the United States is limited. The recent monostrand PT anchorage evaluations conducted at the University of Notre Dame by Walsh and Kurama will be described in detail as they played a crucial role in prompting the multistrand anchorage evaluations described in this report. Prior to the Walsh and Kurama research in 2009, there is only one known source

of published PT anchorage evaluations (Schechter and Boecker 1971). The data presented in this 1971 study is on multistrand anchorages and may be outdated since the materials used are now obsolete and the testing parameters do not meet today's standards. After the Walsh and Kurama report was published, an independent investigation of monostrand PT anchorage systems was carried out by Wiss, Janney, Elstner Associates, Inc. (WJE) on behalf of the Post-Tensioning Institute. The multistrand PT anchorage evaluations presented in this report (as well as the monostrand PT anchorage evaluations described in Section 2.4) were prompted in part by the conflicting Notre Dame and WJE test results.

2.3.1.1 University of Notre Dame Testing

Prompted by the premature fracture of unbonded PT strands within a coupled wall subassembly and the general lack of published research in the area of PT strand/anchorage performance evaluations, the University of Notre Dame undertook a research program titled *Behavior and Design of Unbonded Post-Tensioned Strand/Anchorage Systems for Seismic Applications* (Walsh and Kurama 2009). Following the International Code Council Evaluation Service "Acceptance Criteria for Post-Tensioning Anchorages and Couplers of Prestressed Concrete" (ICC-ES 2007), Walsh and Kurama conducted a multitude of monotonic tensile load tests on monostrand PT strand/anchorage assemblies. The strand/anchorage parameters examined were strand diameter, anchor type (cast and barrel type anchors) and physical properties, number of wedge pieces, and the presence of a binding ring around wedges. Several loading parameters were also investigated including load rate, eccentricity between strand ends, post-yield cyclic loading, and initial strand stress. Some of the most relevant conclusions and recommendations of the final report were:

(1) The ultimate stress and strain capacity of the strands are limited by the fracture of individual strand wire(s) due to the "notching" effect inside the anchor/ wedge assembly.

(2) Due to the brittle nature of the individual wire fracture, a considerable amount of scatter exists within the test data presented. Fracture strains ranged from 0.01 in./in. (or slightly less for a small number of samples) to 0.04 in./in.

(3) Extending the free length of the strand sample tested did not significantly affect the performance of the system.

(4) Cast anchors of the same type and provided by the same manufacturer but with different casting date codes can perform significantly differently.

(5) Strain measurements from a 36-in. gage length extensometer and a 2-in. extensometer are nearly identical. The current ICC-ES requirement to use an extensometer with a minimum gage length of 36 in. is not justified.

(6) The PT strand stress-strain relationship provided by the PCI Design Handbook (PCI 2004) did not correlate well with the relationship observed in the test data presented and needs to be updated.

Most notably, the report suggested that the monostrand anchorage systems tested are not capable of achieving the ultimate strength and strain limits required for certification. Specifically, strands would often fracture prior to achieving the $0.95f_{pu}$ strength requirement and the 2.0% strain requirement of ACI 318-08 Section 18.21.1.

2.3.1.2 Wiss, Janney, Elstner Associates Testing

Due to concern about what appeared to be inconsistent tensile strength results in the Walsh and Kurama report than are normally observed in the acceptance testing of commercially available monostrand anchorage systems, the Technical Advisory Board of the Post-Tensioning Institute retained the services of WJE to perform a series of tensile tests to resolve the apparent discrepancy (Technical Advisory Board, PTI 2010). The testing program implemented by WJE was far less robust than that implemented by Walsh and Kurama in terms of the strand/anchorage and loading parameters that were considered. A total of 23 samples were tested (5 anchorage types with 3 samples each and 2 anchorage types with 4 samples each) in the WJE program in comparison to the 86 samples tested in the Walsh and Kurama program.

Table 2.2: Comparison of average strength, range, and standard deviation between test programs (Technical Advisory Board, PTI 2010).

	Walsh and Kurama Data (86 tests)	**WJE Data (23 tests)**
Average Strength	264 ksi	274 ksi
Range (Difference)	241 ksi – 279 ksi (38 ksi)	263 ksi – 283 ksi (20 ksi)
Standard Deviation	10.12 ksi	5.69 ksi

The WJE report (WJE 2010) showed that all of the tested anchorage assemblies met the ACI 318-08 Section 18.21.1 strength and strain requirements. In a letter to PCI Journal summarizing the WJE results, the PTI Technical Advisory Board also highlighted the reduced range and standard deviation in the WJE results compared to the Walsh and Kurama results (Table 2.2) and suggested that the Walsh and Kurama results may not be representative of typical anchorages and wedges used for 0.5-in. diameter monostrand systems used in the United States.

Walsh and Kurama responded to these criticisms with three primary points. First, the actual strength of the strand used in the two reports differed considerably. The average actual ultimate strength of the Walsh and Kurama strand (286.7 ksi) was 10.6 ksi smaller than that of the WJE strand (297.3 ksi). As shown in Table 2.2, the average strength of the anchorage/strand system in the Walsh and Kurama tests was also 10 ksi smaller than that of the WJE tests. Walsh and Kurama stated that the higher WJE fracture strengths may be due to the higher-strength material that was used. Additionally, the WJE test results were only compared to the ACI 318-08 strength and strain limits. As shown in Table 2.1, ACI 318-08 is the only governing body whose strength requirement is $0.95f_{pu}$. If the fracture strengths were compared to the more stringent limit of $0.95f_{pm,free\text{-}length}$, about two-thirds of the WJE samples would not pass. The WJE report is not clear as to why only the ACI 318-08 acceptance criteria are given consideration.

Second, Walsh and Kurama responded to the PTI criticism of having a greater range and standard deviation than the WJE tests by stating that more test parameters and

variable ranges were included in their testing program than the WJE program. Additionally, Walsh and Kurama dismissed the PTI conclusion that their results may not be representative of typical anchorages and wedges used for 0.5-in. diameter monostrand systems since the Walsh and Kurama testing program included a far greater scope of experimental parameters. Thus, the results presented would actually be more representative of the systems and combinations of systems commonly being used.

Third, Walsh and Kurama called into question the method used by WJE to record and calculate strand elongation. The WJE report states that, "The test machine extensometer recorded the total movement of the sample" (WJE 2010). However, as stated by Walsh and Kurama, the elongation values seem to have been measured using the relative movement of the test machine crossheads, not an extensometer. Using crosshead displacement values to calculate strand strain can be misleading since the deformation of the testing machine fixtures and the seating of the wedges into the anchor are included as strand elongation. Walsh and Kurama presented Figure 2.6 to further illustrate this important difference. The figure shows stress plotted against extensometer and crosshead displacement strain from the same test. The fracture strain is inflated by approximately 0.01 in./in. using the crosshead displacement method, which is a significant difference considering that the strain limit required by both ACI 318-08 and ICC-ES is 0.02 in./in.

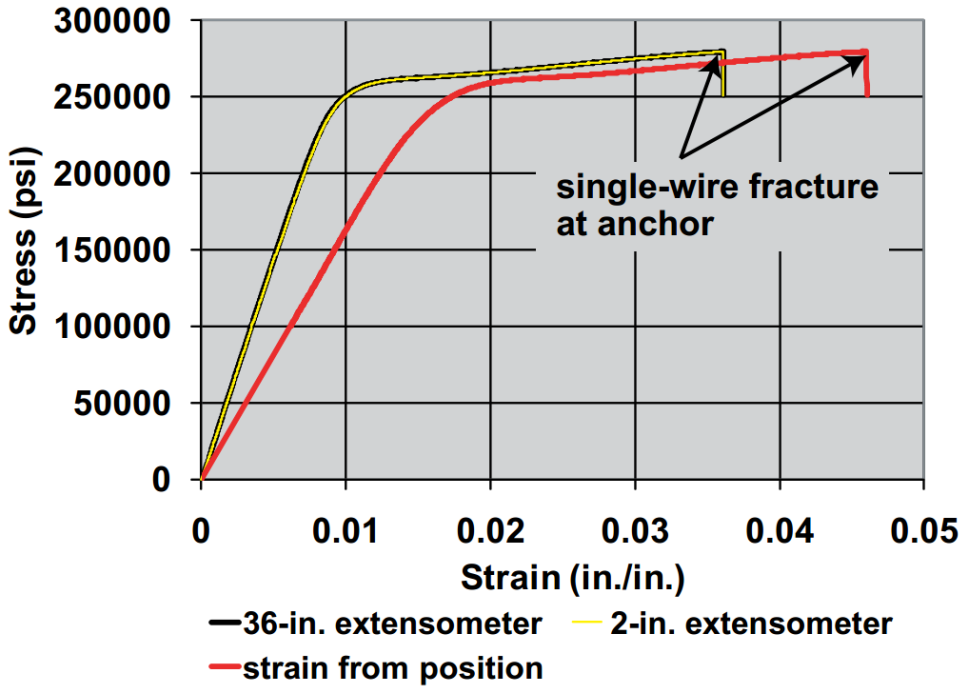

Figure 2.6: Comparison of extensometer and position strains (Walsh and Kurama 2010).

2.3.2 Instrumentation of Post-Tensioning Strand

Previous research has also been conducted on the instrumentation of PT strand (Acosta 1991). The focus of Acosta's research program was to identify favorable methods of instrumenting PT segmental box girder bridges. Instrumentation recommendations were made in terms of the most appropriate systems available at the time of the research based on a survey of existing monitoring devices. The research program encompassed monitoring of all components of PT segmental box girder bridges and made recommendations for instrumentation of an upcoming construction project at the time. In terms of PT strand strain and load measurements specifically, both electrical resistance strain gages and epoxy sleeves were subjected to extensive laboratory testing.

Strain gages are generally bonded to an individual wire of a 7-wire prestressing strand, oriented along the axis of the wire. In doing so, the strain gage measurement reflects the strain of the individual wire rather than that of the strand as a whole. Research conducted previous to the Acosta study indicated that significantly different levels of strain could be observed amongst individual exterior wires at low load levels

(Yates 1988). Yates observed that after a certain load is applied and each wire is fully anchored, the subsequent strain increases are relatively linear with near equivalent slopes. For this reason, Yates recommended that only strain readings corresponding to stresses higher than 50 ksi be considered for the preparation of a linear calibration curve. However, through extensive instrumentation and testing, Acosta later concluded that when all strain gages are installed at one particular cross-section and at an equal distance of at least 24 in. from the anchorage ends, the gages measure similar values of strain even at low stress levels (Acosta 1991).

In a study of a box-girder bridge model (MacGregor 1989), Yates' procedure of omitting low stress readings was adopted and enhanced. MacGregor also performed a linear regression of average gage data values and transformed them into straight lines of equal slope passing through the origin.

In determining modulus of elasticity values to validate strain gage readings, Acosta adopted MacGregor's procedure. Acosta's final data reduction method consisted of constructing a best-fit line through stress-strain data that was defined considering only the data points corresponding to stresses between $0.20f_{pu}$ and $0.80f_{pu}$. This procedure avoids the consideration of initial nonlinearities caused by seating of the strand specimen at the anchor ends as well as nonlinearities present after yielding of the strand has begun. The slope of the best-fit line is then the "apparent" modulus of elasticity of the strand.

Acosta noted that the apparent modulus is slightly larger than the modulus value defined by the manufacturer due to the application of the strain gage to an individual wire along the wire's axis. Strand manufacturers determine moduli values using extensometers which measure the elongation of the strand as a whole. It is difficult to accurately predict how much larger the apparent modulus will be because of factors other than the strand pitch influence (e.g., the exact orientation of the strain gage in relation to the individual wire's axis). However, to help quantify the ratio between the apparent modulus and the manufacturer's modulus, Acosta performed an analytical study of the geometric conditions of the strand under tensile loading (Figure 2.7). The drawing represents a 7-wire strand drawn with an exaggerated high pitch and small wires to better

show the extreme behavior. If this specimen were completely anchored at the beginning and end of the instrumented wire's single loop, the strand strains would be 3.8% to 6.8% higher than the individual wire's strains at the same stress level. This directly implies that the strand's modulus of elasticity is slightly smaller than a single wire's measured modulus due to the different geometric conditions (Acosta 1991).

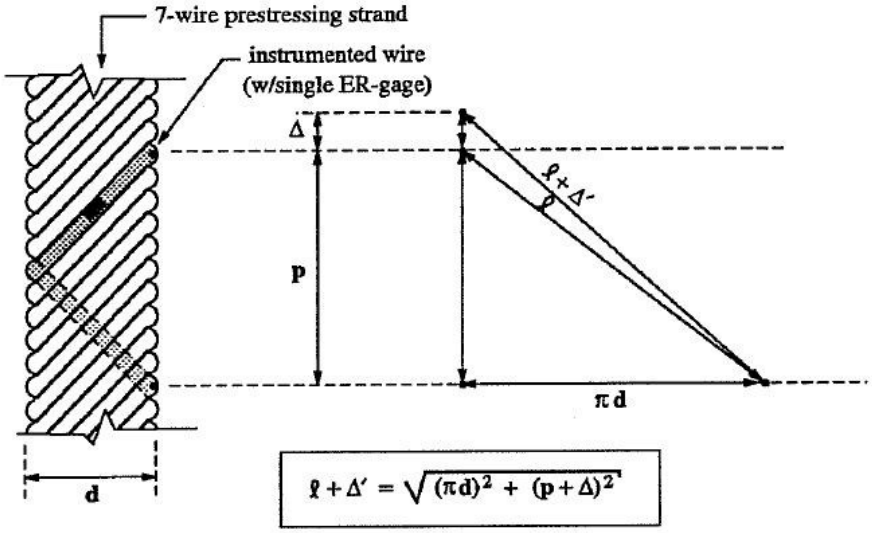

$$\ell + \Delta' = \sqrt{(\pi d)^2 + (p + \Delta)^2}$$

where:
ℓ: length of instrumented wire corresponding to 1 revolution around the strand.
Δ: strand elongation.
Δ′: wire elongation.
ε: strand strain.
ε′: wire strain.
p: pitch of the strand.
d: nominal strand diameter.

* **Manufacturer tolerance in strand's pitch:** 12 to 16 strand diameters.

* **Effect on apparent modulus determined by electrical resistance strain gages:**
(same for ½" ϕ and 0.6" ϕ strands)

Pitch	$\left(\frac{\varepsilon'}{\varepsilon}\right)$
12 d	0.936
16 d	0.963

Figure 2.7: Analytical approximation of a prestressing strand's modulus of elasticity, as determined by electrical resistance strain gages bonded to individual wires (Acosta 1991).

2.4 Preliminary Monostrand Test Results

As an additional experiment within the NEESR project *Unbonded Post-Tensioned Rocking Walls for Seismic Resilient Structures*, monostrand anchorage evaluations were also conducted at the University of Minnesota Duluth (UMD). The primary objectives of these tests were to set a baseline of system performance in terms of strength and strain capacity and to compare the findings with that of Walsh and Kurama and WJE as described in Section 2.3. Although this data has not yet been published in an independent report, some of the preliminary results will be presented here.

The monostrand anchorage tests investigated two cast anchor manufacturers in both coupled and uncoupled setups. The test specimens were loaded both monotonically and under a variety of cyclic load ranges. Table 2.3 contains a summary of the monostrand testing configurations.

Table 2.3: Summary of UMD monostrand test configurations.

Loading Scheme		**Manufacturer**	**Type**	**Repetitions**
Monotonic		1	Anchor only	3
			Coupler	3
		2	Anchor only	3
			Coupler	3
Cyclic (percent of f_{pu})	40-90	1 and 2	Anchor only	6
			Coupler	6
	40-95	1 and 2	Anchor only	6
			Coupler	6
	20-95	1 and 2	Anchor only	6
			Coupler	6
TOTAL MONOSTRAND TESTS CONDUCTED				**48**

The testing apparatus, instrumentation, methodology, and configurations will not be described in detail in this report. Rather, a brief overview of the tests conducted and the fracture stress results will be presented.

The baseline test setup consisted of a single 0.5-in. diameter, 270 ksi low-relaxation PT strand gripped at each end by cast monostrand anchors. The specimen was loaded monotonically at a displacement-controlled rate of 0.361 in./min. Wedges were provided by each respective cast anchor manufacturer to ensure compatibility. One variation of the baseline setup included fixing a coupler (produced by the same manufacturer as the cast anchors being tested) at the mid-height of the specimen. Another variation included cycling the specimen 50 times within a stress range (specified as a percent of f_{pu}) at a frequency of 2 hertz.

The overall test setup is shown in Figure 2.8a and a drawing of the monostrand PT anchor/wedge system is shown in Figure 2.8b.

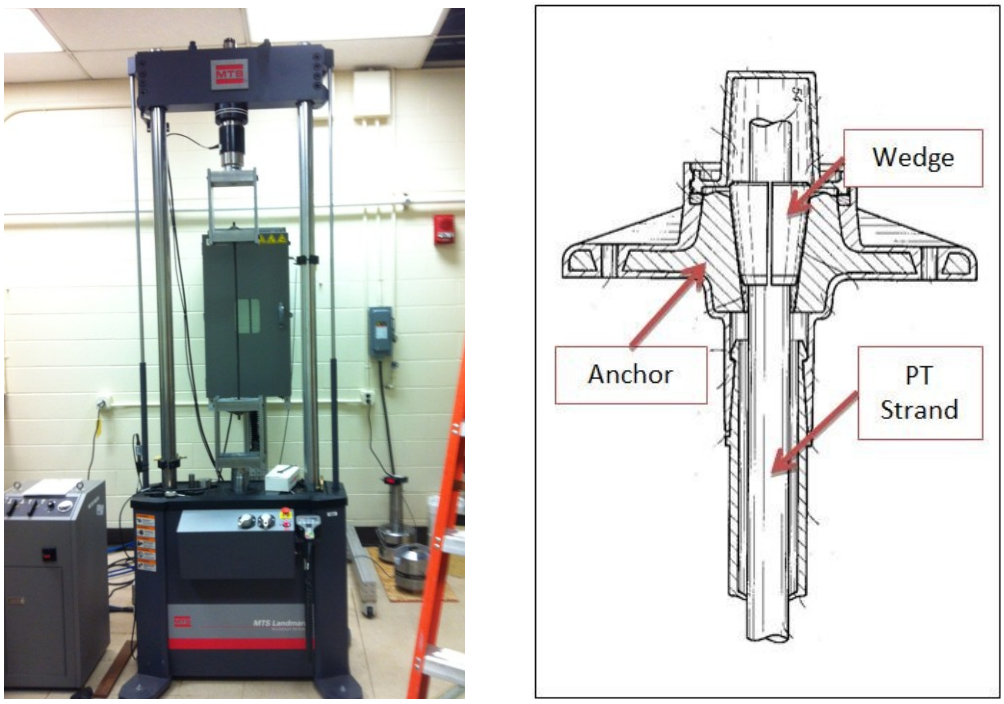

(a) (b)

Figure 2.8: Overall test setup (a) and monostrand cast anchor schematic (b) (Sorkin 1998).

For a number of tests, strain data was collected using a 1-in. extensometer with mixed results. Due to the helical twist of the strand, the extensometer would often shift or twist relative to the strand, rendering all strain readings following this event useless. For this reason, only strength data will be presented in this report, not strain data.

The strength data is presented in terms of fracture stress calculated as the total load recorded by the MTS load cell at the time of wire fracture divided by nominal area of 0.5-in. strand (0.153 in^2). Figure 2.9 shows a summary of the results for the monotonically loaded specimens. Each vertical bar represents an average value, with the maximum and minimum recorded fracture stresses indicated by the upper and lower "whiskers", respectively. The two stress limits are also drawn on each graph. The lower (dashed) line is the ACI 318-08 limit of $0.95f_{pu}$ (256.5 ksi). The upper (dash-dot) line is the ICC-ES (and all others) limit of $0.95f_{pm,free\text{-}length}$ (265.4 ksi). The maximum free-length fracture stress ($f_{pm,free\text{-}length}$) was taken as the breaking strength of the strand as determined by the manufacturer (Appendix A) divided by the nominal cross-sectional area of the strand (Equation 2.1).

$$0.95f_{pm,free-length} = 0.95 * \frac{42.738\ k}{0.153\ in^2} = 265.4\ ksi \qquad (2.1)$$

As shown in Figure 2.9, both monostrand anchor manufacturers exceed the $0.95f_{pu}$ stress limit on average. Additionally, manufacturer 1 exceeded the $0.95f_{pm,free\text{-}length}$ limit in every monotonic test.

A summary of the fracture stress of the cyclically loaded specimens is presented in Figure 2.10. The numbers at the bottom of each grouped data set correspond to the cyclic stress range that the specimen was subjected to, expressed as a percentage of f_{pu} (e.g, "40-90" indicates a cyclic stress range from $0.40f_{pu}$ to $0.90f_{pu}$). All samples tested cyclically exceeded the $0.95f_{pu}$ stress limit. However, for the cyclic tests, manufacturer 1 only exceeds the $0.95f_{pm,free\text{-}length}$ limit occasionally.

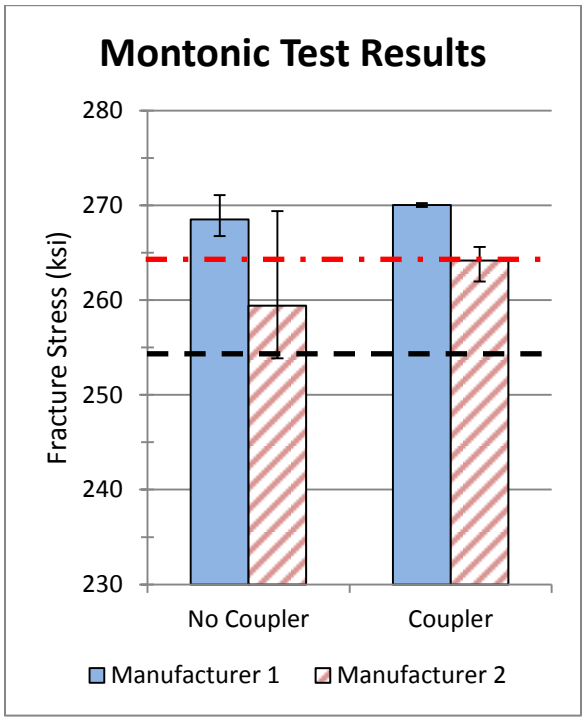

Figure 2.9: Summary of monostrand fracture stress results for monotonically loaded specimens.

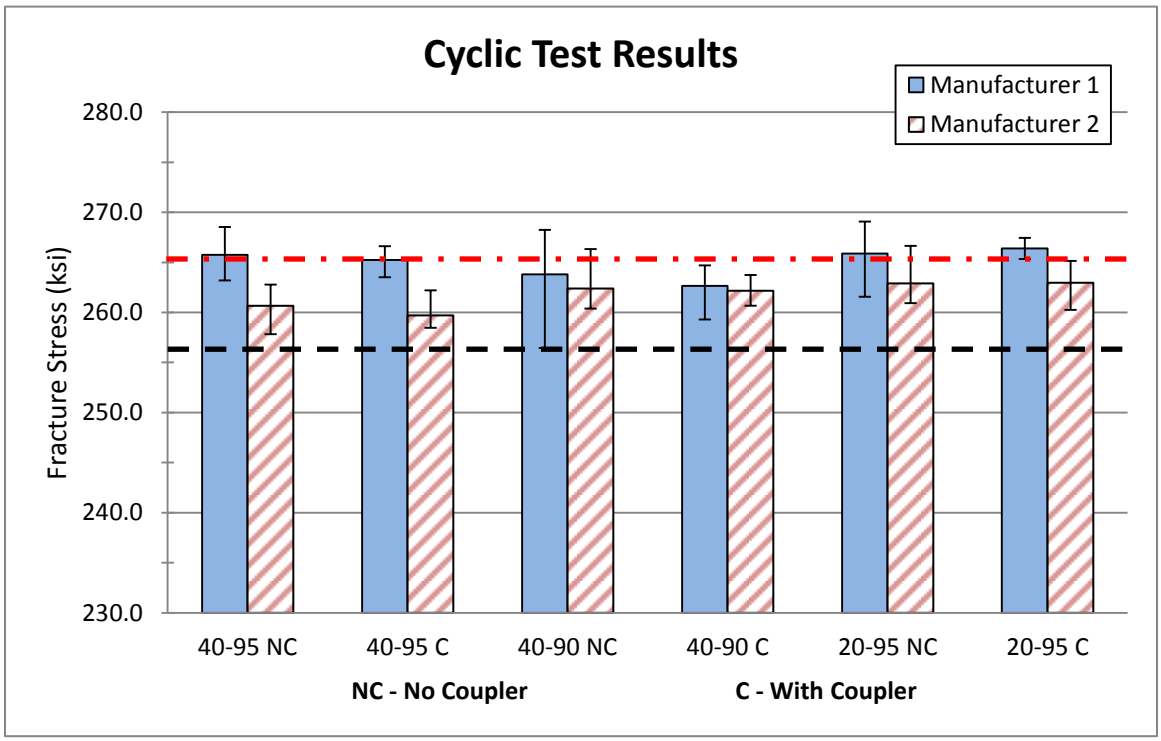

Figure 2.10: Summary of monostrand fracture stress results for cyclically loaded specimens.

Based solely on qualitative analysis of the fracture stress, the following preliminary conclusions were drawn from the monostrand anchorage evaluations:

(1) Manufacturer 1 consistently outperformed manufacturer 2, although anchorages from both manufacturers exceeded the $0.95f_{pu}$ limit on average.

(2) Couplers had no appreciable effect on the performance of the system.

(3) The cyclic loading did not appear to reduce the performance of the system for manufacturer 2, but may have slightly reduced the performance for manufacturer 1.

(4) Varying levels of stress ranges for cyclic loading did not affect the performance of the system.

Additionally, based on the negative results encountered, the use of a 1-inch extensometer is not recommended for measuring post-tensioning strand strain.

CHAPTER 3: TESTING METHODS AND ANALYSIS

3.1 Apparatus

The following sections describe each component of the test specimen, the testing equipment, and the additional components utilized in testing. The test specimen consists of anchorage, strand, and wedge components and is orientated vertically in a 600 kip Material Testing System (MTS) Load Frame and pulled in tension to failure via upward displacement of the top fixture as regulated by the hydraulic cylinder. Figure 3.1 is a schematic drawing of the overall test setup with each of the important elements labeled. Figure 3.2 is a picture of the setup with each element labeled.

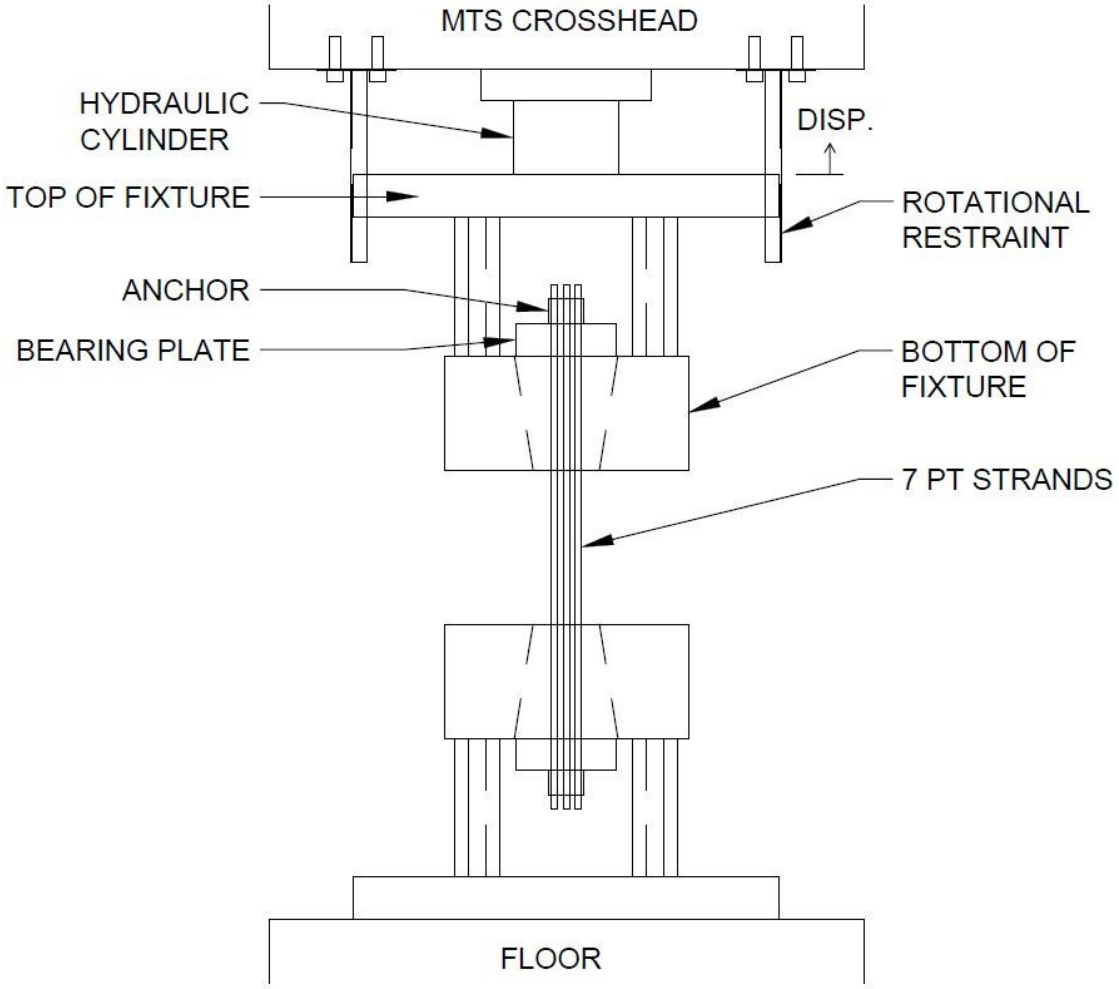

Figure 3.1: Schematic of test setup.

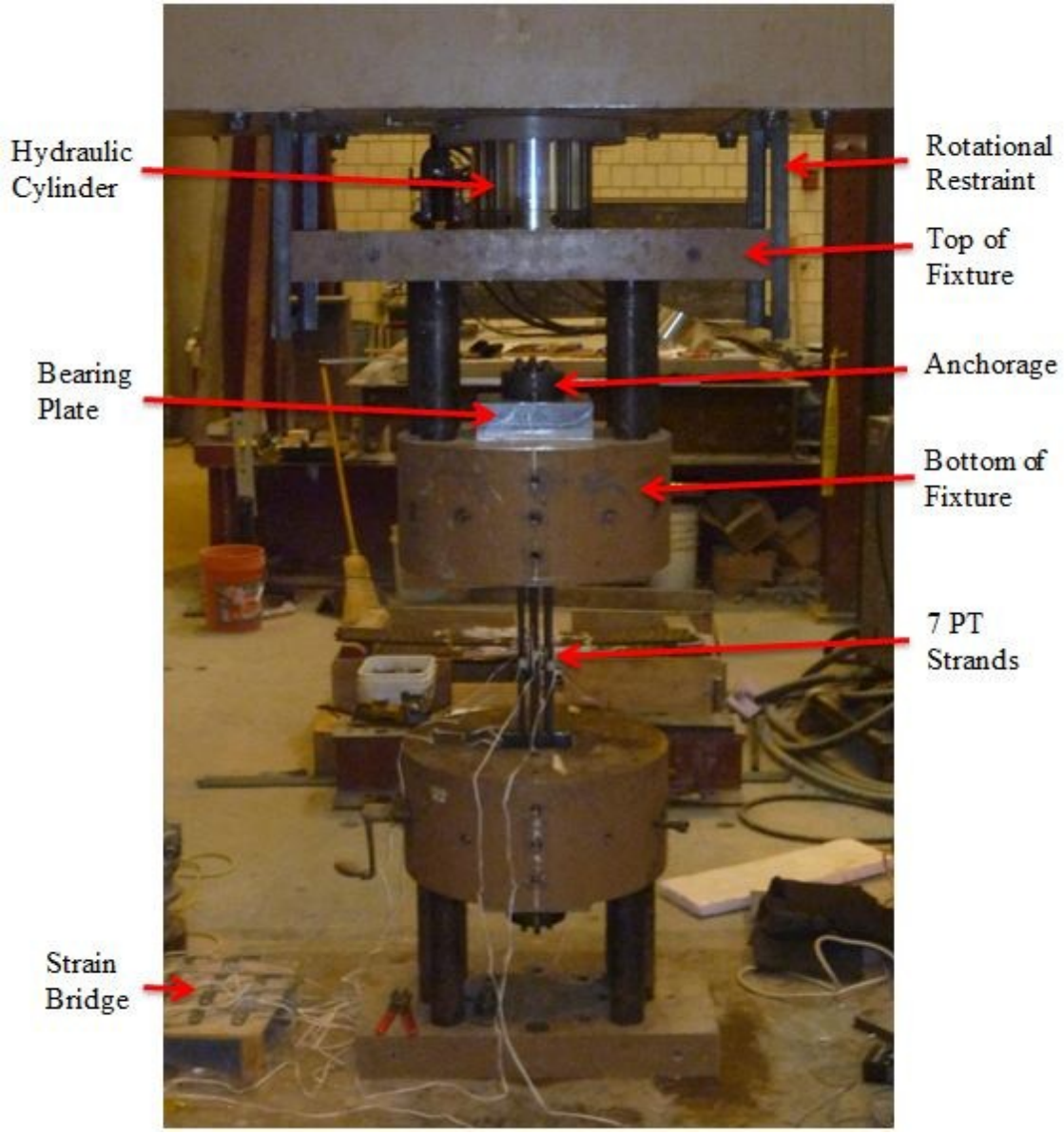

Figure 3.2: Picture of test setup.

3.1.1 Test Specimen

Each test specimen is made up of seven 7-wire PT strands, two wedge plates (i.e., anchorages), and fourteen wedges. Drawings of each component are provided in Figure 3.3. Table 3.1 lists the dimensions of each component taken as the average of the measured value at a minimum of three locations. See Section 3.4.4 for a more detailed discussion of the various wedge geometries used in this testing program. The naming

conventions used for component dimensions are consistent with Walsh and Kurama (2009).

Table 3.1: Measured dimensions of specimen components.

Anchorages				
	H (in.)	**TID (in.)**	**BID (in.)**	**RAD (in.)**
Mfr. A	2.76	1.15	0.70	1.31
Mfr. B	2.16	1.11	0.66	1.38
Wedges				
	H (in.)	**TW (in.)**	**BW (in.)**	**IW (in.)**
2P-A Standard	1.77	1.12	0.71	0.56
3P-B Standard	1.65	0.95	0.59	0.44
2P-A Balanced	1.77	1.12	0.70	0.57
2P-B Balanced	1.66	1.14	0.73	0.57
Seven-wire Strand				
	D_{mw} (in.)	**D_{ow} (in.)**	**d_p (in.)**	**P (in.)**
0.6A	0.205	0.198	0.605	7.9625

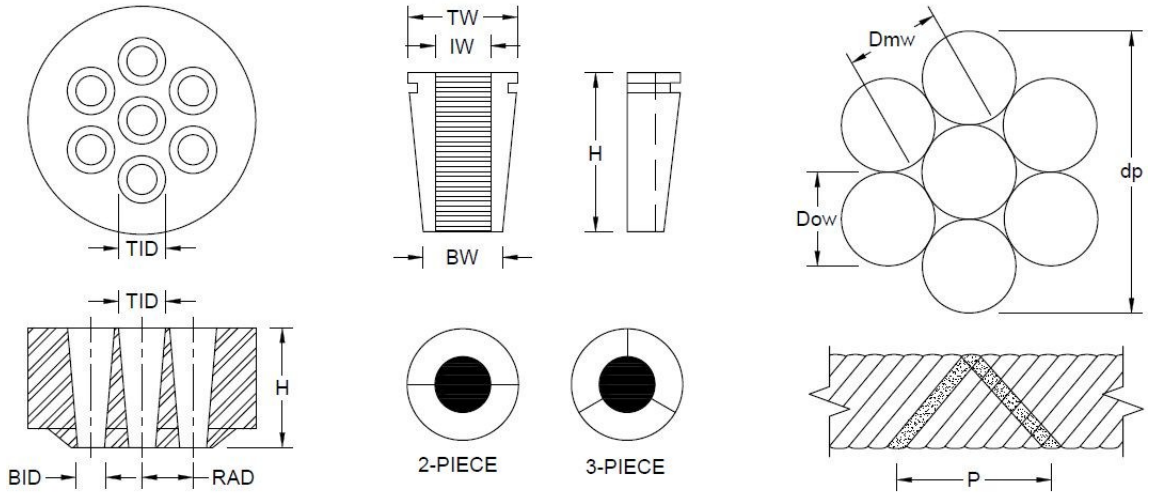

(a) (b) (c)

Figure 3.3: Test specimen components (not to scale): (a) anchorages; (b) wedges; (c) 7-wire strand.

3.1.1.1 Strand

All PT strand came from a single spool and was 0.6-in. diameter, 270 ksi, low-relaxation, uncoated 7-wire steel strand conforming to ASTM A416. Typically, PT strand wires have a surface hardness of about 40-54 Rockwell "C". The strand had an actual breaking strength of 62.393 kips, modulus of elasticity of 28,500 ksi, and cross-sectional area of 0.2227 in^2 as determined by the strand manufacturer and reported on the strand mill certification of inspection (Appendix A). The base material used to produce the strand contained 0.83% carbon and an average ultimate stress capacity of 173.9 ksi. All other chemical and mechanical properties of the base metal are listed in Appendix A.

The strand was cut to approximately 50 inches to ensure a final free-length of at least 42 inches from wedge nose to wedge nose. Actual strand free-lengths varied from 42 to 45 inches due to variability in seating of the wedges and overall anchorage height.

3.1.1.2 Anchorages

Anchorages (labeled as "wedge plate" in Figure 2.2) from two manufacturers were tested. The anchorages are round in nature with six tapered through holes positioned symmetrically around a center tapered through hole. The through holes are shaped to accept conical wedges that grip the strand. Both anchorages were of the same type (i.e., 0.6-in. seven-strand anchorages). Anchorages from manufacturer A were made of cast ductile iron conforming to ASTM A536. Anchorages from manufacturer B were made of forged steel. Both anchorages are components of systems commonly used in the US bridge and building industry.

3.1.1.3 Wedges

Post-tensioning wedges are typically formed by machining, or forging, a single, truncated cone-shaped metal body from a soft steel alloy. A hole is typically drilled in the cone-shaped metal body and the gripping elements are formed inside the hole via threading. Common threads known to be used include so-called "buttress" threads. The exterior surface of each wedge segment is smooth and tapered such that a small diameter exists on one end. The wedge segments are formed such that when applied to the exterior of the strand there is a gap between the circumferential ends of each wedge segment to

enable lateral compression against the strand as the wedge is moved into the receiving bore. Wedges are often heat treated to obtain a surface hardness of about 58-64 Rockwell "C" so that the gripping element of the wedge (threads) can deform the exterior surface of the strand (Hayes and Draginis 2010, a).

In practice, wedges at the dead end (i.e., the end where the prestressing force is not being applied) are typically lightly tapped into place with a cylindrical object. As the prestressing force is applied at the live end and the strand is pulled inward, the wedges also pulled inward causing the wedge pieces to center because of the taper angle. As the tensile load on the strand increases, the normal force of the wedge teeth on the strand increases causing the serrated teeth of the wedge to penetrate the exterior wires of the strand. At the live end, once the stressing operation is complete, the wedges are tapped or hydraulically pressed into place and the strand is released. The restoring force of the strand then enables the same gripping mechanism to ensue at the live end.

In the tests described in this report, the dead end is essentially simulated at both ends. Since the strand is loaded via upward displacement of the top fixture, and not a prestressing jack at one end, there is essentially no "live end". Additionally, the field method of simply tapping the wedges into place to seat them prior to prestressing is conducted in a more repeatable manor as described in Section 3.3.

3.1.2 Testing Equipment

The testing equipment included an MTS Model 311 Material Test Frame with +/- 600 kip capacity and +/- 3-in. stroke. *MTS FlexTest* software was used to program the loading schematics. The in-house data acquisition (DAQ) system used is based on the National Instruments SCXI high performance data acquisition solution. The system is capable of simultaneous sampling of 96 voltage channels at +/- 10 volts and 128 channels of quarter bride 120 ohm strain gage input. Separate *Northern Digital Inc. (NDI) First Principles HD – Dynamic Tracking Software* was also implemented for two trials to collect strain data. This system is discussed in further detail in Section 3.2.2. Data from the separate NDI DAQ system was later synchronized with the in-house DAQ system based on correlated crosshead displacement data as described in Section 3.5.2.2.

3.1.3 Additional Components

A few additional components were necessary to effectively replicate the field PT system as accurately as possible. Bearing plates were installed on the top and bottom MTS fixtures to provide a uniform surface for the wedge plates to bear against (Figure 3.2). The bearing plates essentially acted as the bearing anchor would in a field application (Figure 2.2). The bearing plates were designed to be compatible with anchorages from both manufacturers. They provided a uniform bearing surface similar to that which would be provided by an actual bearing anchor. Additionally, the bearing plates allowed all seven strands to pass freely through a center through hole while centering each wedge plate to avoid any unwanted eccentric loading.

A rotational restraint was installed on the top of the MTS machine to prevent the top MTS fixture from rotating during loading of the test specimen, while allowing the fixture to move freely in the vertical direction (Figure 3.2). The bottom MTS fixture was incapable of rotating because it was fixed to the lab floor.

Additional equipment was also required to complete the hand seating procedure described in Section 3.3. A 15 kip Omegadyne, Inc. load cell (model LC401-15K) and an SPX Power Team 5 ton Sidewinder Mini Jack were used in conjunction with a short pipe section to initially seat the wedges (Figure 3.7).

3.2 Instrumentation

The MTS DAQ system provided elapsed time in seconds, total load in kips, crosshead displacement in inches, and strain gage readings in microstrain. The load data from the internal MTS load cell was important for determining the stress capacity of the system as described in Section 3.5.1. However, it should be noted that the load reading was a total for the entire system (i.e., the load on each individual strand was not recorded). Due to the ductile nature of the strand and the continuation of loading beyond its yield point, the strain data is generally more meaningful than the load data from an analysis standpoint. Additionally, the individual strain of each strand was recorded which allowed for a better understanding of how load is distributed through the system. For that reason, more emphasis is placed on strain data instrumentation and analysis.

3.2.1 Strain Gages

The primary method of collecting strain data was with electrical resistance strain gages fixed to an individual wire of each of the seven strands (i.e., seven strain gages per specimen). While previous research has demonstrated that using only a single strain gage per 7-wire strand is acceptable (Acosta 1991), considerable variation in strain can still exist amongst strands in a multistrand system. The strain instrumentation required by the International Code Council Evaluation Service "Acceptance Criteria for Post-Tensioning Anchorages and Couplers of Prestressed Concrete" (ICC-ES 2007) is a 36-in. extensometer. However, previous research has demonstrated that in the case of unbonded PT strands, extensometer gage length does not appreciably affect the strain measurements (Walsh and Kurama 2009). Additionally, strain gages have been investigated as an instrumentation system for PT segmental box girder bridges with positive results (Acosta 1991). Monostrand testing conducted as a separate experiment of this project (see Section 2.4) at the University of Minnesota Duluth indicated that extensometers with short gage lengths tend to twist during testing because of the helical twist of the strand. The cost of instrumenting all seven strands with extensometers would have also been prohibitive.

Three different strain gage types were used due to the limited availability of pre-wired strain gages that are small enough to fit on an individual strand wire. All strain gages used were from the manufacturer Omega Engineering, Inc. There was no difference in strain data quality or accuracy observed amongst the different strain gage types. The three strain gage types used are summarized in Table 3.2.

Table 3.2: Electrical resistance strain gage properties.

Type	Gage Factor	Gage Length (mm)	Gage Resistance (ohms)	Number of Lead Wires
KFG-1N-120-C1-11L3M3R	2.10	1	120	3
KFG-2N-120-C1-11L3M3R	2.09	2	120	3
KFG-2N-120-C1-11L1M2R	2.09	2	120	2

Strain gage locations varied depending on whether both anchorages were aligned so that the strands were vertically parallel or if one anchor head was rotated causing the strands to touch at the mid-height of the specimen. When the anchorages were aligned, the strain gages were located at the mid-height of the specimen. Although the assumption has already been stated that the local strain along the length of the strand is constant, strain gages were placed at mid-height for consistency and to avoid damaging the strain gages during installation and seating of the strands. When one anchorage was rotated, the strain gages were located 9.5-in. above the mid-height of the specimen. This was done to avoid damaging the strain gages when the strands rubbed together. Figure 3.4 shows the vertical location of strain gages on the strands.

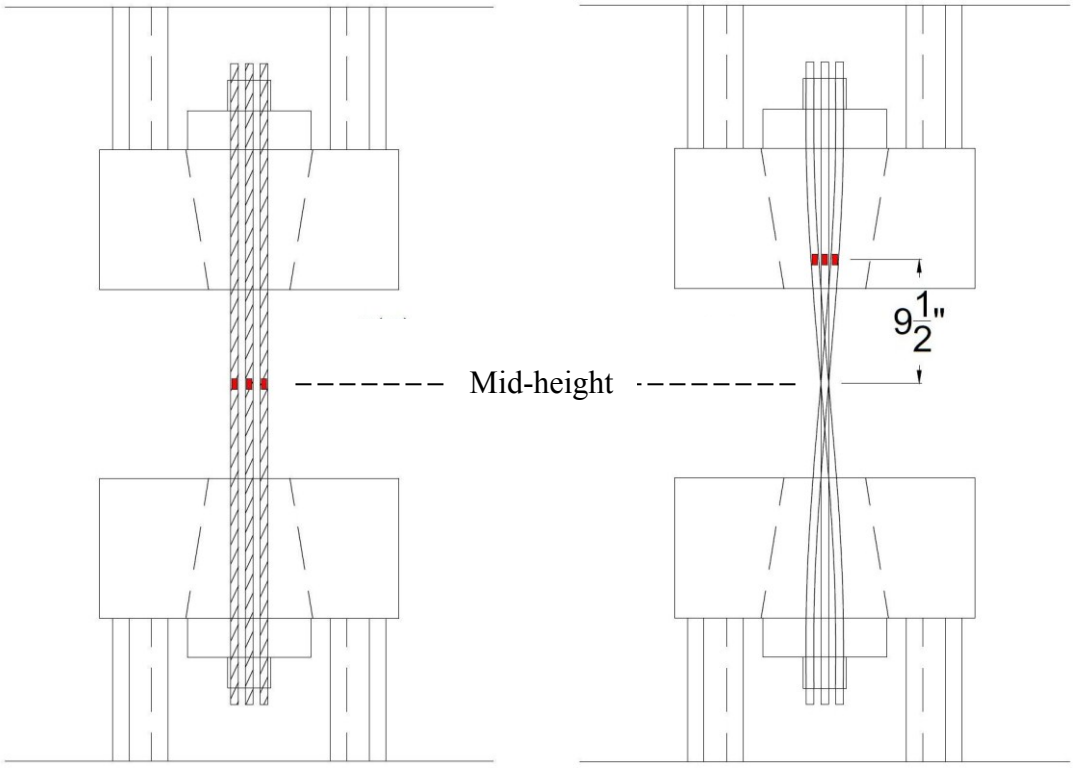

Figure 3.4: Elevation view of strain gage locations for: (a) aligned and (b) rotated anchorages.

3.2.2 NDI Optical Tracking

An *OPTOTRAK Certus HD Dynamic Measuring Machine* was implemented as an alternative method of measuring strain. The *Certus HD Position Sensor* uses high-speed, real-time digital photogrammetry and optical triangulation techniques to track the precise three-dimensional (3D) position of markers. Strain can then be calculated based on the change in the distance between markers divided by the initial distance between markers as described in Section 3.5.2.2. This alternative method of strain measurement was implemented for a select number of trials to verify the strain data collected by strain gages and to test the usefulness of optical strain measurement on PT strands. Note that the NDI strain measurement did not replace the strain gages for these select trials; rather the two methods were used simultaneously so that the data could be compared.

Four NDI markers, spaced at 2 inches, were fixed on three or four strands per test for rotated or aligned anchorages, respectively. The markers were placed surrounding the strain gages so that the local strain in that region could be effectively compared. The NDI system measures the elongation of the strand as compared to the strain gages which record the elongation of an individual wire. By using both methods to collect strain data simultaneously, the relationship between the measurements can be better understood.

Figure 3.5a is a picture of several NDI markers fixed to four strands and the top and bottom MTS fixtures for an aligned anchorage test. Figure 3.5b shows the NDI DAQ system's visual output of marker locations for the same test.

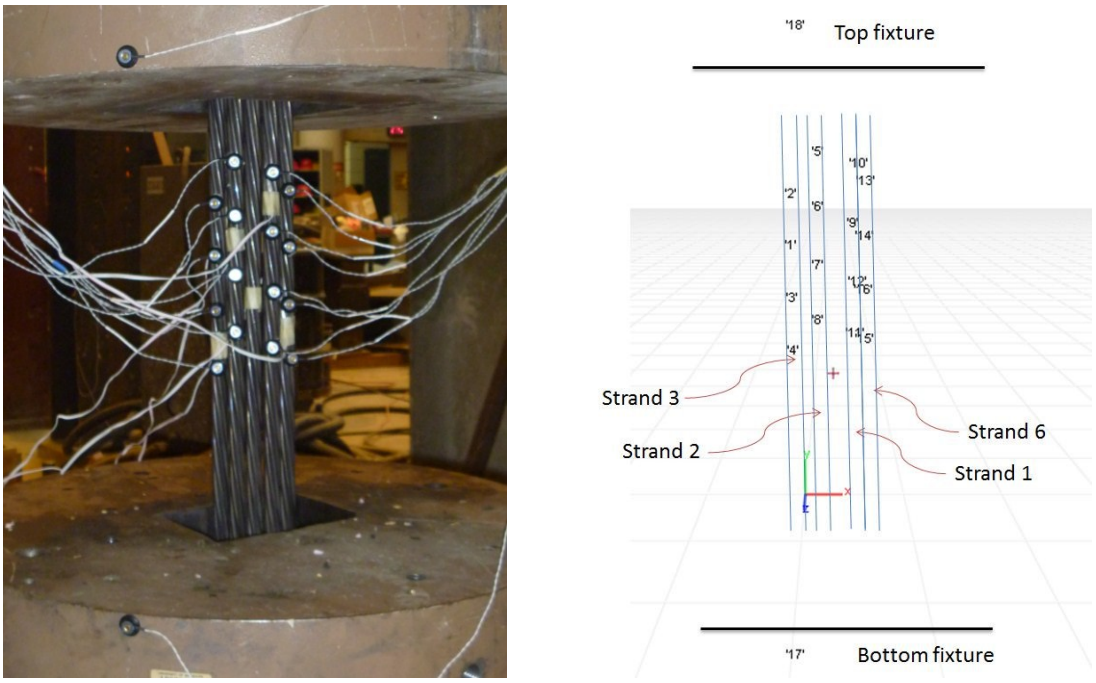

(a) (b)

Figure 3.5: NDI optical tracking markers fixed to strands and MTS fixtures.

3.3 Methodology

The testing procedure was broken into two primary phases: (1) strand preparation and installation and (2) specimen loading. This section describes the first phase in detail. The second phase, which varies depending on the loading scheme of the test, is described in Section 3.4.1.

First, one strain gage was attached to each strand on an individual exterior wire (see *Procedure for Application of Strain Gages* in 0). For tests with aligned anchors, strain gages were attached at the mid-height of the strand. For tests with a rotated anchor head, strain gages were attached at 9.5-in. above the mid-height of the strand. The strain gages were attached prior to installing the strands in the MTS frame to allow for ample curing time of the strain gage adhesive without delaying testing. Each anchor head was also marked with soapstone along the axis of 0^o rotation as well as the axis of 135^o rotation for the rotated anchor tests (Figure 3.6). This ensured easy alignment between the top and bottom anchorages when installing the strands in the MTS load frame.

Figure 3.6: Alignment marks on anchorage head.

With the top anchorage resting on the top bearing plate, seven strands were fed vertically through the top anchorage and one wedge per strand was lightly pressed on, leaving approximately 1.25-in. of strand overhang. The MTS crosshead was then raised and each strand was fed through the bottom anchorage, ensuring proper alignment of each strand with the top anchorage. Again, one wedge per strand was lightly pressed on to hold that bottom anchor in place. A minimum strand overhang of 1.25-in. was left. However, for the bottom wedges, greater emphasis was placed on ensuring that each wedge was at the same elevation. The wedges are kept at the same elevation during seating to ensure that each strand will be loaded as evenly as possible during testing. If the test configuration called for a rotated anchor head, rotation of the bottom anchorage took place at this time.

Next, an initial hand seating of force of 800 lbs. was applied directly to the top and bottom wedges using a low profile hydraulic hand jack, a small load cell, and a pipe section (Figure 3.7). A force of 800 lbs. was chosen based on the ICC-ES AC303 test methods requirement that the applied preload (seating load) not exceed 1000 pounds (for a monostrand system). The hand seating procedure was implemented to ensure consistent wedge seating depths and forces with the goal of loading each of the seven strands as evenly as possible. This initial hand seating procedure emulates the dead end seating procedure in field applications, only it is done in a more repeatable manner.

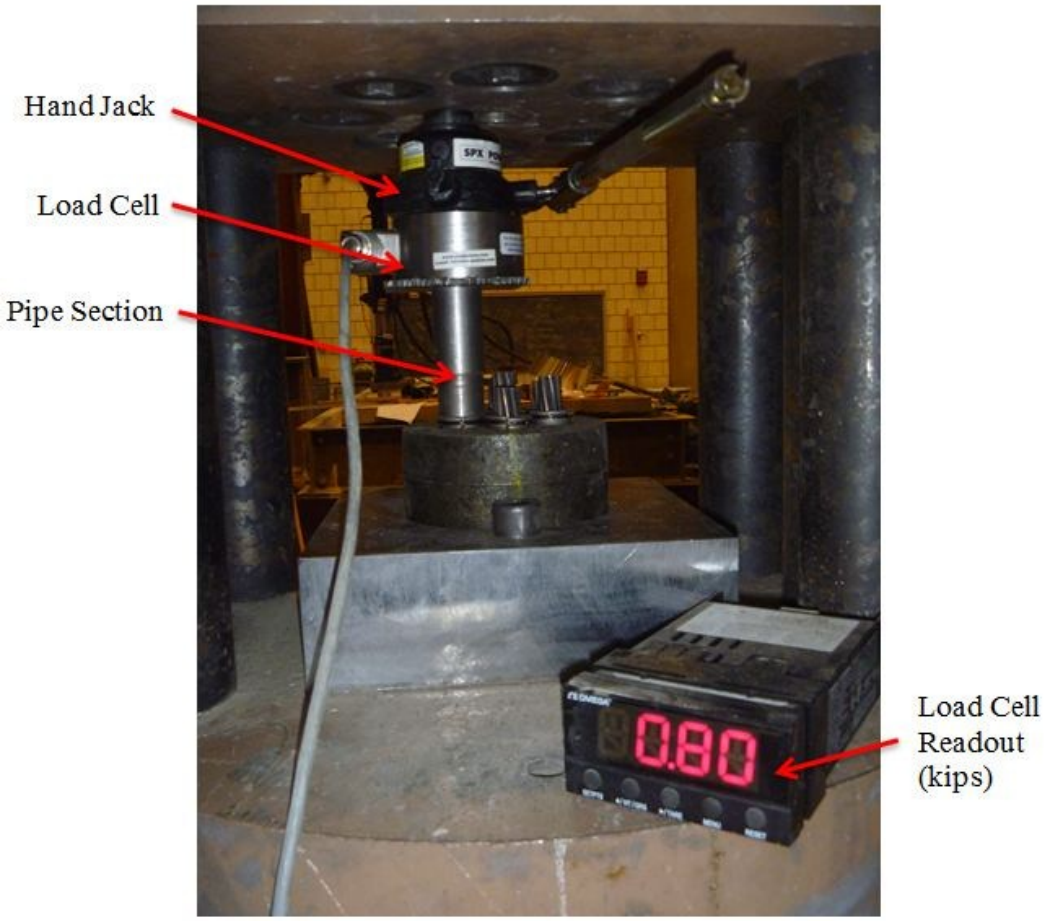

Figure 3.7: Hand seating apparatus.

Strain gage lead wires were then attached to the strain bridge and NDI markers were attached to visible strands, if applicable. A pre-load between 5 and 7 kips was then applied to further seat the wedges and take up any remaining slack in the system. This level of preload was again based on the ICC-ES AC303 requirement that the preload (per strand) not exceed 1000 pounds. The initial specimen length was measured, the anchorage ends protected to prevent flying objects, and offsets taken for strain and displacement. The specimen was then ready to be loaded per the appropriate loading scheme as described in Section 3.4.1.

3.4 Testing Configurations

Thirty-six specimens were tested in twelve unique configurations. The four variables investigated include: (1) loading scheme; (2) anchorage manufacturer; (3) anchorage alignment; and (4) wedge geometry. Table 3.3 contains a summary of the testing configurations.

Table 3.3: Testing configurations summary.

Loading Scheme	Manufacturer	Alignment	Wedge Type	Repetitions
Monotonic	A	Aligned	2P-A Standard	3
		Rotated		3
	A	Aligned	2P-A Balanced	3
		Rotated		3
	B	Aligned	3P-B Standard	3
			3P-B Balanced	3
Cyclic	A	Aligned	2P-A Standard	3
		Rotated		3
	A	Aligned	2P-A Balanced	3
		Rotated		3
	B	Aligned	3P-B Standard	3
			3P-B Balanced	3
TOTAL MULTISTRAND TESTS CONDUCTED				**36**

3.4.1 Loading Scheme

Monotonic and cyclic loading schemes were investigated. Monotonic tests were conducted to set a baseline for multistrand anchorage performance. Cyclic tests were conducted to study the behavior of the PT system under high-range, low-cycle loads. The cyclic loading scheme was intended to replicate the type of loading that the PT system may experience in a rocking wall structure during a seismic event, although the loading

frequency was considerably slower than desired due to limitations of the testing equipment.

The monotonic and cyclic loading schemes were based on the ICC-ES document discussed in Section 3.2.1. The testing procedures and requirements presented in the ICC-ES document are specifically for monostrand assemblages. No such document exists for the testing of multistrand assemblages. Thus, the monostrand guidelines in the ICC-ES document were applied as closely as possible to the multistrand tests discussed in this report.

The monotonic loading protocol consisted of a constant, displacement-controlled load rate of 0.361 in./min., which corresponds to a strain rate of 0.0086 in./in./min. for a 42-in. specimen. The ICC-ES document requires a displacement rate between 0.197 and 0.887 in./min., which corresponds to a strain rate of 0.0047 to 0.021 in./in./min. for a 42-in. specimen. The loading occurred via upward displacement of the top fixture as regulated by the hydraulic cylinder. The bottom anchor remained stationary.

The cyclic loading protocol consisted of three parts: (1) ramp to lower bound; (2) sinusoidal cyclic loading; and (3) ramp to failure.

The ramp to lower bound step was intended to replicate the monotonic load rate of 0.361 in/min for stresses from zero to $0.20f_{pu}$. However, due to limitations of the testing software, this loading step was force-controlled rather than displacement-controlled. This led to crosshead displacement rates as high as 8.0 in/min for portions of the ramp to lower bound step while the wedges were seating. Although the desired load rate was exceeded, the strands were still loaded in a static manner. Additionally, the loading was within the ICC-ES guidelines as no maximum rate is specified for the ramp to lower bound step and 8.0 in/min is slower than the load rate implemented during the cyclic loading step.

The specimen was then cycled 50 times from $0.20f_{pu}$ to $0.85f_{pu}$ at 0.1 hertz. Several deviations from the ICC-ES document were required for this loading step due to limitations of the testing equipment and the anchorage capacities. The ICC-ES document calls for a cycle frequency between 1 and 3 hertz and a cyclic stress range between

$0.40f_{pu}$ and $0.85f_{pu}$. However, monostrand test results (Section 2.4) showed that a cyclic range of $0.40f_{pu}$ to $0.85f_{pu}$ was not large enough to cause any significant reduction in capacity of the system. Thus, the lower limit of the cyclic range was reduced to $0.20f_{pu}$. Monostrand test results also indicated that an upper cyclic range of $0.85f_{pu}$ was not high enough to affect the system's performance or observe the type of post-yield behavior desired. However, preliminary monotonic multistrand test results showed ultimate capacities as low as $0.88f_{pu}$. To avoid wire fractures during cycles, the upper cyclic range was kept at the ICC-ES recommended value of $0.85f_{pu}$. Finally, a cycle frequency of 0.1 hertz was the maximum that could be achieved by the MTS frame under such a large load range.

Upon completion of 50 cycles, the specimen was pulled to failure at a constant, displacement-controlled load rate of 0.361 in./min, which is consistent with the static tests.

3.4.2 Anchorage Manufacturer

Two anchorage manufactures were investigated. The anchorages tested were all of the same type (i.e., 0.6-in. seven-strand anchorages). The anchorage type was chosen based on materials that will likely be implemented in the PreWEC rocking wall system. The two anchorage manufacturers tested are well known and commonly used in the PT industry. Two manufacturers were tested to determine if the system's performance is dependent on manufacturer. The anchorage materials and dimensions differed only slightly amongst manufacturers as described in Section 3.1.1.2.

3.4.3 Anchorage Alignment

Even in a straight tendon, strands will tend to twist along the length between the dead and live end anchorages. This rotation can have an effect on the behavior of the tendon under large deformations and has the potential to reduce the failure load of the tendon. Additionally, strands will tend to rub against one another over the length of the tendon when twist occurs, which may also reduce the performance of the system. Therefore, several trials included a 135^{o} rotation of one anchor head to test the system under eccentric loading conditions, cause the strands to enter the anchorages at an angle,

and to cause the strands to rub together at mid-height. This degree of rotation results in an equivalent strand eccentricity of approximately 6% for the six outside strands, which is likely far greater than what would be expected in an actual system in terms of drift and twist. However, this conservative value was used because it is the degree of rotation required to cause the 42-in. strands to rub against one another at mid-height.

3.4.4 Wedge Geometry

Four different wedge geometries, all produced (but not necessarily designed) by the wedge manufacturer Hayes Specialty Machining, Ltd., were tested. Two-piece wedges are differentiated from three-piece wedges by the naming convention of 2P and 3P, respectively. The four wedge geometries varied as follows:

- 2P-A Standard: 2-piece wedges for anchorage A as designed by manufacturer A.
- 3P-B Standard: 3-piece wedges for anchorage B as designed by manufacturer B.
- 2P-A Modified: 2-piece wedges for anchorage A as designed by the wedge manufacturer Hayes Industries to more evenly balance the stresses within the wedge during peak loading.
- 2P-B Modified: 2-piece wedges for anchorage B as designed by the wedge manufacturer Hayes Industries to more evenly balance the stresses within the wedge during peak loading.

The performance of 2-piece wedges was not compared directly to the performance of 3-piece wedges in this study. Rather, the number of wedge pieces was simply determined by whoever provided the wedges. For the wedges denoted by the name “standard”, the anchorage manufacturer provided wedges just as they would to a contractor in a field application (i.e., wedges were not specified when ordering anchorages). Thus, the shift from 2-piece to 3-piece standard wedges from manufacturer A to manufacturer B was simply the product of differences in the wedge geometry preferred and designed by each respective manufacturer. For the wedges denoted by the name “modified”, the wedge manufacturer Hayes Specialty Machining, Ltd. designed the

wedges based on the dimensions of each anchorage. Hayes always designs its modified wedges as 2-piece wedges because of the added quality control complications introduced with producing 3-piece wedges. Hayes believes that the principles introduced through their modified wedges are applicable as either a 2-piece or 3-piece wedge system, but choses to implement a 2-piece wedge system because of the tighter tolerance levels to which they can be machined. Additionally, 3-piece wedges are more expensive to manufacture.

The physical change in wedge geometry that allows a more balanced load along the gripped length of strand is the product of two primary principles implemented by the wedge manufacturer Hayes Specialty Machining, Ltd. Used in conjunction, these two principles can provide a wedge system close to that of a "pure" wedge system in which failure occurs along the free length of the strand rather than within the anchorage at the nose of the wedge. Although all of the specimens in the tests described in this report failed due to wire fractures within the anchorage (for both wedge types), the modified wedge geometry often allowed the system to exceed the ultimate design strength of the strand (f_{pu}) as well as meet the strain certification requirement of 2.0% elongation at ultimate. It should also be noted that this significant increase in performance is achieved without any substantial changes to the wedge manufacturing process or base material and is compatible with anchorages currently used in the industry.

3.4.4.1 Principle of Angle Differential

The first principle is referred to by Hayes as "angle differential" (Patent No. US 7,765,752 B2). This principle was previously introduced and patented for fiber reinforced plastic (FRP) tendons (Shrive, et al. 2000); however several differences exist between the Shrive and Hayes wedge systems. Most notably, the system patented by Shrive introduced a sleeve element to protect the exterior FRP tendon surface. It also substantially increased the wedge length and, therefore, required changes to the dimensions of the anchorage systems they are used in conjunction with. Alternatively, the wedge system developed by Hayes has a geometry that is compatible with anchorage

systems currently being used in the PT industry and does not require additional elements or an increased wedge length.

The wedges denoted by the name "standard" have a geometry in which the taper angle of the exterior surface of the wedge matches the taper angle of the wedge receiving bore and both are approximately 7 degrees (Figure 3.8a). This type of wedge geometry, which is the current industry standard, forces all of the wedge teeth to engage on the strand simultaneously when loading begins. Once the entire wedge length has engaged, elongation of the strand within the anchorage is significantly restrained. Thus, the load along the length of the wedge is concentrated at the nose. This so-called "elongation nose loading" begins early in the loading and propagates as loading continues. Eventually, this stress concentration causes the shear failure of an individual wire within the anchorage at the nose of the wedge.

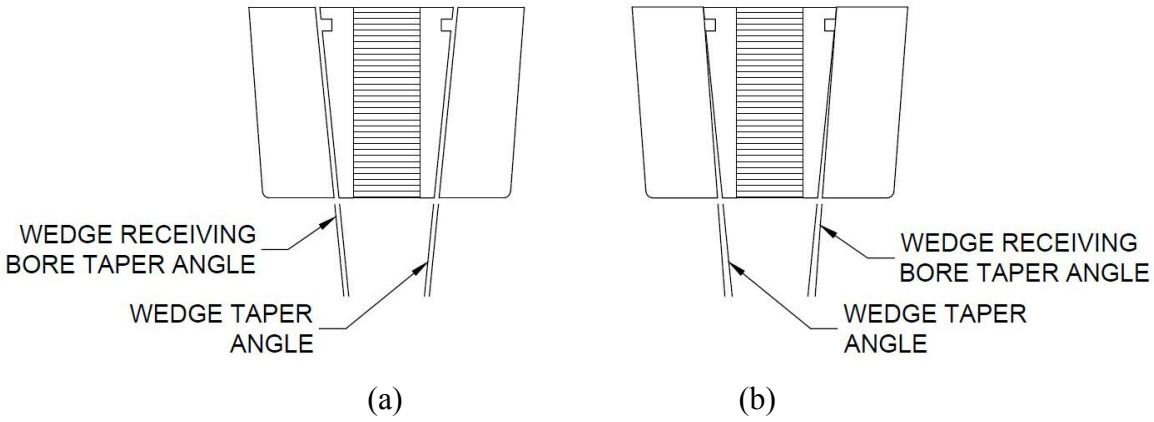

Figure 3.8: (a) Matched angle (standard) wedge geometry; (b) angle differential (modified) wedge geometry.

Alternatively, the wedges denoted by the name "modified" have an exterior surface taper angle that is 1 to 2 degrees greater than that of the wedge receiving bore (Figure 3.8b). This angle differential allows the wedge to grip the strand sequentially from the "back" or wide end of the wedge to the "nose" or narrow end of the wedge as load increases. This fundamental change in the engagement of wedge teeth allows elongation of the strand to occur within the wedge throughout loading and up to failure. As a result, the normal force on the strand along the length of the wedge is more balanced

as the load approaches the actual free-length breaking strength of the strand. Figure 3.9 shows the difference in load distribution on the strand along the length of the wedge due to the angle differential.

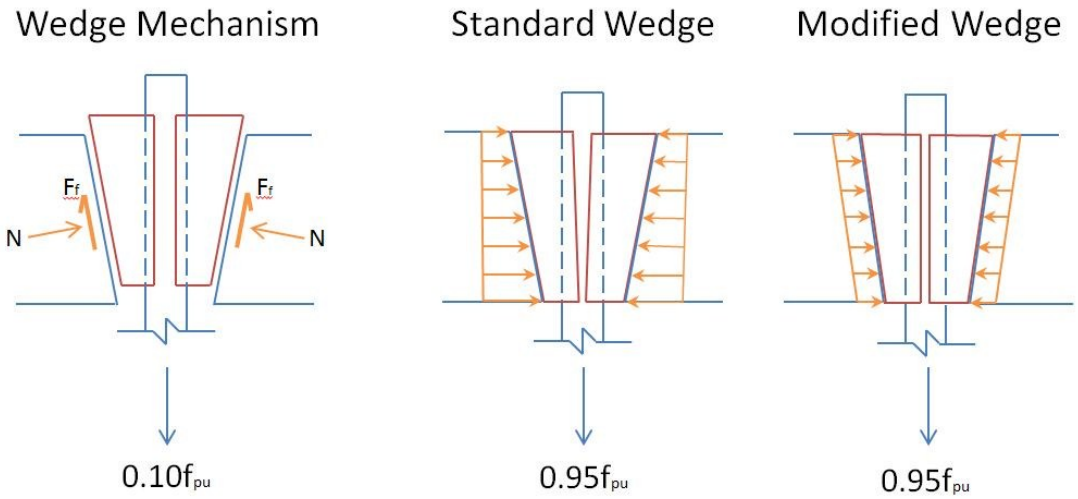

Figure 3.9: Load distribution within wedge due to angle differential principle.

The angle differential principle is further illustrated by the cracking patterns of wedge pieces that have been used in retaining a strand loaded to failure. Figure 3.10 shows characteristic cracking patterns of (a) standard and (b) modified wedge pieces. The single horizontal crack near the top of the standard wedge pieces (Figure 3.10a) indicates a tensile rupture type failure of the wedge as it is pulled apart by the strand. This is due to all of the wedge teeth engaging simultaneously early in the loading, which forces elongation of the strand within the wedge pieces to deform and crack the wedge pieces. Alternatively, the distributed, spider web cracking along the length of the modified wedge pieces (Figure 3.10b) indicates a flexural type failure as the wedge pieces are forced to flex from the back to the nose to match the angle of the receiving bore as load increases.

(a) (b)

Figure 3.10: Cracking pattern after retaining strand loaded to failure of (a) standard and (b) modified wedge pieces.

3.4.4.2 Principle of Gap Control

The second principle of the modified wedge geometry is referred to by Hayes as "gap control" (Patent No. US 7,726,082 B2). When wedges are placed around the strand prior to loading, an initial (uncompressed) gap exists between wedge pieces. The uncompressed gap is defined as the gap that exists when the wedge segments are applied to the exterior of the tendon without force sufficient to substantially deform the metal of the exterior surface of the strand. In some instances, the radius of curvature of the wedge segments at the inner surface of the threads may be slightly smaller than the exterior of the strand. Therefore, some metal deformation may take place in such cases when the wedge segments are applied to the tendon prior to lateral compression into the wedge plate, but the condition still fits the description of "substantially no deformation" of the surface of the tendon (Hayes and Draginis 2010, b).

As the prestressing force increases, the wedge pieces compress laterally, closing this initial gap. If the gap between wedge pieces is allowed to close completely, the wedges are no longer be able to move inward and grip the strand as load increases. This

leaves the system potentially susceptible to a "pull-out" failure in which the gripping force of the wedge is no longer sufficient to restrain the tensile force of the strand.

The wedges denoted by the name "standard" have a geometry in which the wedge pieces will remain in "free float" (i.e., will never come in contact) throughout the loading sequence (Figure 3.11a). Depending on how symmetrically the individual wedge segments are positioned about the exterior of the strand, the gaps between the wedge segments may be equal in size, or may be unequal in size. However, wedge segments made according to methods and dimensions currently used in the industry (i.e., the "standard" wedge geometry) will provide a total gap (the sum of all the individual gaps between circumferential ends of all the wedge segments) which is greater than the total expected amount of diameter reduction (lateral compression) of the wedge due to the gripping elements (treads) penetrating the exterior surface of the strands. As an example, for a typical 0.5-in. wedge with a thread depth of 0.021 inches, it would be expected that the wedge would be reduced in diameter by at least 0.042 inches (two times the thread depth) from an uncompressed state to fully laterally compressed state when pulled into the wedge receiving bore. In this case, the wedges are cut or formed so that in the uncompressed state a total gap of at least 0.063 inches (three times the thread depth) is provided (Hayes and Draginis 2010, b).

Alternatively, Hayes has determined experimentally that allowing the wedge pieces to come into contact, with reasonable limitation, is actually beneficial to the operation of the anchor system overall. The wedges denoted by the name "modified" are manufactured to have a smaller uncompressed gap between wedge pieces. The axial motion of the wedge is limited such that the lateral compression is in a range of about 0.24 to 2.4 (most preferably 0.40 to 1.8) times the height of the gripping elements. Using the previous example of a 0.5-in. wedge with a thread depth of 0.021 inches, the total maximum uncompressed gap would be about 0.050 inches (Hayes and Draginis 2010, b).

When this smaller initial gap is implemented, the centering movement of the wedges is stopped late in the loading sequence due to the wedge pieces coming into

contact. This allows the wedges to penetrate the exterior strand wires only enough to avoid a pull-out failure without "over-penetrating" the strand (Figure 3.11b).

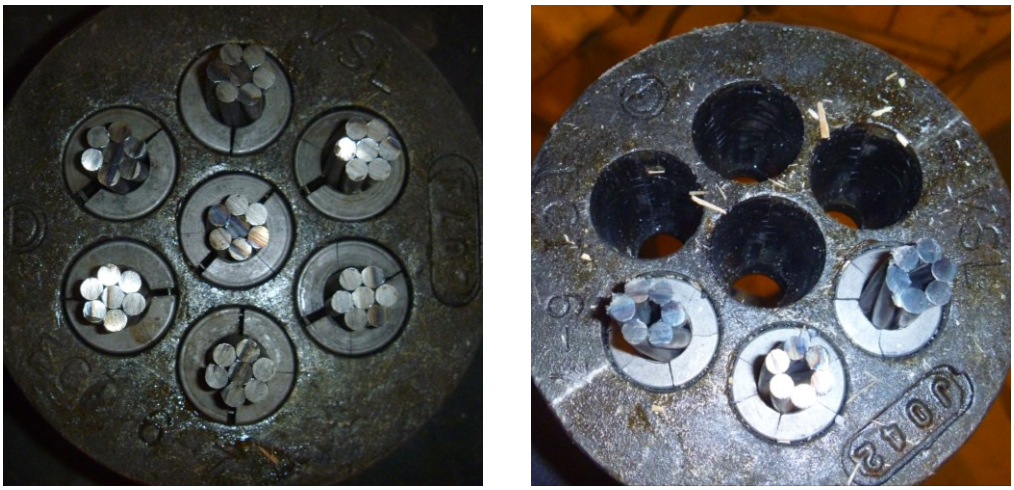

(a) (b)

Figure 3.11: Gap between (a) standard and (b) modified wedge pieces after being loaded to failure.

3.5 Analysis

The following sections describe the data reduction methods for stress capacity, strain capacity, and modulus of elasticity determination. As discussed in Section 3.2, more emphasis is placed on the analysis of the strain capacities of the system due to the large change in strain that occurs for a small change in stress after yielding. Additionally, strain in each individual strand was recorded via strain gages whereas load data was recorded as a total of the system as a whole. Therefore, more information about the distribution of load amongst strands can be derived from the strain data.

In a multistrand system, individual strands can be subjected to considerably different levels of load and elongation depending on the initial distance between wedges on a strand and any slack that exists after the preload is applied. To ensure that the hand seating method implemented (described in Section 3.3) did not negatively affect the performance of the system (i.e., that one strand was not initially loaded substantially more or less than the rest), a maximum strain differential limit of 2000 microstrain was adopted for loads less than $0.80f_{pu}$. If an absolute strain differential greater than 2000

microstrain existed at any point in the loading up to $0.80f_{pu}$, the test was discarded and repeated. The 2000 microstrain limit was selected experimentally based on test data including tests not discussed in this report which implemented an insufficient hand seating procedure that resulted in strain differentials greater than 2000 microstrain at loads less than $0.80f_{pu}$. It should be noted that once strands begin to yield, a considerable amount of strain differential is introduced. While this phenomenon is not investigated in detail in this report, it is likely the primary contributing factor in causing the fracture of an individual wire at a load less than the ultimate load. Differentiation between fracture and ultimate stress and strain are described in detail in their respective sections.

3.5.1 Stress Capacity

The stress capacity of each specimen was derived from MTS load cell data. The data acquisition system provided the total load, in kips, of the system. The load was then divided by the effective cross-sectional area of the 0.6-in. 7-strand system (i.e., 0.217 in^2 * 7 = 1.519 in^2).

As discussed in Section 3.5, an individual wire of a strand would occasionally fracture at a stress level lower than the ultimate stress achieved by the system (Figure 3.12). Therefore, two stress values are reported: (1) fracture stress, and (2) ultimate stress. The fracture stress is the stress of the specimen at the time of initial wire fracture. The ultimate stress is the maximum stress that the specimen achieves. Consequently, the facture stress may be equivalent to the ultimate stress if the initial fracture stress is the maximum stress that the specimen achieves, or the ultimate stress may exceed the fracture stress if the system achieves a higher stress level after initial fracture.

Additionally, in accordance with the ICC-ES document discussed in Section 3.2.1, the yield stress of each specimen is reported in Appendix C. The yield stress is defined as the stress corresponding to a strain of 1.0% as determined by the maximum of individual strain gage readings.

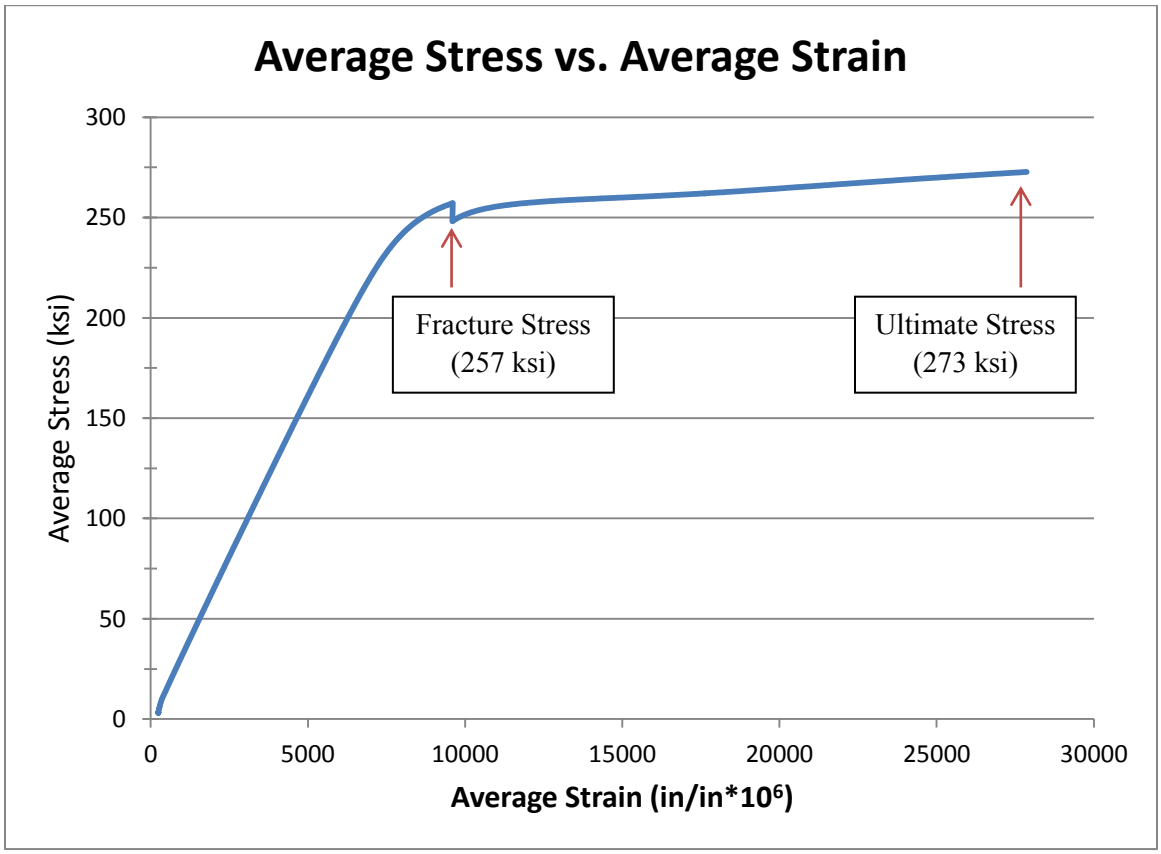

Figure 3.12: Stress-strain curve showing difference between fracture and ultimate stress.

Despite the occasional occurrence of the system achieving an ultimate stress greater than the stress at the time of initial wire fracture, the stress in the system was always calculated using the initial effective cross-sectional area of 1.519 in^2. This stress calculation is referred to as the "engineering stress" of the system. That is, the cross-sectional area of the specimen is not adjusted in the stress calculation during loading. In the same way that the cross-sectional area of the specimen is not adjusted for effects such as necking in the strand or the indentations caused by wedge teeth during loading, it is also considered to remain constant for the sake of calculating stress after a wire fracture occurred. Additionally, the engineering stress is more representative than the "true stress" of the actual system performance for the purpose of making design recommendations. Ultimately, the design engineer is interested in how much drift the wall can undergo and the load on the strand associated with that level of drift. The ability

of the PT system to achieve a higher stress than fracture but not a higher load is unimportant from a structural design standpoint. Furthermore, dividing load by a smaller cross-sectional area amplifies the calculated stress, potentially leading to a design recommendation that is not conservative. For comparison, Figure 3.13 shows the "true" stress-strain curve of a specimen where the cross-sectional area is reduced after a single wire fracture alongside the engineering stress-strain curve for the same test.

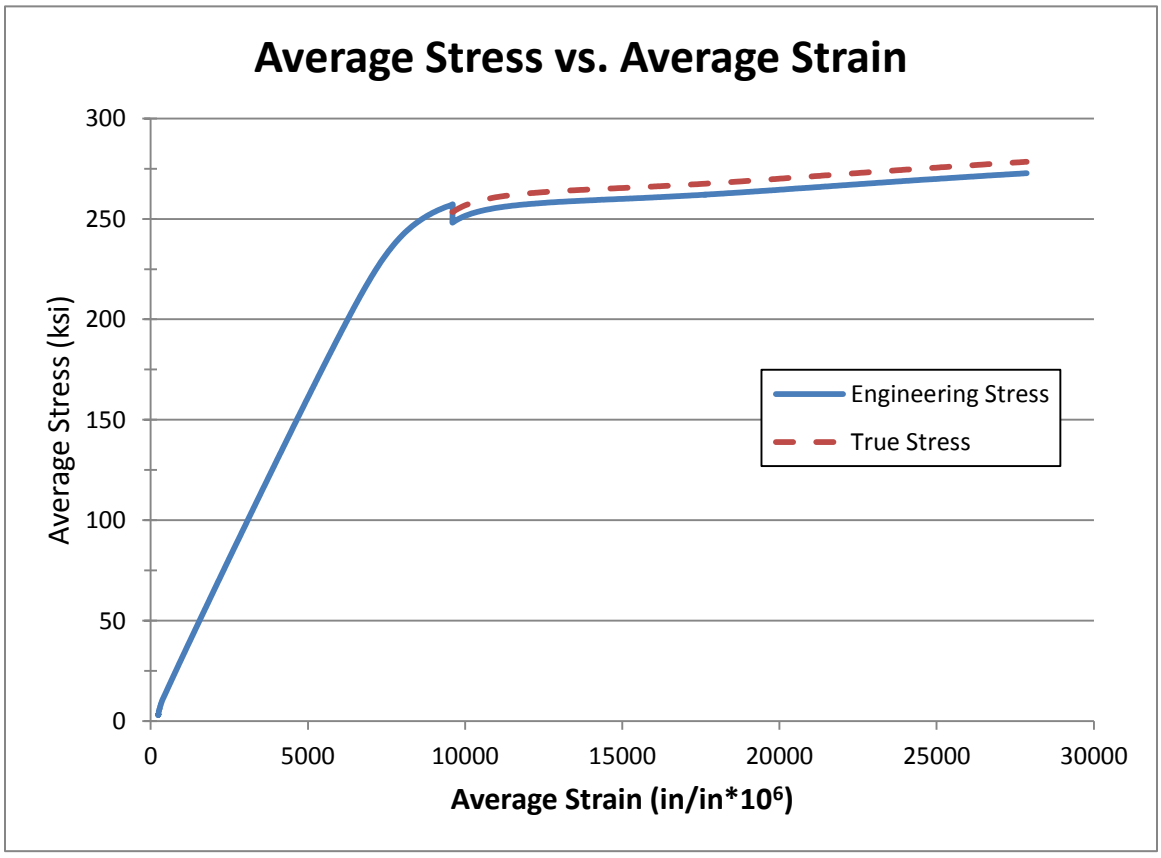

Figure 3.13: Comparison of engineering and "true" average stress.

3.5.2 Strain Capacity

Strain in each individual strand was measured with electrical resistance strain gages. Strain data was verified with the use of NDI Optical Tracking equipment on a select number of tests. Recording the strain of each strand was especially useful in understanding how the stresses are distributed throughout the system (i.e., to each strand).

The strain gage data represents the strain in an individual wire rather than the actual elongation of the strand as a whole. For the purposes of making design recommendations for rocking wall structures, the strand elongation and, thus, the system elongation is the desired value. Unfortunately, it is not reasonable to use crosshead displacement data to calculate the system elongation because of wedge seating that occurs throughout much of the loading cycle – an effect that is magnified in a laboratory specimen with a relatively short free length. Thus, strain gage data from an individual wire of each strand was considered to be representative of the system as a whole. This is a conservative assumption since the measured strain of an individual wire will be approximately 3.8% to 6.8% lower than the strand at the same stress level (Acosta 1991).

3.5.2.1 Strain Gages

The primary method of collecting strain data was with electrical resistance strain gages fixed to an individual wire of each of the seven strands (i.e., seven strain gages per specimen). The DAQ system recorded strain gage readings in units of microstrain ($in/in*10^6$) at a scan rate of 2 and 4 hertz for monotonic and cyclic tests, respectively. Prior to commencement of the appropriate loading scheme, a pre-load of approximately 5 to 7 kips was applied to the specimen. At this time, offsets of the strain gages were taken. However, an offset of the MTS load was not taken. This was done because the actual force required to cause failure of the system was desired, not the maximum load minus the pre-load. Taking offsets of strain gages but not the load after the application of a pre-load made it necessary to translate (or shift) the strain data horizontally to account for the strain that was not recorded between zero load and the pre-load.

The strain gage data was adjusted so that the linear portion of the stress-strain curve intersects the origin. The linear portion of the curve was taken as the data corresponding to a stress level between $0.20f_{pu}$ and $0.50f_{pu}$. The least squares method was used to fit a linear best-fit line to the corresponding data (Equation 3.1). The slope and y-intercept of this line were then used to calculate the horizontal translation value as shown below (Equation 3.2). Finally, the horizontal translation value was added to the original strain gage reading to get the derived strain value (Equation 3.3).

$$Line\ Equation: y_{(0.2fpu-0.5fpu)} = mx + b \quad (3.1)$$

$$Horizontal\ Translation: \frac{b}{m}\ [microstrain] \quad (3.2)$$

$$Derived\ SG\ Strain = Gage\ Reading + Translation \quad (3.3)$$

It is reasonable to assume that the variability in strain amongst strands was greater in the test specimen than would be observed in a full scale system due to the relatively short length of strand being tested (42-in. free-length minimum). The primary basis for justification of this assumption is the ratio of wedge seating depth to total specimen length. In a 42-in. specimen, this ratio is approximately 1.19%, assuming a total wedge seating of 0.5-in (0.25-in. at each end). In a full scale system (e.g., 120-in.), this ratio would be approximately 0.42%. In a full scale system, the effects of slightly different levels of strand seating and wedge engagement would be negligible. Thus, the strains in each strand would be much closer together.

The aforementioned discrepancy in strain variability between the test specimen and a full-scale assemblage led to the strain being derived in terms of both the average and maximum strain at fracture and ultimate (Figure 3.14). The four types of strain derived from strain gage readings are:

- Average fracture strain: The average strain reading of all working strain gages at the time of initial wire fracture.
- Maximum fracture strain: The maximum strain reading of all working strain gages at the time of initial wire fracture.
- Average ultimate strain: The average strain reading of all working strain gages at the time that ultimate stress is achieved.
- Maximum ultimate strain: The maximum strain reading of all working strain gages at the time that ultimate stress is achieved.

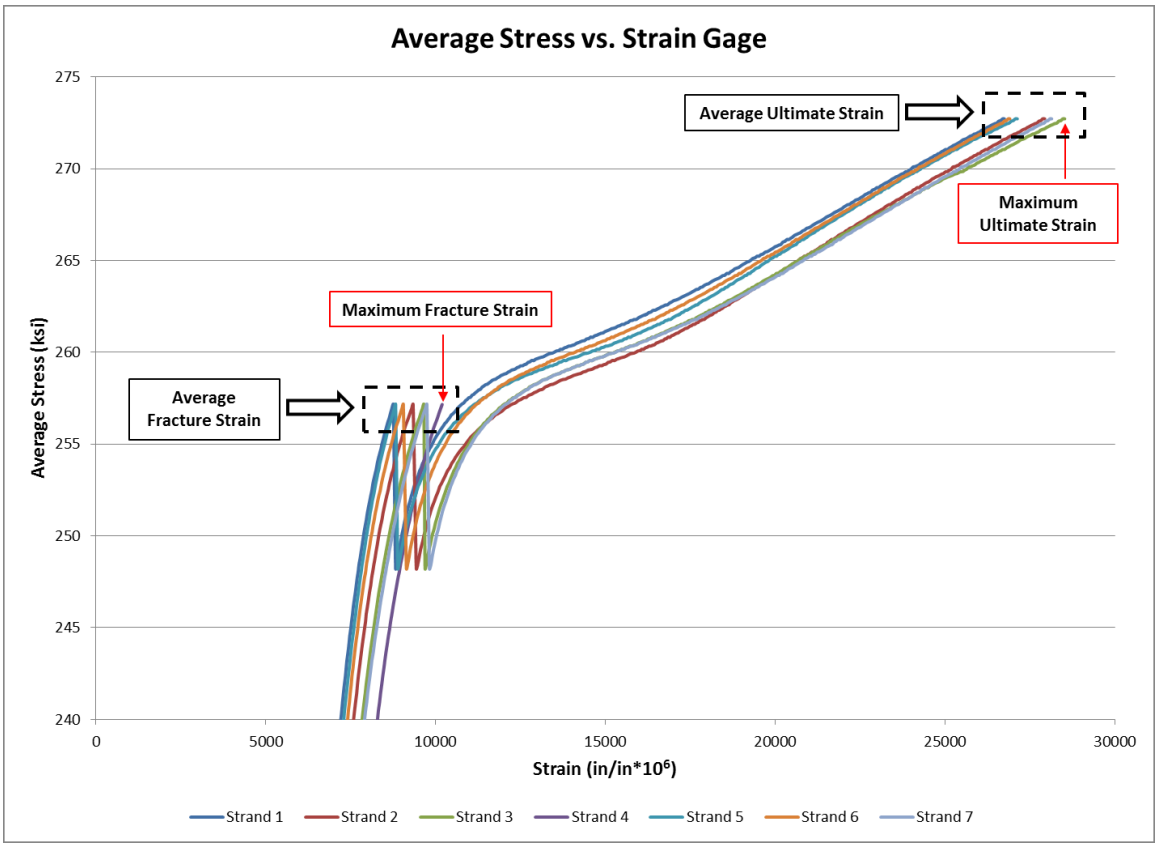

Figure 3.14: Average and maximum fracture and ultimate strain.

The average strain, which is calculated as a straight average of all working strain gages at a particular time, is the most conservative strain measurement. In this calculation, the assumption is made that if one strand is loaded "early", the other six strands will experience a reduced strain at a given load. Thus, an average of all seven strains will provide the actual system strain. While this approach makes sense conceptually, it is likely overly conservative.

The maximum strain is taken simply as the maximum value of all working strain gages at a particular time. In the test specimen, the strand with the greatest strain represents the true maximum strain that an individual strand in the system can withstand. Considering this fact, it is reasonable to assume that the maximum strain measured in the 42-in. test specimen is the most representative value of the limiting strain expected in a full scale system where the strain in each strand will be more consistent.

3.5.2.2 NDI Optical Tracking

The NDI Optical Tracking system was implemented for a select number of trials to verify strain gage readings, compare strand strain to individual wire strain (i.e., verify the findings of Acosta's analytical approximation method), and assess the effectiveness of optical tracking devices for measuring strain in PT strands. NDI output is in the form of three-dimensional (3D) coordinates of each marker. Four NDI markers, spaced at 2 inches, were fixed on three or four strands per test for rotated or aligned anchorages, respectively.

The NDI data acquisition (DAQ) system was independent from the MTS DAQ. Additionally, the NDI DAQ only recorded the frame of each scan, not a timestamp. For this reason, it was necessary to first align the two data sets based on the crosshead displacement. Markers on strands could not be used to align the data due to differences in initial seating and engagement of individual wedges at low stress levels (i.e., unadjusted NDI strain data did not clearly correlate with strain gage data at low stress levels). For each test, one NDI marker was placed on the top and bottom MTS fixture (Figure 3.5). The change in distance between these two markers was calculated and compared to the crosshead displacement value recorded by the MTS DAQ versus time. While some deflection of the fixtures at increased loads was recorded by the NDI markers and not by the MTS displacement, the initiation of crosshead movement at the beginning of the loading sequence is clearly defined in both data sets. In this way, the two data sets were aligned (Figure 3.15).

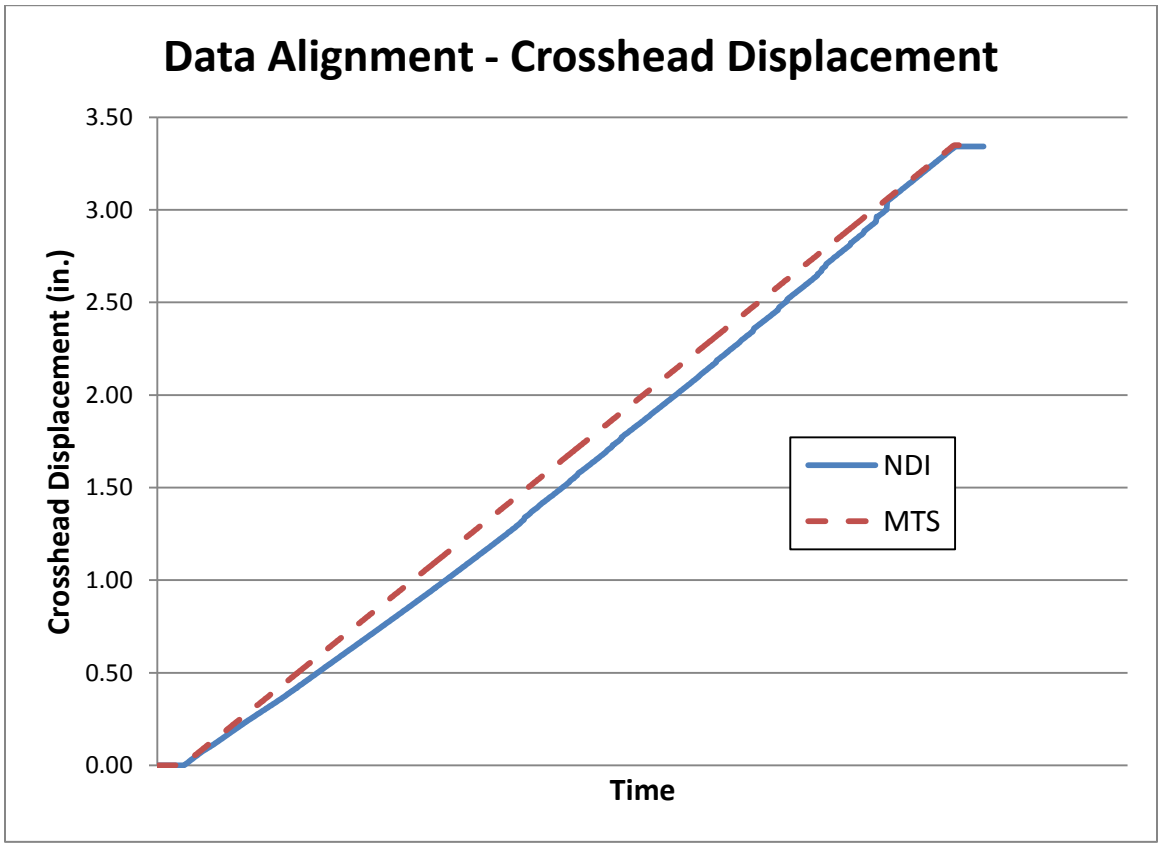

Figure 3.15: Comparison of crosshead displacement as measured by the NDI and MTS DAQ systems.

Strain in a strand is derived by calculating the change in 3D Euclidean distance between two markers on a strand and dividing by their initial distance (equation 3.4). The 3D Euclidean distance, d, was calculated using equation 3.5. It was determined that the derived strain calculated using an average of three distances between all four markers (spaced at 2-inches each) was equivalent to the derived strain calculated using simply the uppermost and lowermost markers (spaced at 6-inches). Thus, the derived strain is calculated considering only the uppermost and lowermost markers on a strand.

$$Derived\ NDI\ Strain = \frac{\Delta l}{L} = \frac{d - d_0}{d_0}\ [{}^{in}/_{in}] \tag{3.4}$$

$$d = \sqrt{(x_2 - x_1)^2 + (y_2 - y_1)^2 + (z_2 - z_1)^2}\ [in] \tag{3.5}$$

At low stress levels, the strands tend to twist and straighten while initial seating and engagement of each wedge occurs and any remaining slack in the system is removed. If this out-of-plane motion is not properly accounted for, it will be interpreted as "strain" using the derived strain equation. Additionally, this portion of the curve cannot simply be eliminated or zeroed as some amount of strand elongation occurs during this time. Thus, some data reduction is required to determine the initial distance (d_0) value of each strand.

Movement of the strand in the out-of-plane direction causes nonlinearity in early portions of the NDI-calculated stress-strain curves. However, based on the fact that a linear relationship exists between the stress and strain of PT strand at loads less than yield, a graphical method was implemented to determine d_0. First, the distance between the uppermost and lowermost markers was plotted against load. A best-fit line was then applied over the portion of data corresponding to $0.20f_{pu}$ to $0.50f_{pu}$ (linear portion) using the least squares method. The intersection of the best-fit line with the distance axis was then taken as the initial distance (d_0). Figure 3.16 shows how d_0 was determined using the distance versus load plot. A graphical comparison of the derived strain data when calculated with an unadjusted versus adjusted initial distance is provided in Figure 3.17.

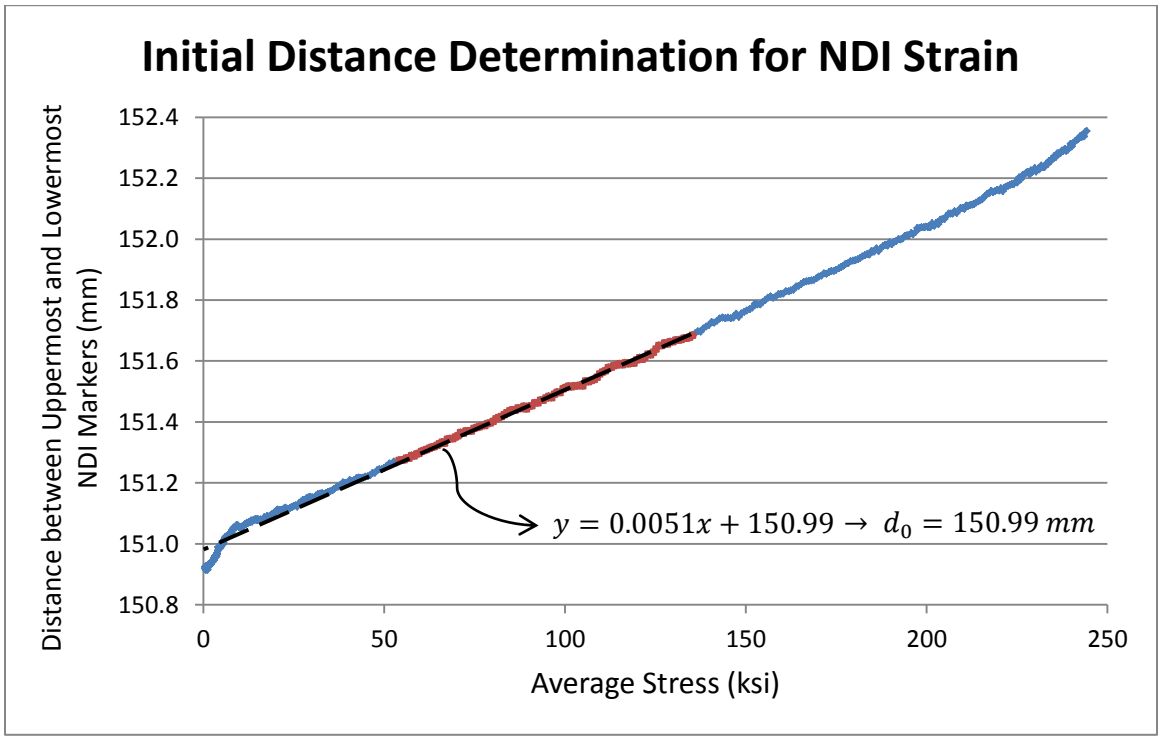

Figure 3.16: Graphical description of d_0 determination for NDI strain calculation.

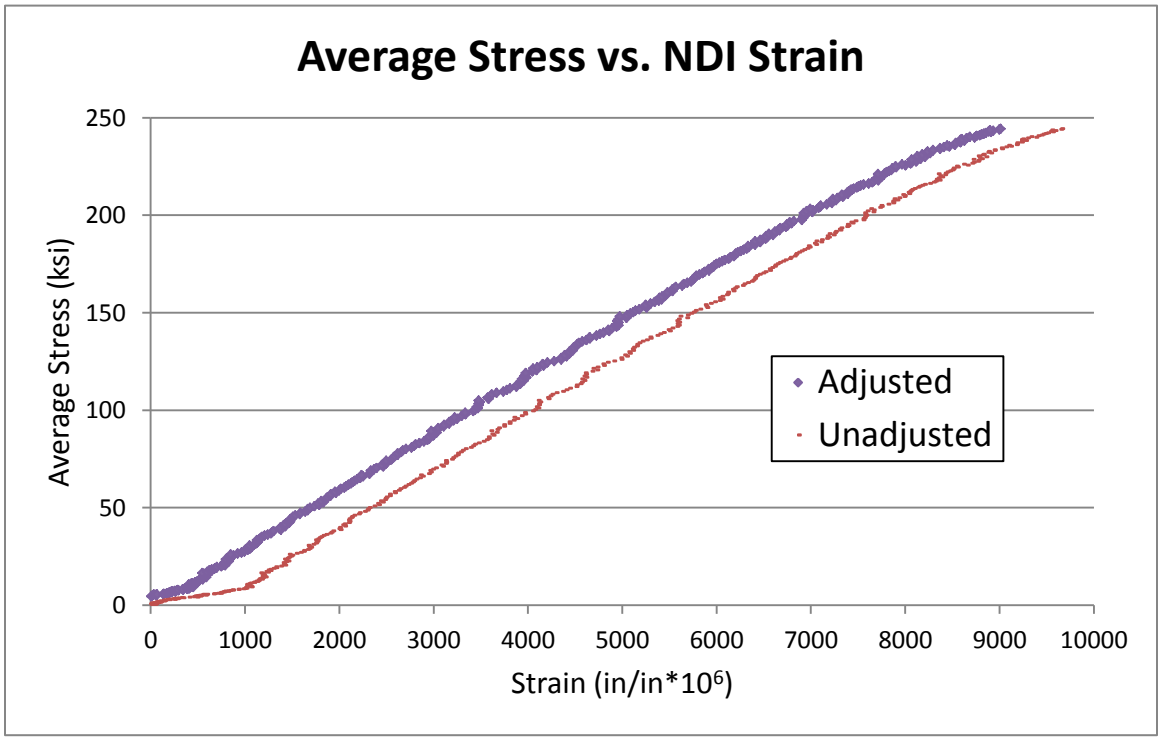

Figure 3.17: Comparison of NDI derived strain with and without initial distance adjustment.

3.5.3 Modulus of Elasticity

In general, the method described in Acosta (1991) was followed for determining the modulus of elasticity of each strand. In this procedure, a best-fit line of strain in each strand (using either strain gage or NDI optical tracking data) was computed considering only the data points that corresponded to stresses between $0.20f_{pu}$ and $0.80f_{pu}$. Stresses less than 0.20fpu are not considered because of variability that can exist due to wedge seating. Stresses greater than $0.80f_{pu}$ are not considered because of strand yielding that can ensue as early as $0.85f_{pu}$. Slightly different methods of data reduction were followed for monotonic and cyclic tests as described in the following sections.

The analytical approximation method developed by Acosta (Figure 2.7) was then verified by comparing modulus of elasticity values determined using strain gages fixed to an individual wire to elastic modulus values determined for the strand as a whole using NDI optical tracking. The manufacturer provided elastic modulus was also compared to the NDI measured modulus of the strand as a whole.

3.5.3.1 Monotonic Load Tests

The data analysis procedure for monotonic load tests followed Acosta's procedure exactly. For each of the seven strands, a best-fit line was computed only considering the data points corresponding to stresses located between $0.20f_{pu}$ and $0.80f_{pu}$. The slope of this line was then taken as the elastic modulus of the strand.

3.5.3.2 Cyclic Load Tests

The data analysis procedure for cyclic load tests was similar to the Acosta procedure, but required some modifications. The cyclic loading schematic includes 50 cycles between $0.20f_{pu}$ to $0.85f_{pu}$. Thus, for each strand, the slope of a best-fit line was computed for the data points corresponding to stresses located between $0.20f_{pu}$ and $0.80f_{pu}$ for the "loading side" of cycles two through eleven (Figure 3.18). These ten values were then averaged to obtain a final modulus of elasticity. The first cycle was not included to avoid any wedge seating that may have still been occurring, which can cause nonlinearity in the stress versus strain curve. Additionally, if the strand had a wire

fracture prior to completing eleven cycles, then an average of the completed cycles (excluding the first cycle) was used.

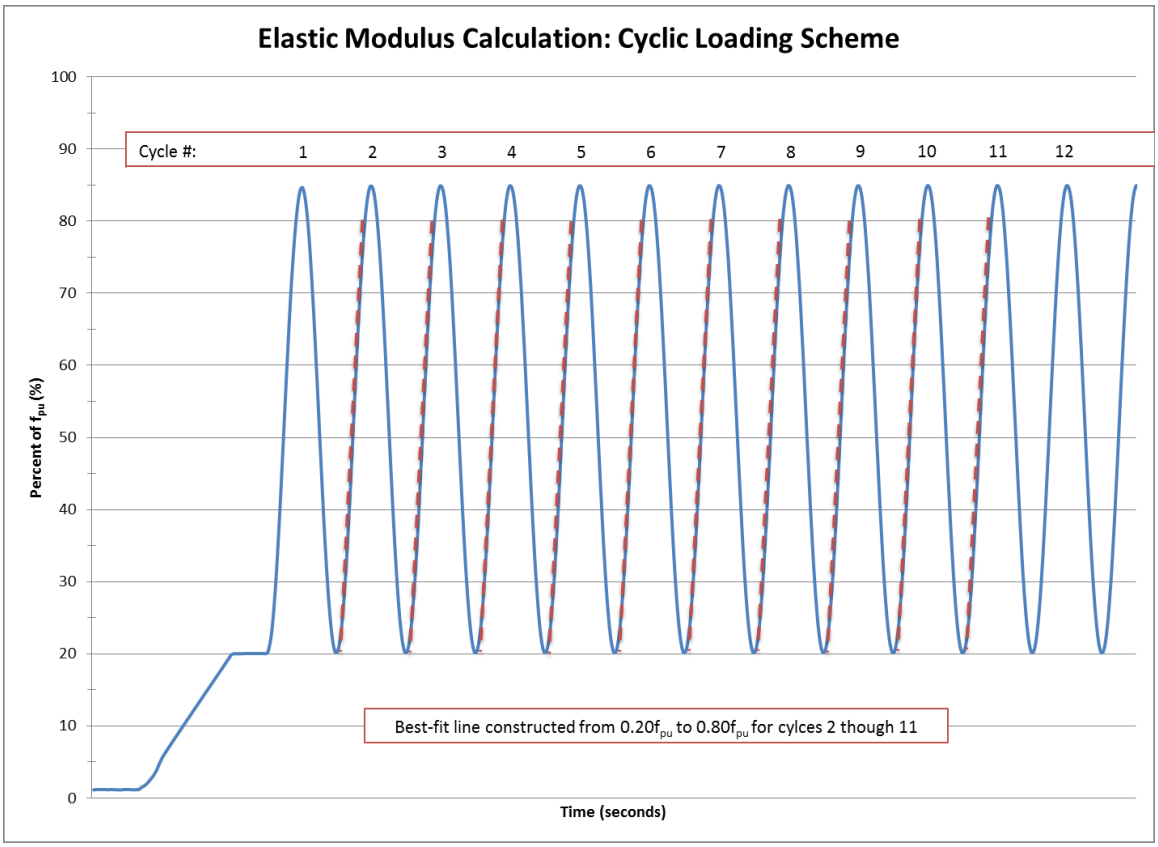

Figure 3.18: Elastic modulus calculation for cyclic loading scheme.

CHAPTER 4: TEST RESULTS

The test results presented in the following sections are organized by stress capacity, strain capacity, and modulus of elasticity. Several figures are provided in this chapter for enhanced visual comparison of stress, strain, and elastic modulus values. Tables of numerical values are provided in Appendix C.

The published strength and deformation requirements that the anchoring system must allow the strand to achieve prior to failure are listed in Table 2.1. Traditionally, the certification of strand/anchorage systems is done with a single strand, even for multistrand anchorages. When testing a single strand, failure occurs when an individual wire fractures within the anchorage at the nose of the wedge. The peak load at the time of failure is then the ultimate load. However, in multistrand systems where several strands are loaded simultaneously, it is possible for the system to achieve a higher load (ultimate load) than was achieved at the time of initial fracture of an individual wire (fracture load) (see Section 3.5), despite an even distribution of strain amongst strands at loads up to $0.80f_{pu}$. For this reason, stress and strain capacity results are presented in terms of both fracture and ultimate values.

Discrepancies also arise in the terminology of certification requirements because they are currently intended for strand/anchorage systems in which only a single strand is being tested. In terms of strength requirements, the ICC-ES document states, "Each test assembly shall demonstrate *failure* of the strand at a test load of at least 95 percent of the actual breaking strength of the strand used in the tests." For a multistrand test assembly, the failure load is interpreted as the load at initial wire fracture. However, the ICC-ES deformation requirement states, "The elongation of the strand of each tested assembly at the *ultimate* load shall be at least 2 percent." As discussed previously, for a multistrand test assembly, the ultimate load may not correspond to the fracture load. Due to this difference in terminology, for the purpose of determining certification conformance, the *fracture stress* of the system is compared to the stated strength limit while the *ultimate strain* of the system is compared to the stated deformation limit.

It should be noted, however, that while a system may surpass the published deformation limit of 2 percent at ultimate, in the context of rocking walls designed for seismic resiliency, the fracture strain is of the upmost importance to the design engineer due to the fact that an individual wire fracture during a seismic event will likely require replacement of the post-tensioning. Thus, for the purpose of making design recommendations, the *fracture strain* will be cited as the limiting condition.

4.1 Stress Capacity

The strength of the multistrand PT anchorage system was analyzed in terms of average engineering stress (i.e., total load [kips] divided by nominal cross-sectional area [in^2] of all seven strands). See Section 3.5.1 for a description of the stress capacity data analysis procedure and differentiation between fracture and ultimate stress.

A summary of the stress capacity of the system under each configuration is provided in the figures below. Figure 4.1 shows the results for the monotonically loaded tests and Figure 4.2 shows the results from the cyclically loaded tests. Three repetitions were conducted for each configuration, each represented by a vertical bar. The lowermost (blue shaded) bar represents the fracture stress of the system and the uppermost (red hatched) bar represents the ultimate stress of the system. If only one bar is present, the ultimate stress is equal to the fracture stress.

The two stress limits are also drawn on each graph. The lower (black) line is the ACI 318-08 limit of $0.95f_{pu}$ (256.5 ksi). The upper (red) line is the ICC-ES (and all others) limit of $0.95f_{pm,free\text{-}length}$ (273.1 ksi). The maximum free-length fracture stress ($f_{pm,free\text{-}length}$) was taken as the breaking strength of the strand as determined by the manufacturer (Appendix A) divided by the nominal cross-sectional area of the strand (Equation 4.1).

$$0.95f_{pm,free-length} = 0.95 * \frac{62.393\ k}{0.217\ in^2} = 273.1\ ksi \qquad (4.1)$$

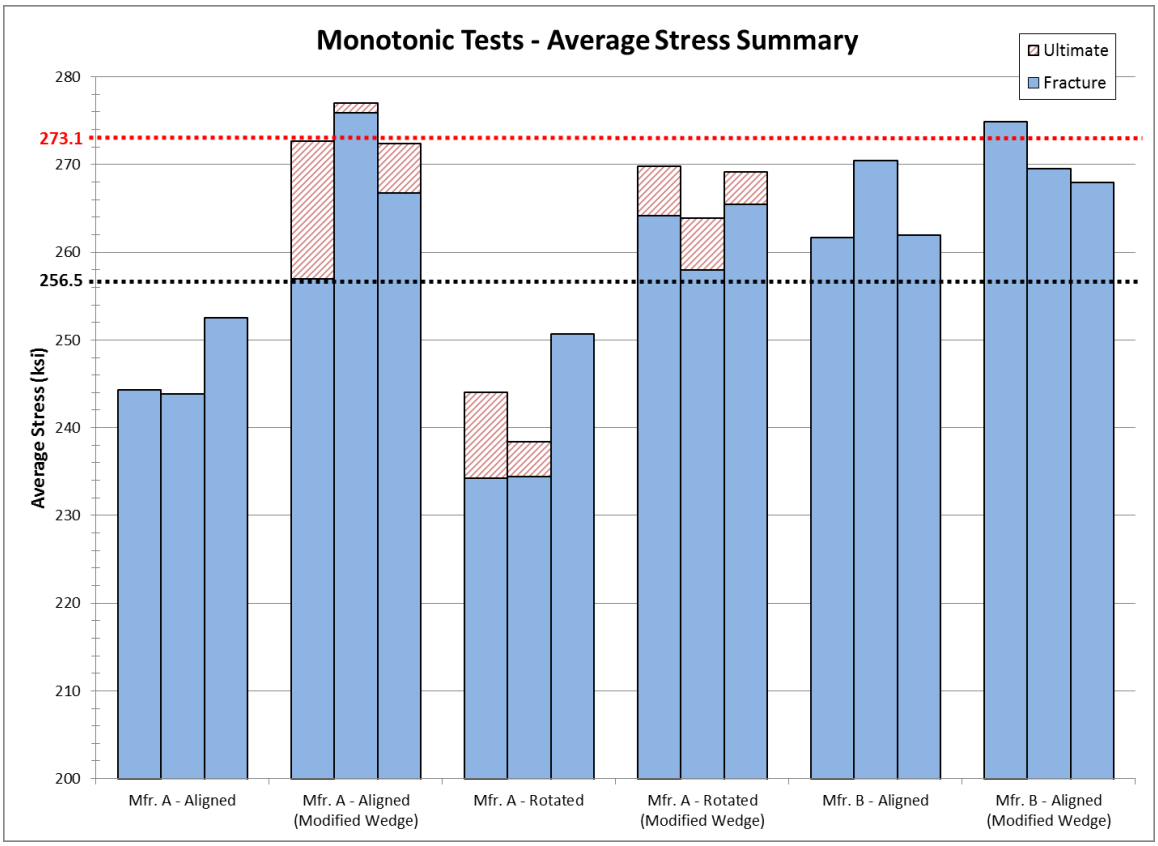

Figure 4.1: Summary of average stress results for monotonically loaded specimens.

As shown in Figure 4.1, anchorages from manufacturer A tested with standard wedges did not meet the ACI 318-08 strength requirement of $0.95f_{pu}$ at fracture. All of the other configurations, however, exceeded $0.95f_{pu}$ at fracture. On average, manufacturer A tested with aligned anchorage heads and modified wedges was able to exceed $0.95f_{pm,free\text{-}length}$ at ultimate. However, fracture strength, not ultimate strength, is the limiting value for strength certification. Therefore, on average, none of the configurations met the $0.95f_{pm,free\text{-}length}$ limit when loaded monotonically.

The cyclically loaded specimens (Figure 4.2) showed very similar results to those loaded monotonically. Again, anchorages from manufacturer A tested with standard wedges did not meet the $0.95f_{pu}$ limit at fracture, while all other configurations did. The only change in performance occurred with manufacturer A tested with aligned anchorage heads and modified wedges. When subjected to the cyclic loading scheme, the specimen was able to exceed $0.95f_{pm,free\text{-}length}$ at fracture for all three repetitions.

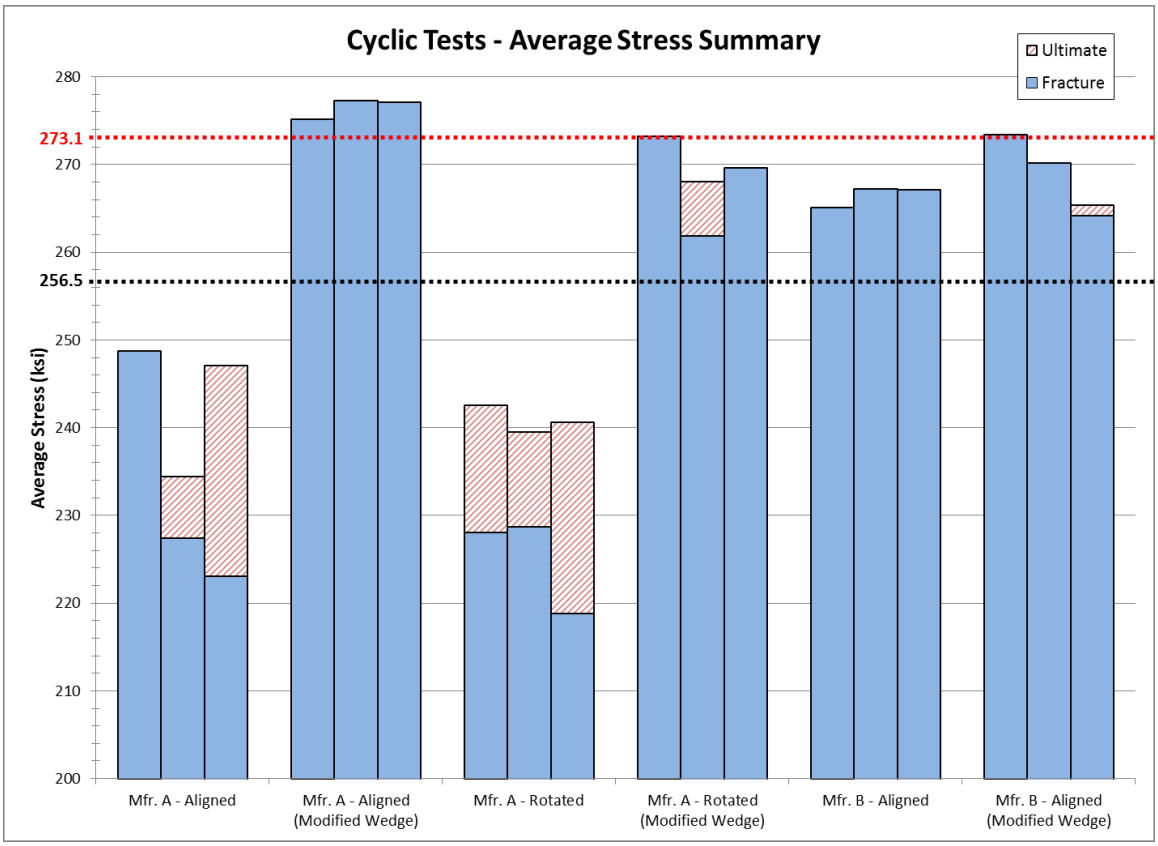

Figure 4.2: Summary of average stress results for cyclically loaded specimens.

Visual inspection of the bar graphs suggests qualitatively that the modified wedge geometry improves the performance of anchorages from both manufacturers and that anchorage rotation may reduce the strength capacity of the system. To quantify these apparent trends, a statistical analysis of fracture stresses was conducted for each of the four test variables. By comparing tests in which only one variable changes, several direct comparisons could be drawn and statistically analyzed to determine if a certain parameter caused a statistically significant change in the mean fracture stress capacity of the system.

Two-tailed Student's t-tests were used to evaluate the null hypothesis of equivalent means for the loading scheme, anchorage manufacturer, anchorage alignment, and wedge geometry variables. For all tests, it was assumed that the two populations are unpaired and have about the same spread (i.e., they are homoscedastic).

Table 4.1: Direct comparisons drawn for statistical analysis.

Trial 1				Trial 2				Changing Variable
Load	**Mfr.**	**Alignment**	**Wedge**	**Load**	**Mfr.**	**Alignment**	**Wedge**	
Static	A	Aligned	Standard	Cyclic	A	Aligned	Standard	Load
Static	A	Rotated	Standard	Cyclic	A	Rotated	Standard	Load
Static	A	Aligned	Modified	Cyclic	A	Aligned	Modified	Load
Static	A	Rotated	Modified	Cyclic	A	Rotated	Modified	Load
Static	B	Aligned	Standard	Cyclic	B	Aligned	Standard	Load
Static	B	Aligned	Modified	Cyclic	B	Aligned	Modified	Load
Static	A	Aligned	Standard	Static	B	Aligned	Standard	Mfr.
Static	A	Aligned	Modified	Static	B	Aligned	Modified	Mfr.
Cyclic	A	Aligned	Standard	Cyclic	B	Aligned	Standard	Mfr.
Cyclic	A	Aligned	Modified	Cyclic	B	Aligned	Modified	Mfr.
Static	A	Aligned	Standard	Static	A	Rotated	Standard	Alignment
Static	A	Aligned	Modified	Static	A	Rotated	Modified	Alignment
Cyclic	A	Aligned	Standard	Cyclic	A	Rotated	Standard	Alignment
Cyclic	A	Aligned	Modified	Cyclic	A	Rotated	Modified	Alignment
Static	A	Aligned	Standard	Static	A	Aligned	Modified	Wedge
Static	A	Rotated	Standard	Static	A	Rotated	Modified	Wedge
Static	B	Aligned	Standard	Static	B	Aligned	Modified	Wedge
Cyclic	A	Aligned	Standard	Cyclic	A	Aligned	Modified	Wedge
Cyclic	A	Rotated	Standard	Cyclic	A	Rotated	Modified	Wedge
Cyclic	B	Aligned	Standard	Cyclic	B	Aligned	Modified	Wedge

Table 4.1 shows the direct comparisons that were drawn for each variable. A method of "variable elimination" was implemented to increase the sample size of tests being directly compared. For example, by showing statistically that no significant difference in means exists amongst monotonic and cyclic load tests, the loading parameter could be eliminated as being unique. Thus, when comparing manufacturer A with standard wedges to manufacturer B with standard wedges, fracture stresses from both monotonic and cyclic load tests were used. Additionally, for this example, the anchorage alignment variable was eliminated since no rotated anchorage tests were conducted for manufacturer B.

Table 4.2 shows a summary of the results from the statistical analysis conducted for fracture stress. The following sections (4.1.1-4.1.4) present the individual results from each variable with discussions of what the results indicate. A 95% confidence interval was used to determine significance. Thus, a p-value of less than 0.05 indicates a significant difference in means.

Table 4.2: Fracture stress statistical analysis results summary.

Variable	Configuration	Variable A		Variable B	P-value
Loading Scheme	All	Monotonic	=	Cyclic	> 0.05
Anchorage Manufacturer	Standard Wedge	A	<	B	4.967E-4
	Modified Wedge	A	=	B	0.6890
Anchorage Alignment	Standard Wedge	Aligned	=	Rotated	0.2765
	Modified Wedge	Aligned	=	Rotated	0.1563
Wedge Geometry	Mfr. A – Aligned	Standard	<	Modified	3.249E-4
	Mfr. A – Rotated	Standard	<	Modified	4.945E-5
	Mfr. B – Aligned	Standard	=	Modified	0.0604

4.1.1 Loading Scheme

For the loading scheme parameter, individual t-tests were conducted for each of the direct comparisons drawn in Table 4.1. The t-tests showed that none of these comparisons had a significant difference in their means. Thus, for the remainder of the statistical tests, the loading scheme parameter was eliminated as a unique variable (i.e., tests that varied only by loading scheme were considered to be a part of the same population).

4.1.2 Anchorage Manufacturer

For the statistical analysis of anchorage manufacturer, the anchorage alignment variable was eliminated since alignment was not investigated for manufacturer B (i.e., only the aligned anchorage tests for manufacturer A were used to compare to the aligned anchorage tests for manufacturer B). Additionally, the loading scheme parameter was eliminated previously. Therefore, the only variables remaining to compare were anchorage manufacturer and wedge geometry.

Figure 4.3a shows the box-and-whisker plot for manufacturers A and B when the standard wedges are used and Figure 4.3b shows the box-and-whisker plot for the modified wedge configuration. The box-and-whisker plots are provided so that the difference in the mean and the spread of the data sets can be viewed. The upper and lower whiskers indicate the maximum and minimum observed values, respectively. The bottom of the shaded (blue) box is the first quartile, the top of the hatched (red) box is the third quartile, and where the boxes meet is the median value. The yellow "X" on the plots indicates the mean of the data set.

The calculated p-values for the standard and modified wedge configurations are 4.967E-4 and 0.6890, respectively. This indicates that when each manufacturer uses their respective standard wedges, manufacturer B has a significantly greater mean fracture stress than manufacturer A. However, when the modified wedge geometry is used, the mean fracture stress of manufacturer A actually exceeds that of manufacturer B, but not to a statistically significant extent. The difference in anchorage performance amongst changing wedge geometries indicates that anchorage performance is highly dependent on

anchor/wedge compatibility. That is, anchorage A is capable of performing as well as anchorage B when compatible wedge geometries are used.

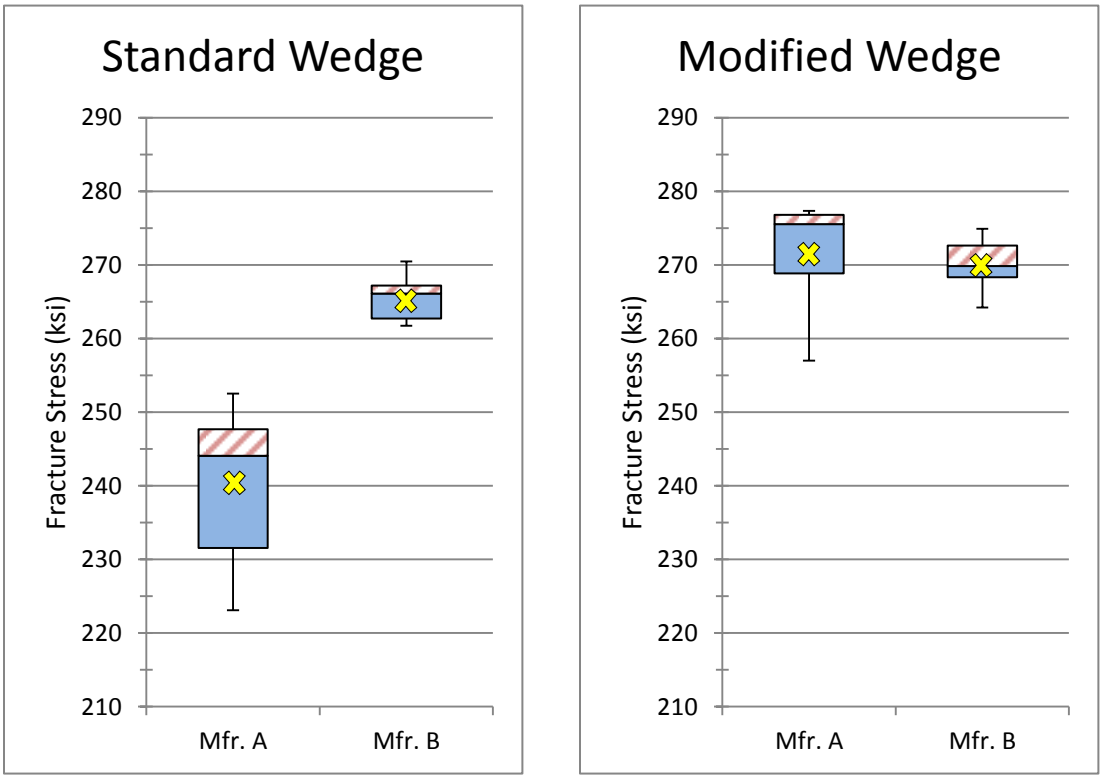

(a) (b)

Figure 4.3: Box-and-whisker plots comparing manufacturer A and manufacturer B with (a) standard and (b) modified wedge geometries.

4.1.3 Anchorage Alignment

Anchorage alignment was only investigated with anchorages from manufacturer A, therefore anchorage manufacturer was eliminated for the investigation of anchorage alignment. Additionally, the loading scheme parameter was eliminated previously. Therefore, the only variables remaining to compare were anchorage alignment and wedge geometry.

Figure 4.4a shows the box-and-whisker plot for the aligned and rotated anchorages when the standard wedges are used and Figure 4.4b shows the box-and-whisker plot for the modified wedge configuration.

The calculated p-values for the standard wedge and modified wedge configurations are 0.2765 and 0.1563, respectively. This indicates that while the mean fracture stress of the system was reduced when the anchorage ends were rotated, the reduction was not significant at a 95% confidence level.

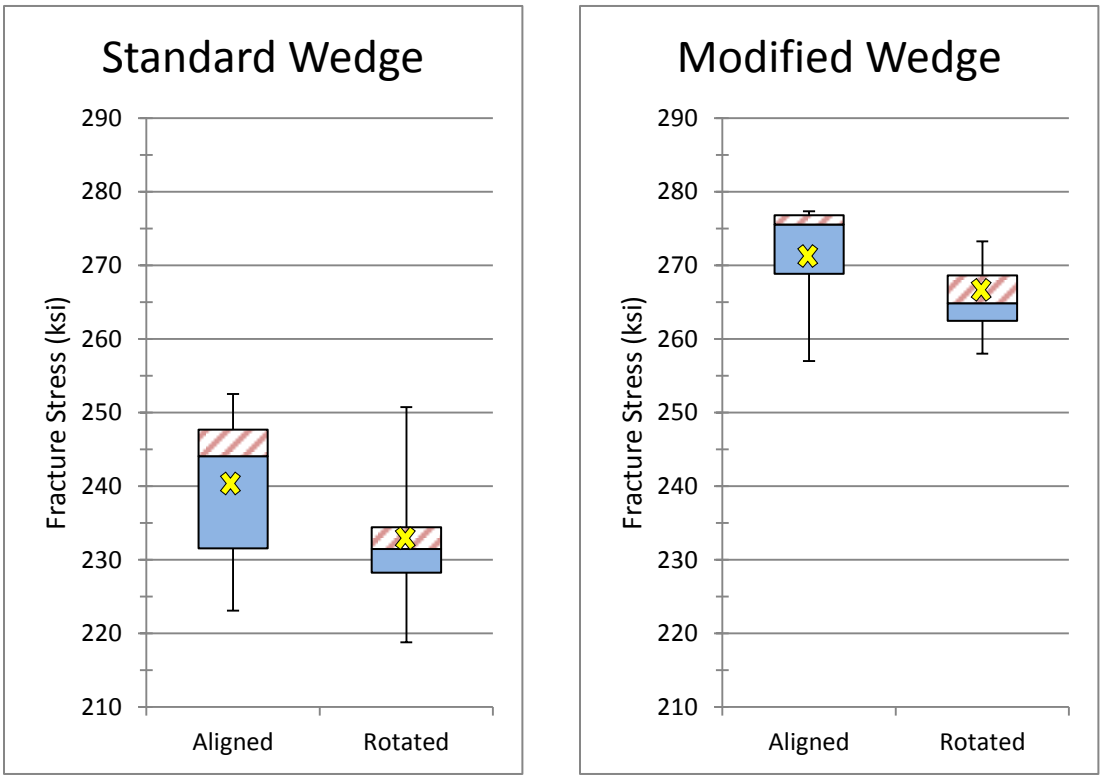

(a) (b)

Figure 4.4: Box-and-whisker plots comparing aligned and rotated anchorages with (a) standard and (b) modified wedge geometries.

4.1.4 Wedge Geometry

A side-by-side comparison was made with the standard versus modified wedge geometries for all of the tested configurations. The loading scheme parameter was eliminated previously leaving three variables to be compared: (1) wedge geometry, (2) anchorage manufacturer, and (3) anchorage alignment.

Figure 4.5a shows the box-and-whisker plot for the standard and modified wedge geometries when anchorage manufacturer A was tested with aligned anchorages. Figure

4.5b shows the box-and-whisker plot for manufacturer A with the rotated anchorage configuration. Figure 4.5c shows the box-and-whisker plot for manufacturer B with aligned anchorages.

The calculated p-values for the manufacturer A–aligned, manufacturer A–rotated, and manufacturer B–aligned configurations are 3.249E-4, 4.945E-5 and 0.0604, respectively. This indicates that the modified wedge geometry significantly increased the fracture stress for anchorages from manufacturer A when tested in both the aligned and rotated configurations. The modified wedge also increased the mean fracture stress capacity of anchorages from manufacturer B; however the increase was not significant using a 95% confidence interval.

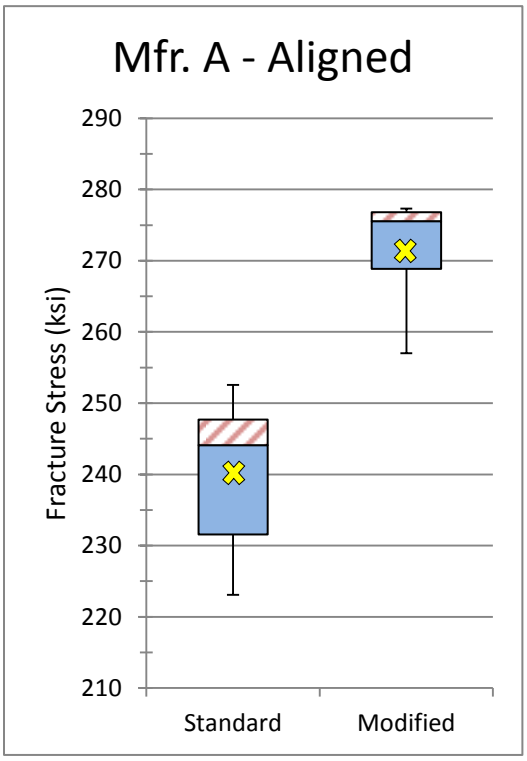

(a)

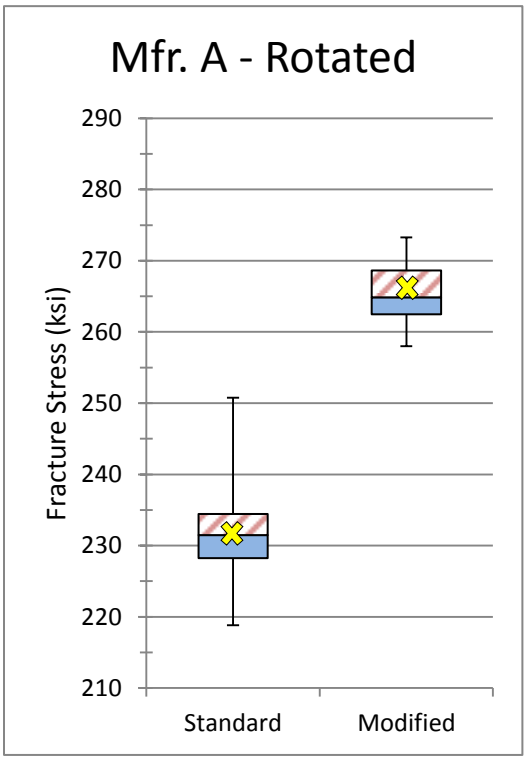

(b)

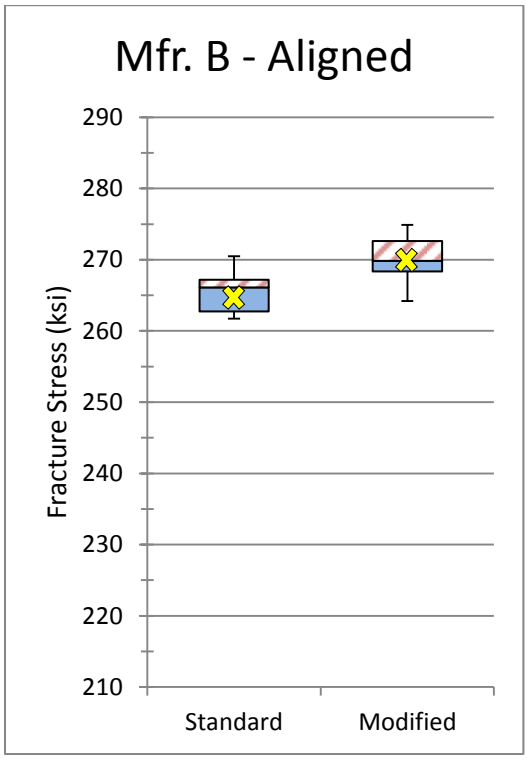

(c)

Figure 4.5: Box-and-whisker plots comparing standard and modified wedge geometries with (a) mfr. A-aligned (b) mfr. A-rotated, and (c) mfr. B-aligned configurations.

4.2 Strain Capacity

The strain capacity of the multistrand PT anchorage system was analyzed in terms of microstrain as determined by strain gages applied to an individual wire of each strand (i.e., one strain gage per strand). See Section 3.5.2.1 for a description of the strain gage data analysis procedure and differentiation between fracture and ultimate strain. Section 3.5.2.1 also describes the four types of strain that were derived from strain gage readings.

In each of the figures below, the maximum fracture and ultimate strain values are presented. Tables containing each of the derived strain values are provided in Appendix C. The maximum strain is defined as the maximum strain reading of all working strain gages at a particular time. While this value is less conservative than the average strain, the researchers believe it is a more accurate representation of the limiting strand strain that would be observed in a full scale application due to the longer strand lengths

resulting in a more uniform strain distribution. Additionally, maximum strain as determined by strain gages will still be conservative since it is a measurement of individual wire strain and not strand elongation as a whole (see Section 3.5.2).

A summary of the strain capacity of the system under each configuration described in Section 3.4 is provided in the figures below. Figure 4.6 shows the results for the monotonically loaded tests and Figure 4.7 shows the results from the cyclically loaded tests. Three repetitions were conducted for each configuration, each represented by a vertical bar. The lowermost (blue shaded) bar represents the fracture strain of the system and the uppermost (red hatched) bar represents the ultimate strain of the system. If only one bar is present, the ultimate strain is equal to the fracture strain. The deformation requirement of 2.0% at ultimate is also drawn on each graph.

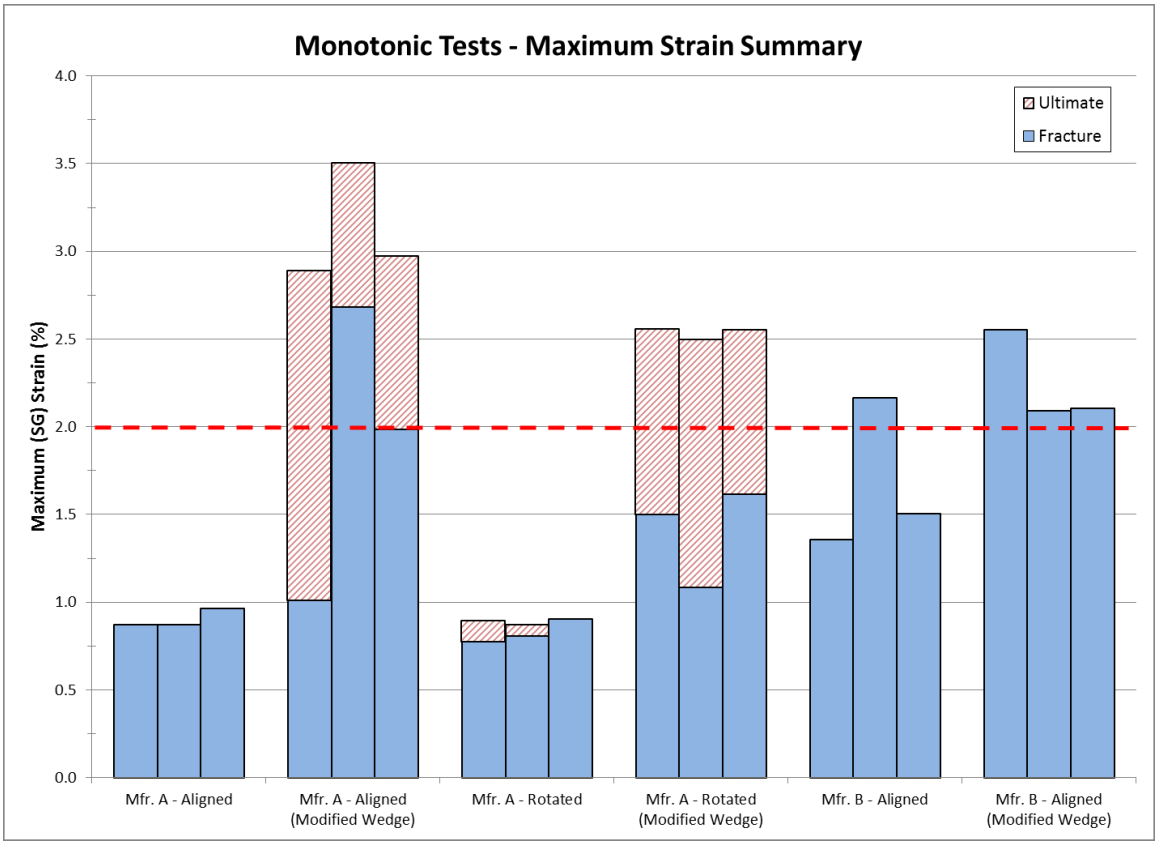

Figure 4.6: Summary of maximum strain results for monotonically loaded specimens.

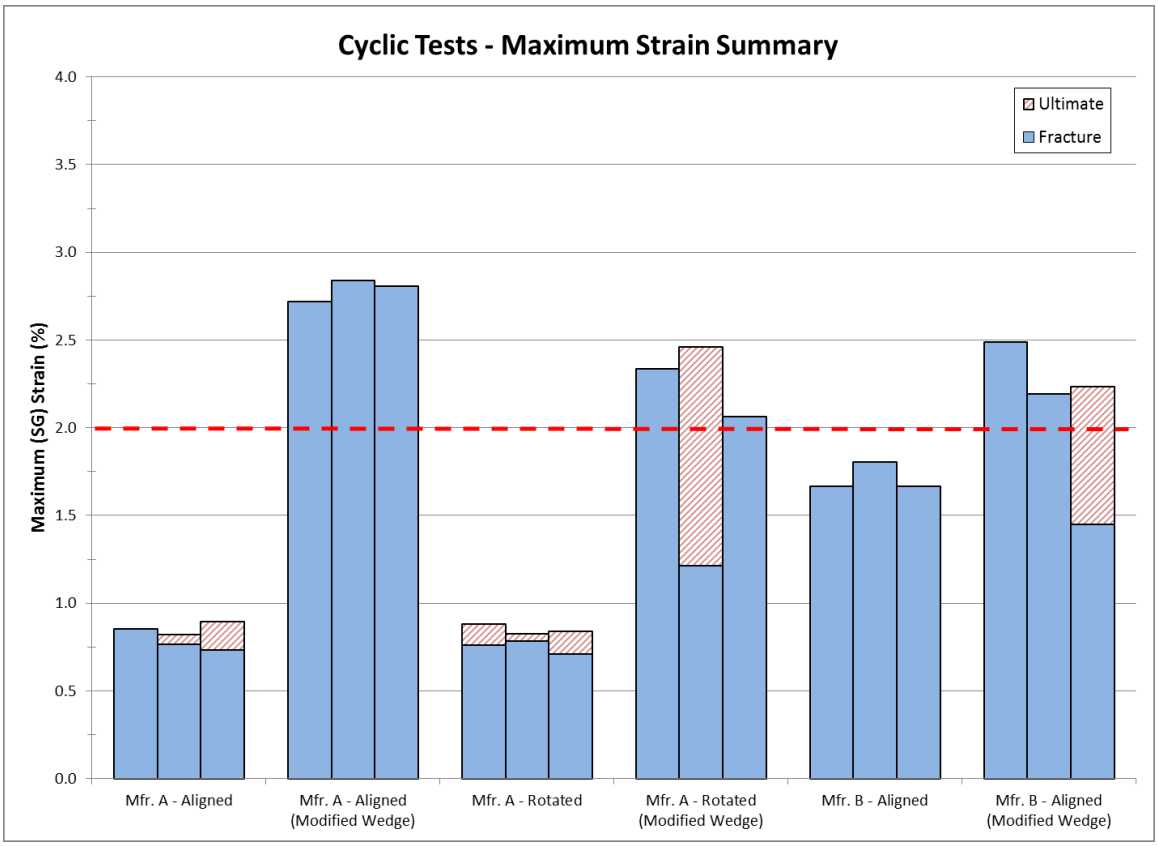

Figure 4.7: Summary of maximum strain results for cyclically loaded specimens.

As shown in Figure 4.6 and Figure 4.7, on average anchorages from both manufacturers tested with standard wedges did not meet the elongation requirement of 2.0% at ultimate. Recalling that manufacturer B with standard wedges did meet the $0.95f_{pu}$ strength limit at fracture indicates another discrepancy in the ACI 318-08 certification requirements. That is, the system was able to meet the strength requirement without meeting the elongation requirement. This is essentially due to the fact that $0.95f_{pu}$ (256.5 ksi) does not correspond to a strain of 2.0% on the PCI-defined stress-strain curve for PT strand. Rather, a strand strain of 2.0% corresponds to a stress of about 264.3 ksi. Essentially, this makes the less stringent strength limit of $0.95f_{pu}$ obsolete because the strain limit will always control. However, in the case of the more stringent $0.95f_{pm,free\text{-}length}$ limit, the strength requirement may or may not control depending on the actual breaking strength of the strand. For this reason, it is recommended that the strength limit of $0.95f_{pm,free\text{-}length}$ be adopted by ACI 318-08.

In each of the configurations utilizing the modified wedge geometry, the elongation requirement of 2.0% at ultimate is always achieved. It is important to note, however, that the limiting strain in terms of the design of rocking walls for seismic resiliency is the fracture strain. While the modified wedge geometry allowed fracture strains of more than 2.5% in some cases, premature fractures were also recorded as low as 1.0% when the modified wedge was being used. This large range in maximum fracture strain indicates the need for further research in the area of wedge geometry development. Additionally, the possibility of wire fractures at strains as low as 1.0% requires that a strand strain limit of 1.0% elongation be used in the design of self-centering rocking wall structures.

4.3 Modulus of Elasticity

The modulus of elasticity of each strand was determined following the procedure presented in Acosta (1991) (see Section 3.5.3). Strain gages were implemented for all tests, with one gage applied to each strand. Due to the fact that strain gages were attached to an individual wire of the strand and oriented along the wire's axis, the "apparent" modulus value calculated is expected to be 3.8% to 6.8% greater than the manufacturer specified elastic modulus of the strand as a whole (see Figure 2.7). Figure 4.8 shows a summary of the apparent modulus values of individual strand wires as measured by strain gages for monotonically loaded specimens. Figure 4.9 shows the apparent moduli for cyclically loaded specimens. The average moduli for the monotonic and cyclic data sets (marked on each graph by the horizontal dashed line) are 31,640 ksi and 31,360 ksi, respectively. The standard deviation for the cyclically loaded specimens was considerably lower (610 ksi) than the monotonically loaded specimens (1127 ksi) due to the fact that the modulus calculation was based on an average of several cycles for cyclic tests rather than a single slope as in the monotonic tests. Combining all of the results, the average apparent elastic modulus was 31,500 ksi with a combined standard deviation of 920 ksi.

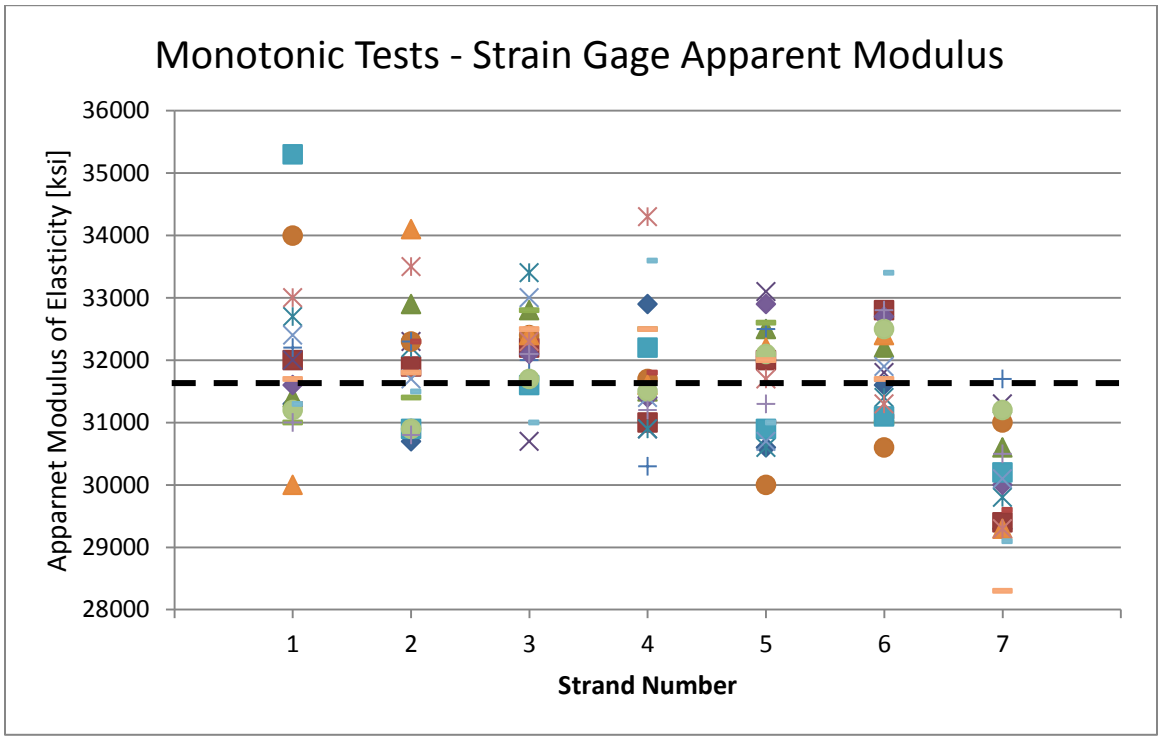

Figure 4.8: Apparent modulus values of individual wires for monotonically loaded specimens.

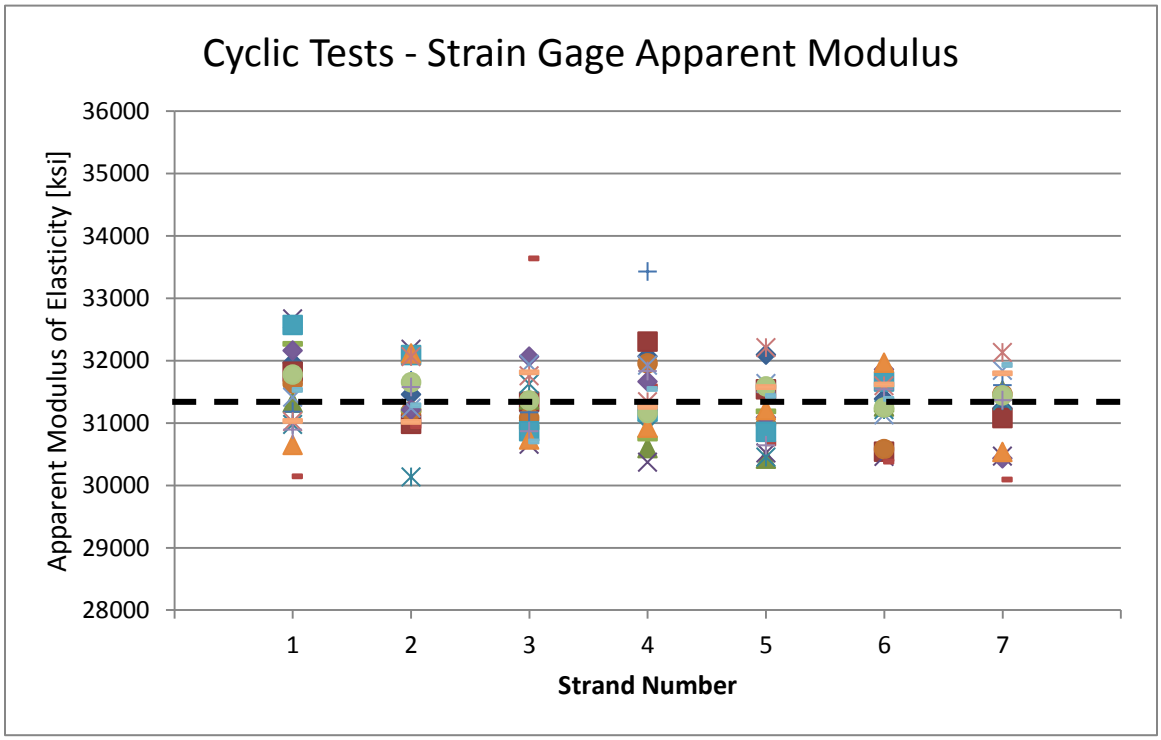

Figure 4.9: Apparent modulus values of individual wires for cyclically loaded specimens.

Figure 4.10 shows the strand modulus of elasticity values as determined using NDI optical tracking. The NDI system was only implemented during 4 tests with a total of 14 strands being instrumented with optical tracking markers. Thus, considerably less data points exist for the strand modulus compared to the apparent modulus. The average modulus (marked on Figure 4.10 by the horizontal dashed line) is 28,860 ksi with a standard deviation of 722 ksi.

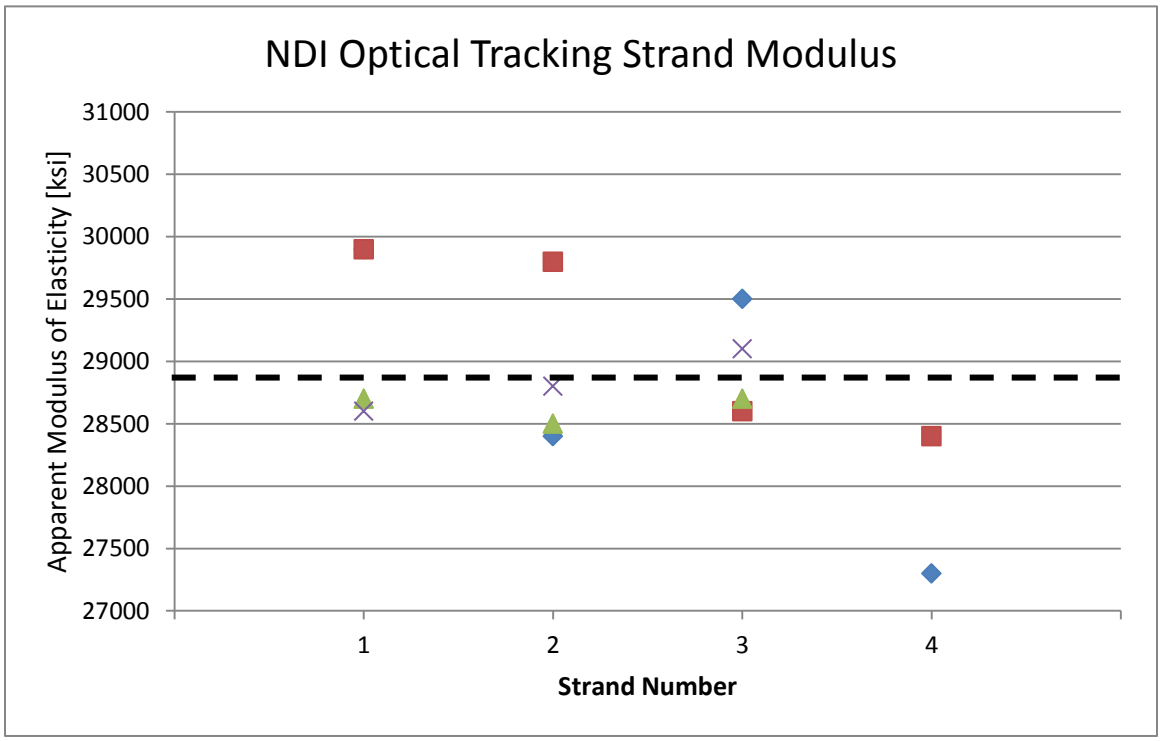

Figure 4.10: Strand modulus values as determined using NDI optical tracking.

The manufacturer specified modulus of elasticity for the spool of strand used for all tests was 28,500 ksi (Appendix A), which is very close to the average strand modulus of 28,860 ksi determined using NDI optical tracking. Additionally, the ratio of the average apparent modulus of an individual wire to the average modulus of the strand as a whole is 0.916 (Table 4.3), which correlates very closely to the analytical modulus ratio range of 0.936 to 0.963. The pitch of the strand used for testing was measured to be approximately 7.9625 inches, which corresponds to about 13.3 times the nominal strand diameter (0.6 inches). Using linear interpolation, this correlates to an analytical modulus

ratio of approximately 0.945. The experimental modulus ratio likely falls outside of the expected range due to factors that are not considered in the analytical approximation method. While these findings support the fact that the strain gages provided reasonable and useful data, a more robust study of the ratio between PT strand and individual wire strain is required before strain gage readings can confidently be converted to strand strain using this ratio.

Table 4.3: Strand and wire modulus of elasticity ratio as determined analytically and experimentally.

Analytical Results		
Strand Pitch	12 d (lower limit)	16 d (upper limit)
$\frac{E_{strand}}{E_{wire}} = \frac{\epsilon_{wire}}{\epsilon_{strand}}$	0.936	0.963
Experimental Results (Ratio of Elastic Moduli)		
Range	Min.	$\frac{28{,}451}{32{,}303} = \mathbf{0.881}$
	Max.	$\frac{28{,}352}{29{,}415} = \mathbf{0.964}$
Average		$\frac{28{,}860}{31{,}500} = \mathbf{0.916}$

CHAPTER 5: SUMMARY, CONCLUSIONS, AND RECOMMENDATIONS

This thesis presents results from a comprehensive laboratory evaluation of the fracture and ultimate strength and deformation capacities of multistrand post-tensioning (PT) anchorage systems for use in seismic resilient rocking wall structures. The testing program encompassed two anchorage manufacturers, two anchorage alignment configurations, and two wedge geometries under both monotonic and cyclic loading. The testing requirements of the International Code Council Evaluation Service "Acceptance Criteria for Post-Tensioning Anchorages and Couplers of Prestressed Concrete" (ICC-ES 2007), which are intended for monostrand assemblies, were followed as closely as possible. All individual numerical test data is listed in Appendix C.

Due to the increased variability in strain distributions amongst strands after yielding, the system would often fracture an individual wire at a load less than the ultimate load. For this reason, the strength and deformation capacities of the system were analyzed in terms of both fracture and ultimate stress and strain. According to the terminology used in the ICC-ES document, for determination of certification compliance, the fracture stress of the system is compared to the strength limits and the ultimate strain is compared to the deformation limit. The following conclusions regarding certification conformance of multistrand PT anchorages can be made based on this investigation:

(1) The multistrand anchorage system only met both the strength ($0.95f_{pu}$) and deformation (2.0%) requirements of ACI 318-08 when the modified wedge geometry was used.

(2) Only one of the tested configurations (aligned anchorages from manufacturer A with modified wedges loaded cyclically) met both the strength ($0.95f_{pm,free\text{-}length}$) and deformation (2.0%) requirements of ICC-ES 2007.

(3) Anchorages from manufacturer A with standard wedges was the only configuration that failed to meet the ACI 318-08 strength requirement of $0.95f_{pu}$.

(4) Anchorages from manufacturer B with standard wedges met the ACI 318-08 strength requirement ($0.95f_{pu}$), but not the deformation requirement (2.0%).

The following conclusions regarding the variables and configurations investigated can be made:

(1) The cyclic loading scheme implemented in this report did not significantly affect the performance of the system under any configuration.

(2) The performance of the system varied greatly depending on the anchorage manufacturer, however neither anchorage was found to be superior. Rather, it was determined that compatibility of the anchorages and wedges is the primary factor in anchorage performance.

(3) Rotation of an anchorage inducing the effects of eccentricity, an angled entrance of the strand into the anchorage, and fretting did not significantly affect the performance of the system.

(4) The geometrically-modified wedge significantly improved the performance of anchorages produced by manufacturer A. They also allowed anchorages from manufacturer B to meet the strength and deformation requirements of ACI 318-08, although the improvement was not statistically significant at a 95% confidence interval.

Based on this investigation, it is recommended that:

(1) Unbonded post-tensioned rocking wall structures be detailed by the structural design engineer to include the wedge modification principles presented in this report.

(2) A strand strain limit of 1.0% elongation be used in the design of unbonded post-tensioning in rocking wall structures due to the potential for premature wire fracture at strains as low as 1.0% even with the modified wedge geometry.

(3) The more stringent strength requirement of $0.95f_{pm,free\text{-}length}$ be adopted by ACI 318-08 as the current limit ($0.95f_{pu}$) does not correlate to the deformation requirement (2.0%) based on the PCI-defined stress-strain relationship of PT strand.

(4) Further research be conducted in the area of wedge geometry development especially regarding the modified wedge geometry principles presented in this report.

(5) Further research be conducted in the relation of individual wire strain determined using strain gages to strand elongation as a whole.

For the purpose of developing acceptance testing criteria for multistrand PT anchorages in which multiple strands are loaded simultaneously, it is recommended that:

(1) Each strand be instrumented such that the strain in each strand is recorded.

(2) Wedges at each end of the assembly be hand seated to a constant load (less than 1000 pounds) prior to the application of the preload.

(3) Specimens with an absolute strain differential greater than 2000 microstrain at any point in the loading up to $0.80f_{pu}$ be discarded and the test repeated.

(4) Limits relevant to current multistrand PT anchorage systems be developed based on achievable fracture and ultimate strength and deformation capacities. Based on the current limits in place, it is recommended that the fracture stress and strain values be compared to the more stringent strength ($0.95f_{pm,free\text{-}length}$) and elongation (2.0%) limits introduced by the Post-Tensioning Institute.

BIBLIOGRAPHY

Aalami, Bijan O. "Critical Milestones in Development of Post-Tensioned Buidlings." *Concrete International*, 2007: 52-56.

Aaleti, S., and S. Sritharan. "A Precast Wall with End Columns (PreWEC) for Seismic Applications." *8th Pacific Conference on Earthquake Engineering (8PCEE).* Singapore, 2007.

ACI 318-08. *Building Code Requirements for Structural Concrete and Commentary.* Farmington Hills: American Concrete Institute, 2008.

Acosta, Jose Antonio Arrellaga. *Instrumentation Systems for Post-Tensioned Segmental Box Girder Bridges.* Master's Thesis, Austin: University of Texas at Austin, 1991.

Billington, David P. "Historical Perspective on Prestressed Concrete." *PCI Journal*, 2004: 14-30.

Dinges, Tyson. *The History of Prestressed Concrete: 1888 to 1963.* Master's Thesis, Manhattan: Kansas State University, 2009.

DSI. *DYWIDAG Post-Tensioning Systems* . DYWIDAG-Systems International, 2006.

El-Sheikh, Magdy T., Richard Sause, Stephen Pessiki, and Le-Wu Lu. "Seismic Behavior and Design of Unbonded Post-Tensioned Precast Concrete Frames." *PCI Journal*, May-June 1999: 54-62.

FHWA. "Post-Tensioning Tendon Installation and Grouting Manual Appendix A - Terminology." *Bridge Technology.* April 17, 2013. http://www.fhwa.dot.gov/bridge/pt/ptappa.cfm (accessed April 17, 2013).

Hayes, Norris O., and Randy Draginis. Anchor System with Substantially Longitudinally Equal Wedge Compression. United States of America Patent 7,765,752 B2. August 3, 2010, a.

Hayes, Norris O., and Randy Draginis. Anchor Wedge Configuration for Tendon Anchors. United States of America Patent 7,726,082 B2. June 1, 2010, b.

Henry, Richard S., Sriram Aaleti, Sri Sritharan, and Jason M. Ingham. "Concept and Finite-Element Modeling of New Steel Shear Connectors for Self-Centering Wall

Systems." *Journal of Engineering Mechanics* 136, no. 2 (February 2010): 220-229.

Holden, Tony, Jose Restrepo, and John B. Mander. "Seismic Performance of Precast Reinforced and Prestressed Concrete Walls." *Journal of Structural Engineering* 129, no. 3 (March 2003): 286-296.

Housner, George W. "The Behavior of Inverted Pendulum Structures During Earthquakes." *Bulletin of the Seismological Society of America* 53, no. 2 (February 1963): 403-417.

ICC-ES. *Acceptance Criteria for Post-Tensioned Anchorages and Couplers of Prestressed Concrete.* Evaluation Report AC303, Whittier: International Code Council Evaluation Service, 2007.

Kurama, Yahya. "Seismic Design of Partially Post-Tensioned Precast Concrete Walls." *PCI Journal* 50, no. 4 (2005): 100-125.

Kurama, Yahya, Brad Weldon, and Qiang Shen. "Experimental Evaluation of Post-Tensioned Hybrid Coupled Wall Subassemblages." *Journal of Structural Engineering* 132, no. 7 (2006): 1017-1029.

Kurama, Yahya, Richard Sause, Stephen Pessiki, and Le-Wu Lu. "Seismic Behavior and Design of Unbonded Post-Tensioned Precast Concrete Walls." *PCI Journal* 44, no. 3 (1999): 72-89.

MacGregor, R. J. G. *Evaluation of Strength and Ductility of a Three Span Externally Post-Tensioned Box Girder Bridge Model.* Ph.D. Dissertation, Austin, TX: The University of Texas at Austin, 1989.

NEES@Nevada. *Unbonded Post-Tensioned Rocking Walls for Seismic Resilient Structures.* 2010. http://nees.unr.edu/projects/rocking-walls (accessed April 2, 2013).

PCI. *PCI Design Handbook, 6th Edition.* Chicago, IL: Precast/Prestressed Concrete Institute, 2004.

Perez, Felipe J., Richard Sause, and Stephen Pessiki. "Analytical and Experimental Lateral Load Behavior of Unbonded Post-Tensioned Precast Concrete Walls." *Journal of Structural Engineering* 133, no. 1 (2007): 1531-1540.

Perez, Felipe, J., Stephen Pessiki, and Richard Sause. "Lateral Load Behavior of Unbonded Post-Tensioned Precast Concrete Walls with Vertical Joints." *PCI Journal*, March-April 2004: 48-64.

Priestley, M. J. Nigel, and Jian Ren Tao. "Seismic Response of Precast Prestressed Concrete Frames With Partially Debonded Tendons." *PCI Journal*, January-February 1993: 58-69.

Priestley, M.J. Nigel, Sri Sritharan, James R. Conley, and Stefano Pampanin. "Preliminary Results and Conclusions From the PRESSS Five-Story Precast Concrete Test Building." *PCI Journal*, November-December 1999: 42-67.

PTI. *Acceptance Standards for Post-Tensioned Systems.* Phoenix: Post-Tensioning Institute, 1998.

PTI. *What is Post-Tensioning?* Phoenix: Post-Tensioning Institute, 2000.

Restrepo, Jose I., and Amar Rahman. "Seismic Performance of Self-Centering Structural Walls Incorporating Energy Dissipators." *Journal of Structural Engineering* 133 (2007): 1560-1570.

Schechter, Edward, and Henry C. Boecker. "Wedge Anchorage System for Strand Post-Tensioning." *PCI Journal*, July-August 1971: 49-63.

Shrive, Nigel G., Ezzeldin Y. Sayed-Ahmed, Eric Damson, Daniel Tilleman, and Gamil Tadros. Prestressing Anchorage System for Fiber Reinforced Plastic Tendons. United States of America Patent 6,082,063. July 4, 2000.

Sorkin, Felix L. Anchor of a Post-Tension Anchorage System with an Improved Cap Connection. United States of America Patent 6023894. February 15, 1998.

Sritharan, Sri. *NEESR-CR: Unbonded Post-Tensioned Rocking Walls for Seismic Resilient Structures.* September 23, 2010. http://nees.org/warehouse/project/946 (accessed March 12, 2013).

Sritharan, Sri, Sriram Aaleti, Rick Henry, Keh-Chyuan Tsai, and Kuang-Yen Liu. "Introduction to PreWEC and Key Results of a Proof of Concept Test." *M.J. Nigel Priestley Symposium*, August 2008: 95-106.

Technical Advisory Board, PTI. "Post-Tensioning Institute Technical Board Shares Alternative Research Program, Testing Results." *PCI Journal*, Summer 2010: 9-10.

Walsh, Kevin Q., and Yahya C. Kurama. *Behavior and Design of Unbonded Post-Tensioning Strand/Anchorage Systems for Seismic Applications.* Master's Thesis, Notre Dame: University of Notre Dame, 2009.

—. "Post-Tensioning Institute Technical Board Shares Alternative Research Program, Testing Results." *PCI Journal*, Summer 2010: 11-14.

WJE. *Post-Tension Anchorage Testing for the Post Tensioning Institute.* WJE No. 2009.3214, Northbrook, IL: Wiss, Janney, Elstner Associates Inc., 2010.

Yates, D. L. *A Study of Fretting Fatigue in Post-Tensioned Concrete Beams.* M.S. Thesis, Austin, TX: The University of Texas at Austin, 1988.

APPENDIX A: STRAND MILL CERTIFICATES OF INSPECTION

SUMIDEN WIRE PRODUCTS CORPORATION
710 Marshall Stuart Drive
Dickson, TN 37055
(615) 446-3199
Fax (615) 740-1518
SWPC

*** MILL CERTIFICATE OF INSPECTION *** PAGE 1 OF 1

ORDER NUMBER : D18062 ISSUE DATE : 10/20/10

COMMODITY : STEEL STRAND, UNCOATED SEVEN-WIRE FOR PRESTRESSED CONCRETE
SPECIFICATION : ASTM A416-LATEST
Size 1/2 Low Relaxation

CUSTOMER : UNIVERSITY OF MINNESOTA - DULUTH
P.O. NUMBER : 342597
STATE JOB NO :
MANUFACTURER : Sumiden Wire Product Corporation
DESTINATION : DULUTH MN

PACK NUMBER CERTIFIED: -----REPRESENTATIVE-----

NO.	PACK#	HEAT#	GRADE (ksi)	B.S (lb)	EL (%)	Y.P (lb)	CURVE#	AREA (sq.in.)	ELASTIC MODULUS (M psi)
1	D120759B	D617830	270	42,738	6.1	38,652	D100000R	0.1528	28.7

We hereby certify that:
* We have accurately carried out the inspection of commodity as described above in accordance with all applicable specifications of the contract.
* The raw material, and all manufacturing processes used in the production of the strand described above occurred in the USA, in compliance with the Buy America requirements of the Surface Transportation Assistance Act of 1982, as amended.
* The material described above will bond to concrete of a normal strength and consistency in conformance with the prediction equations for transfer and development length given in the ACI/AASHTO specifications.

Quality Assurance Section

Load-Elongation Curve

For Uncoated Seven Wire Steel Strand for Prestressed Concrete

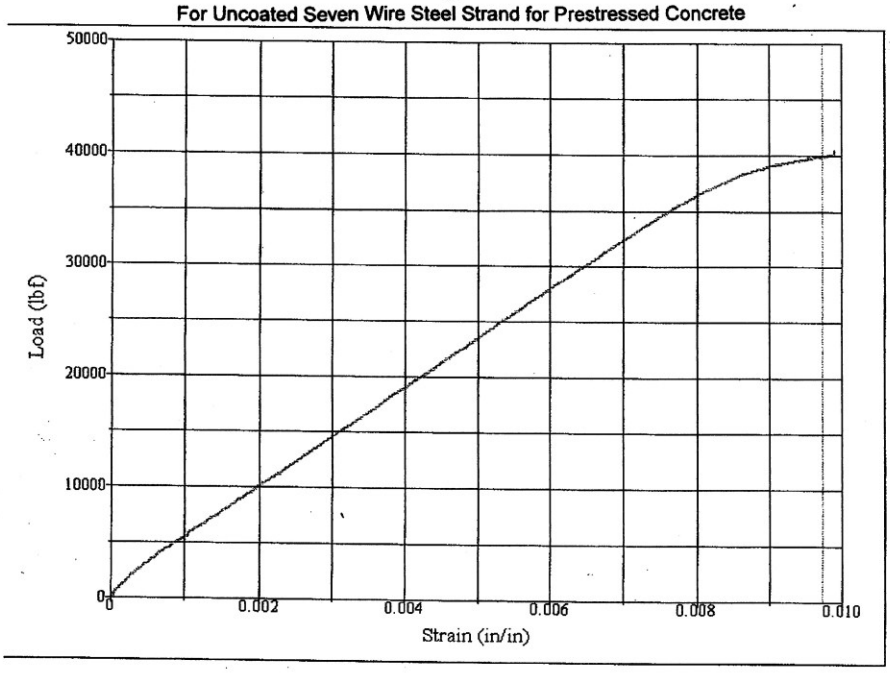

***Vertical Line is drawn at 1% Extension Under Load**

Pack #	D100000R
Area	0.1528 in²
Modulus	28.7 Msi
Size	1/2"
Grade	270k

SWPC

Approval

SUMIDEN WIRE PRODUCTS CORPORATION
710 Marshall Stuart Drive
Dickson, TN 37055
(615) 446-3199
Fax (615) 740-1518

SWPC

*** MILL CERTIFICATE OF INSPECTION *** PAGE 1 OF 1

ORDER NUMBER : D20915 ISSUE DATE : 01/26/12

COMMODITY : STEEL STRAND, UNCOATED SEVEN-WIRE
FOR PRESTRESSED CONCRETE
SPECIFICATION : ASTM A416-LATEST
Size 0.6 Low Relaxation

CUSTOMER : UNIVERSITY OF MINNESOTA - DULUTH
P.O. NUMBER : 0000509877
STATE JOB NO :
MANUFACTURER : Sumiden Wire Product Corporation
DESTINATION : DULUTH MN

PACK NUMBER CERTIFIED: ----REPRESENTATIVE----

NO.	PACK#	HEAT#	GRADE (ksi)	B.S (lb)	EL (%)	Y.P (lb)	CURVE#	AREA (sq.in.)	ELASTIC MODULUS (M psi)
1	D322516A	D247217	270	62,393	5.9	56,731	D300000R	0.2227	28.5

We hereby certify that:
* We have accurately carried out the inspection of commodity as described above in accordance with all applicable specifications of the contract.
* The raw material, and all manufacturing processes used in the production of the strand described above occurred in the USA, in compliance with the Buy America requirements of the Surface Transportation Assistance Act of 1982, as amended.
* The material described above will bond to concrete of a normal strength and consistency in conformance with the prediction equations for transfer and development length given in the ACI/AASHTO specifications.

Quality Assurance Section

Load-Elongation Curve

For Uncoated Seven Wire Steel Strand for Prestressed Concrete

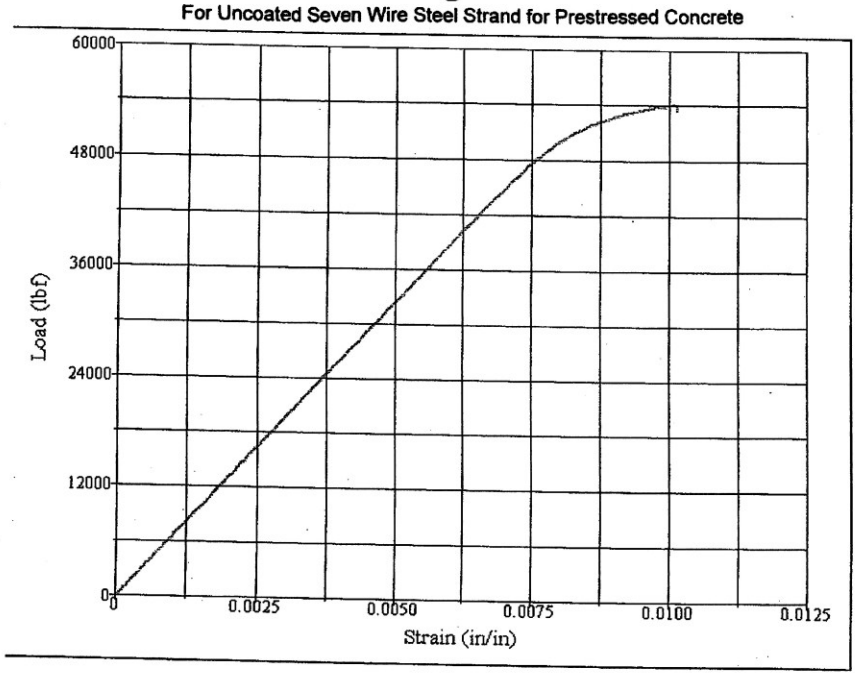

***Vertical Line is drawn at 1% Extension Under Load**

Pack #	D300000R
Area	0.2227 in²
Modulus	28.5 Msi
Size	0.6"
Grade	270K

SWPC

Approval

EVRAZ ROCKY MOUNTAIN STEEL
A DIVISION OF EVRAZ INC. NA

P.O. Box 316
Pueblo, CO 81002 USA

MATERIAL TEST REPORT

Date Printed: 18–NOV–11

Date Shipped: 18–NOV–11 **Product:** ROD 1/2" **Specification:** ASTM–A–510 AISI 1080M
Mts ASTM A–510 **FWIP:** 77186608 **Customer:** SUMIDEN WIRE PRODUCTS CORP **Cust. PO:** 8036

CHEMICAL ANALYSIS

Heat Number	C	Mn	P	S	Si	Cu	Ni	Cr	Mo	Al	V	B	Cb	Sn	N	Ca	Ti
547217	0.83	0.70	0.009	0.008	0.21	0.20	0.06	0.14	0.013	0.002	0.030	0.0003	0.001	0.011	0.0071	0.0003	0.001

MECHANICAL PROPERTIES

	Ultimate (Psi)	Red/Area (%)	Size	Ovality
Minimum	171210	10.0	.495	.005
Maximum	176760	18.4	.496	.006
Average	173924	13.2	.496	.005
Std. Dev	1668	2.8	.000	.000
Count	9	9	9	9

All melting and manufacturing processes of the material subject to this test certificate occurred in the United States of America.
ERMS also certifies this material to be free from Mercury contamination.

This material has been produced and tested in accordance with the requirements of the applicable specifications. We hereby certify that the above test results represent those contained in the records of the Company.

Reported %R/A results are from unaged samples. Fully aged will be >25%
"TR" designated heats are certified to +/– 5 ksi from the designated grade

Mark F Lupanec

Quality Assurance Department

APPENDIX B: STRAIN GAGE INSTALLATION PROCEDURE

Procedure for Application of Pre-wired Strain Gages to PT Strand using M-Bond 200 Adhesive from Micro-Measurements

Modified procedure adapted from Micro-Measurements Strain Gage Installations with M-Bond 200 Adhesive: http://www.vishaypg.com/docs/11127/11127_b1.pdf

The following products are used in this procedure:

- M-Bond 200 adhesive
- M-Bond 200 catalyst
- Degreaser (or isopropyl alcohol)
- Silicon-carbide paper (320- and 400-grit)
- M-Prep Conditioner A
- M-Prep Neutralizer 5A
- Gauze sponges
- Cotton applicators
- Gage installation tape

The following pre-wired Omega strain gages are recommended for this application:

- KFG-1N-120-C1-11L3M3R
- KFG-2N-120-C1-11L3M3R
- KFG-2N-120-C1-11L1M2R

Step 1
Thoroughly degrease the gaging area with degreaser or isopropyl alcohol. Simply spray the area of the strand where the gage will be applied and wipe dry with a clean rag or paper towel.

Step 2
Thoroughly wet the individual wire that the strain gage will be applied to with M-Prep Conditioner A and abrade with 320-grit silicon-carbide paper. This is followed by wiping dry with a gauze sponge. Repeat this wet abrading process with 400-grit silicon-carbide paper, and then dry by slowly wiping through with a gauze sponge.



Repeatedly apply M-Prep Conditioner A and scrub with cotton-tipped applicators until a clean tip is no longer discolored. Remove all residue and Conditioner by again slowly wiping through with a gauze sponge. Never allow any solution to dry on the surface because this invariably leaves a contaminating film and reduces chances of a good bond.



Step 3
Now apply a liberal amount of M-Prep Neutralizer 5A to the prepared wire and scrub with a cotton-tipped applicator. With a single, slow wiping motion of a gauze sponge, carefully dry this surface. Do not wipe back and forth because this may allow contaminants to be re-deposited.

Note: The cotton-tipped applicator should be clean after scrubbing since the conditioner was applied until the applicator was clean. If the applicator is not clean, repeat the second part of step two until the applicator is clean.

Step 4
Remove the pre-wired strain gage from the transparent envelope. Be careful not to touch the bonding surface of the strain gage directly as natural hand oils may contaminate the gage and reduce chances of a good bond.

Note: Gages have been treated for optimum bonding conditions and require no pre-cleaning before use unless contaminated during handling. If contaminated, the back of any gage can be cleaned with a cotton-tipped applicator slightly moistened with M-Prep Neutralizer 5A.

Step 5
The M-Bond **catalyst** can now be applied to the bonding surface of the gage. Very little catalyst is need, and it should be applied in a thin, uniform coat. Lift the brush-cap out of the catalyst bottle and wipe the brush approximately 10 strokes against the inside of the neck of the bottle to wring out most of the catalyst. Holding the strain gage by the lead wires with the bonding side up, set the brush down on the gage and swab the gage backing. Do not stroke the brush in a painting style, but slide the brush over the entire gage in a single motion. Allow the catalyst to dry at least **one minute** under normal ambient conditions before proceeding.

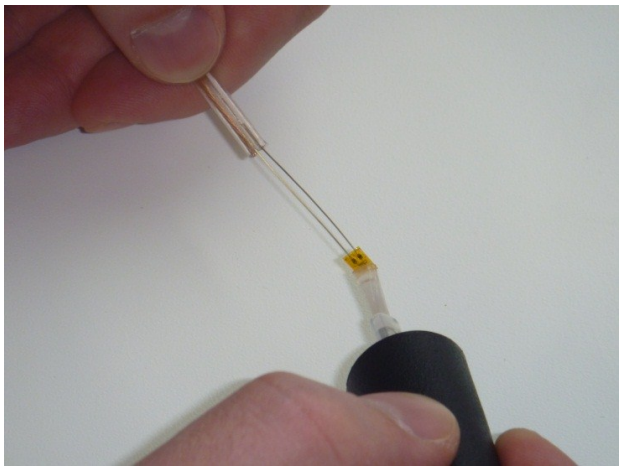

Step 6
Once the catalyst has been allowed to thoroughly dry for at least one minute, place the gage (bonding side down) on a chemically clean glass plate. Cut an approximately 2-in. long piece of gage installation tape in half the long way.

Apply the tape over the gage, slightly overlapping the lead wire insulation at one end and extending beyond the end of the strain gage at the other. Take care to center the gage on the tape. Holding the free end of the tape strip off of the glass plate, gently press on the top of the tape to ensure a good bond is formed between the tape and the gage.

Carefully lift the tape at a shallow angle (about 45 degrees to the glass surface), bringing the gage up with the tape and removing the assembly from the glass plate.

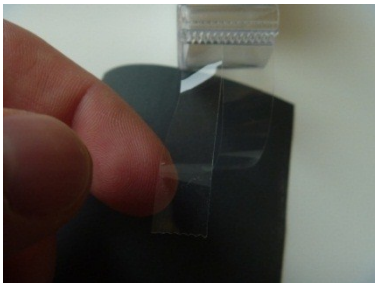
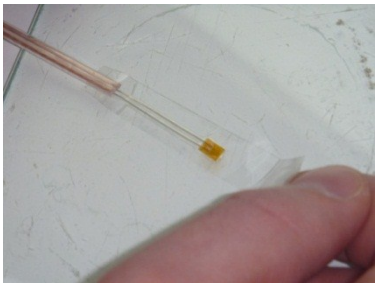
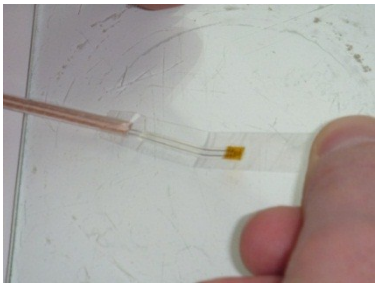

Step 7
Holding the assembly by the free end of the tape and strain gage lead wires, align the gage with the wire to be instrumented. Apply the free end of the tape to the individual strand wire so that the strain gage remains unattached and will be aligned with the individual wire once it is glued in place.

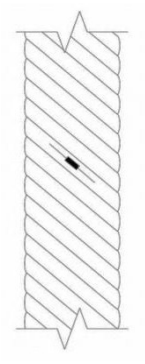
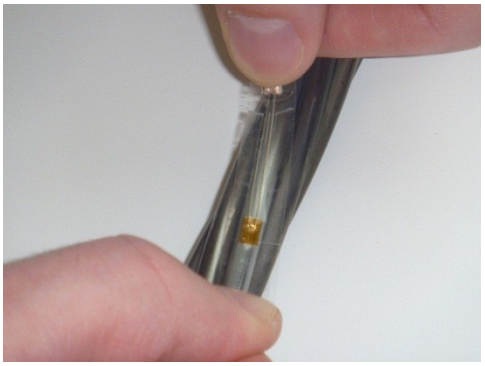
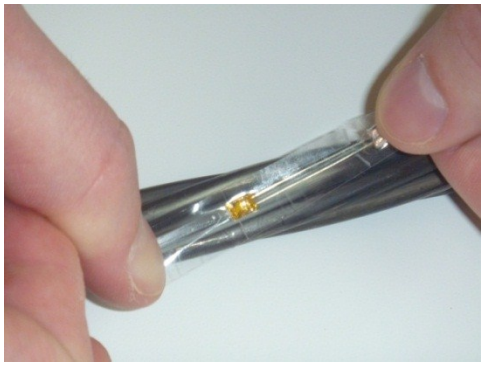

Note: The next three steps must be completed in the sequence shown, within 3 to 5 seconds. Read steps 8, 9, and 10 before proceeding.

Step 8
Lift the free end of the tape assembly so that a fold is formed in the tape approximately 0.5-in. from the strain gage. Holding in this position, apply one or two drops of M-Bond 200 **adhesive** at the fold formed by the junction of the tape and specimen surface. This adhesive application should be approximately 0.5-in. outside the actual gage installation area to ensure that local polymerization that takes place when the adhesive comes in contact with the specimen surface will not cause unevenness in the gage glueline.

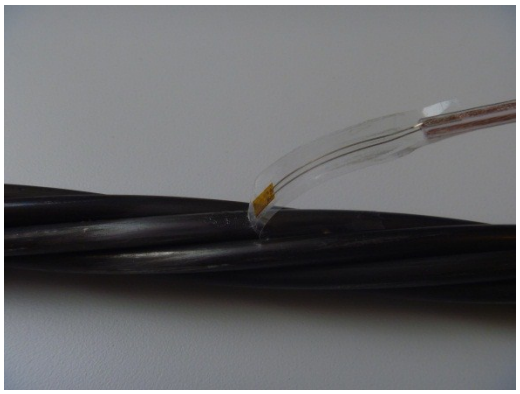
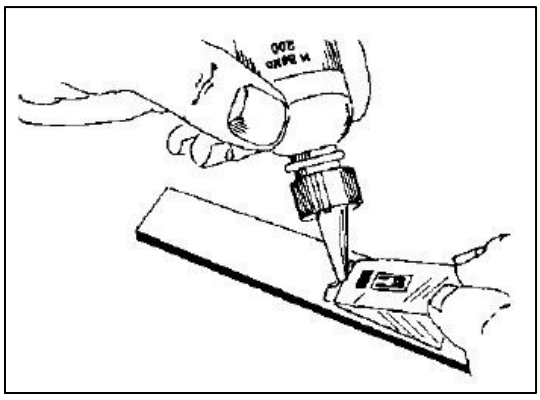

Step 9
Immediately rotate the tape to approximately a 30-degree angle so that the gage is bridged over the installation area. While holding the tape slightly taut, slowly and firmly make a single wiping stroke over the gage/tape assembly with your finger bringing the gage back down over the specimen. Use firm pressure when wiping over the gage. A very thin, uniform layer of adhesive is desired for optimum bond performance.

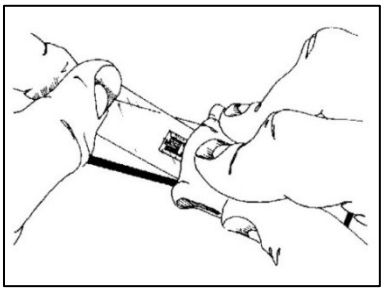
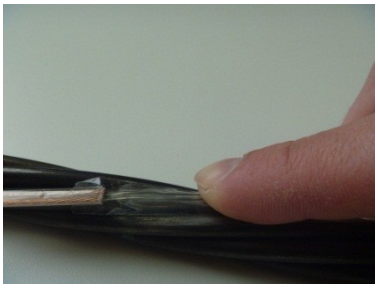
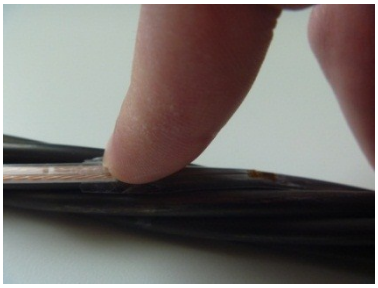

Step 10
Immediately upon completion of step 9, firm thumb pressure must be applied to the gage area. This pressure should be held for at least **one minute** (at room temperature conditions). Note that direct use of the thumb or finger rather than with a gauze pad is important because "thumb heat" helps to speed adhesive polymerization. If a gauze pad or other buffer is used, pressure-application time should be extended to ensure proper bond.

Step 11
Place a strip of masking tape around the gage lead wire insulation near its terminus. The tape should be placed tightly enough so that in the event that the lead wires are inadvertently tugged on or pulled, the force will be absorbed by the masking tape and lead wire insulation rather than the strain gage itself. Take care not to tug on the freshly glued strain gage while placing the masking tape.

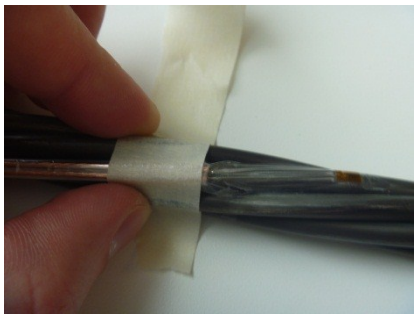
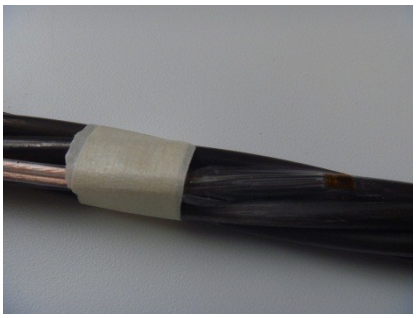

Note: Neither the masking tape nor the gage installation tape need to be removed prior to testing. Leaving them in place offers the best probability of a working (undamaged) strain gage at the time of testing.

APPENDIX C: DATA TABLES

Table C1: Stress and strain gage elongation data for monotonic load tests.

Test Config.	Rep	Stress (ksi)			Percent Elongation (%)			
		Yield	Fract.	Ult.	Average fracture	Max fracture	Average ultimate	Max ultimate
Mfr. A Aligned Standard	1	N/A	244.30	244.30	0.8303	0.8714	0.8303	0.8714
	2	N/A	243.90	243.90	0.8142	0.8741	0.8142	0.8741
	3	N/A	252.54	252.54	0.8804	0.9636	0.8804	0.9636
Mfr. A Aligned Modified	1	256.70	257.00	272.72	0.9608	1.0122	2.7863	2.8902
	2	253.03	275.97	277.05	2.5775	2.6847	3.3710	3.5074
	3	252.72	266.76	272.47	1.6417	1.9840	2.7191	2.9725
Mfr. A Rotated Standard	1	N/A	234.28	244.10	0.7575	0.7738	0.8612	0.8929
	2	N/A	234.50	238.40	0.7686	0.8083	0.8291	0.8735
	3	N/A	250.74	250.74	0.8674	0.9033	0.8674	0.9033
Mfr. A Rotated Modified	1	255.92	264.20	269.83	1.4568	1.4995	2.5247	2.5551
	2	253.86	258.00	263.90	0.9789	1.0846	2.3286	2.4988
	3	253.04	265.50	269.20	1.4708	1.6469	2.4130	2.5530
Mfr. B Aligned Standard	1	254.15	261.73	261.73	1.1483	1.3564	1.1483	1.3564
	2	254.37	270.49	270.49	2.0020	2.1676	2.0020	2.1676
	3	254.82	261.96	261.96	1.1646	1.5038	1.1646	1.5038
Mfr. B Aligned Modified	1	255.84	274.91	274.91	2.4054	2.5531	2.4054	2.5531
	2	252.71	269.53	269.53	1.9324	2.0936	1.9324	2.0936
	3	249.51	267.97	267.97	1.8535	2.1074	1.8535	2.1074

Table C2: Stress and strain gage elongation data for cyclic load tests.

Test Config.	Rep	Stress (ksi)			Percent Elongation (%)			
		Yield	Fract.	Ult.	Average fracture	Max fracture	Average ultimate	Max ultimate
Mfr. A Aligned Standard	1	N/A	248.82	248.82	0.8275	0.8539	0.8275	0.8539
	2	N/A	227.46	234.42	0.7317	0.7680	0.7621	0.8226
	3	N/A	223.09	247.08	0.7286	0.7361	0.8556	0.8949
Mfr. A Aligned Modified	1	252.55	275.16	275.16	2.7214	2.7214	2.5217	2.7214
	2	250.91	277.33	277.33	2.7294	2.8412	2.7294	2.8412
	3	255.48	277.12	277.12	2.7328	2.8091	2.7328	2.8091
Mfr. A Rotated Standard	1	N/A	228.10	242.63	0.7311	0.7631	0.8296	0.8801
	2	N/A	228.70	239.50	0.7346	0.7830	0.7966	0.8280
	3	N/A	218.80	240.62	0.6842	0.7112	0.8260	0.8409
Mfr. A Rotated Modified	1	254.37	273.25	273.25	2.2919	2.3382	2.2919	2.3382
	2	257.04	261.92	268.10	1.0921	1.2136	2.3499	2.4623
	3	256.88	269.68	269.68	2.0047	2.0663	2.0047	2.0663
Mfr. B Aligned Standard	1	250.92	265.09	265.09	1.5074	1.6660	1.5074	1.6660
	2	256.02	267.23	267.23	1.6592	1.8078	1.6592	1.8078
	3	254.38	267.17	267.17	1.6224	1.6667	1.6224	1.6667
Mfr. B Aligned Modified	1	251.44	273.44	273.44	2.3197	2.4913	2.3197	2.4913
	2	252.07	270.20	270.20	2.0207	2.1929	2.0207	2.1929
	3	250.45	264.20	265.41	1.2706	1.4485	2.0501	2.2354

Table C3: NDI optical tracking modulus and strain at fracture data.

Test Config.	Repetition 1			Repetition 2		
	Strand	Modulus (ksi)	Strain at fracture (%)	Strand	Modulus (ksi)	Strain at fracture (%)
Static Mfr. A Aligned Standard	1	29905	0.8595	1	29873	0.8766
	2	28422	0.9013	2	29822	0.8607
	3	29529	0.8673	3	28607	0.8844
	6	27318	0.9390	7	28352	0.9038
Static Mfr. A Rotated Standard	1	28651	0.9374	1	28566	0.8767
	2	28451	0.8383	2	28750	0.8694
	3	28675	0.8505	3	29103	0.8389

Table C4: Strain gage elastic modulus data.

Test Configuration	Strand	Elastic modulus (ksi)					
		Monotonic Load Tests			Cyclic Load Tests		
		Rep 1	Rep 2	Rep 3	Rep 1	Rep 2	Rep 3
Mfr. A Aligned Standard	1	31316	32009	31386	31964	31823	31323
	2	30730	31888	32916	31457	30987	--
	3	--	32230	32788	31042	31339	31373
	4	32873	30985	31521	32066	32306	30598
	5	30601	32025	32514	32095	31540	30428
	6	31556	32829	32189	31385	30540	31263
	7	29346	29415	30587	31240	31079	31520
Mfr. A Aligned Modified	1	31997	32731	33955	32669	30975	31630
	2	32333	32207	32336	32182	30136	31187
	3	30662	33353	32403	30656	31630	31083
	4	30880	30862	31722	30368	30900	31956
	5	33076	30649	30000	30519	30454	30982
	6	31532	31370	30632	30463	31210	30581
	7	31267	29767	30965	30468	31354	31463

Test Configuration	Strand	Elastic modulus (ksi)					
		Monotonic Load Tests			Cyclic Load Tests		
		Rep 1	Rep 2	Rep 3	Rep 1	Rep 2	Rep 3
Mfr. A Rotated Standard	1	32235	31295	31041	31181	30145	32270
	2	32303	32252	31433	31682	30948	31205
	3	31936	32342	32833	31170	33640	30930
	4	30257	31830	32486	33427	31587	30749
	5	32511	30977	32638	30843	30670	31187
	6	31105	31133	30984	31710	30382	31212
	7	31746	29567	--	31609	30091	--
Mfr. A Rotated Modified	1	31593	35330	30047	32160	32572	30648
	2	30857	30891	34084	31210	32090	32114
	3	32102	31632	32388	32062	30866	30732
	4	31432	32225	31630	31665	31180	30922
	5	32926	30889	32233	31090	30858	31208
	6	32742	31075	32430	31860	31663	31967
	7	29960	30169	29293	30432	--	30534

Test Configuration	Strand	Elastic modulus (ksi)					
		Monotonic Load Tests			Cyclic Load Tests		
		Rep 1	Rep 2	Rep 3	Rep 1	Rep 2	Rep 3
Mfr. B Aligned Standard	1	32354	33001	31187	31413	31020	31777
	2	31706	33540	30916	31235	32062	31655
	3	32982	32279	31715	31939	31758	31359
	4	31355	34305	31522	31924	31340	31163
	5	30657	31656	32143	31631	32206	31585
	6	31864	31303	32502	31132	31594	31249
	7	30087	29261	31163	31841	32131	31440
Mfr. B Aligned Modified	1	30982	31339	31667	30894	31527	31034
	2	30810	31472	31797	31576	31283	31018
	3	32063	31007	32509	30867	30702	31810
	4	31230	33620	32462	31833	31546	31258
	5	31299	30972	31987	30642	31434	31575
	6	32767	33382	31686	31539	31387	31614
	7	30458	29112	28299	31367	31931	31798